BERICHTE
aus dem Fachbereich Geowissenschaften
der Universität Bremen

Nr. 225

Panteleit, B.

GEOCHEMISCHE PROZESSE IN DER SALZ- SÜßWASSER ÜBERGANGSZONE

Berichte, Fachbereich Geowissenschaften, Universität Bremen, Nr. 225,
106 Seiten, Bremen 2004

ISSN 0931-0800

Die "Berichte aus dem Fachbereich Geowissenschaften" werden in unregelmäßigen Abständen vom Fachbereich 5, Universität Bremen, herausgegeben.

Sie dienen der Veröffentlichung von Forschungsarbeiten, Doktorarbeiten und wissenschaftlichen Beiträgen, die im Fachbereich angefertigt wurden.

Die Berichte können bei:

Frau Monika Bachur

Forschungszentrum Ozeanränder, RCOM

Universität Bremen

Postfach 330 440

D 28334 BREMEN

Telefon: (49) 421 218-8960

Fax: (49) 421 218-3116

e-mail: MBachur@uni-bremen.de

angefordert werden.

Zitat:

Panteleit, B.

Geochemische Prozesse in der Salz- Süßwasser Übergangszone.

Berichte, Fachbereich Geowissenschaften, Universität Bremen, Nr. 225, 106 Seiten, Bremen, 2004.

ISSN 0931-0800

Geochemische Prozesse
in der
Salz-Süßwasser Übergangszone

Dissertation zur Erlangung
des Doktorgrades in den Naturwissenschaften
am Fachbereich Geowissenschaften
der Universität Bremen

vorgelegt von
Dipl. Geol. Björn Panteleit
Bremen, Juli 2003

Tag des Kolloquiums: 12. Dezember 2003

Gutachter:

1. Herr Prof. H. D. Schulz (Universität Bremen FB 5)

2. Herr Prof. H. Villinger (Universität Bremen FB 5)

Prüfer:

1. Herr Prof. R. Stein (Alfred Wegener Institut Bremerhaven)

2. Herr F. Binot (GGA-Institut, Hannover)

Danksagung

An dieser Stelle möchte ich den Menschen danken, die mich in den letzten 3 Jahren auf die eine oder andere Weise unterstützt haben. An erster Stelle seien hier Herr Prof. Dr. H.D. Schulz und Herr Dr. W. Kessels genannt, die diese Arbeit fachlich betreut und bei der Vergabe dieser interessanten Arbeit an mich gedacht haben. Herrn Prof. Dr. H. Villinger danke ich für die Übernahme des Zweitgutachtens.

Die Arbeit zwischen zwei Instituten bringt es mit sich, dass man oft allein vor Fragen steht. Ich hatte aber das Glück, dass immer jemand ein offenes Ohr für mich hatte. Bezüglich der Felduntersuchungen im Raum Cuxhaven waren dies hauptsächlich die Kollegen aus dem Geozentrum Hannover. Hier sind vor allem Frau Haifa Rifai und Herr F. Binot zu nennen, denen ich auch viele fröhliche Stunden in der Marsch verdanke, und die nicht nur einmal auch ein paar aufmunternde Worte für mich hatten. Für interessante fachliche Diskussionen und Hinweise danke ich weiterhin Herrn Dr. J. Fritz, Herrn Dr. A. Suckow, Dr. R. Kringel, Herrn T. Willert, Herrn Dr. C. Thorenz, Herrn Dr. C. Fulda, Herrn M. Neuß und vielen weiteren Mitarbeiten des Instituts für Geowissenschaftliche Gemeinschaftsaufgaben, des Niedersäschischen Landesamtes für Bodenforschung und der Bundesanstalt für Geowissenschaften und Rohstoffe, die ich in dieser Zeit kennen lernen und mit denen ich zusammen arbeiten durfte.

Die Laboruntersuchungen fanden an der Universität Bremen statt. Für die fachliche und technische Unterstützung im Labor standen mir die Mitarbeiter der Arbeitsgruppe Geochemie Karsten Enneking, Susanne Siemer, Sylvana Hessler, Thomas Wilkop und Siegrid Hinrichs zur Seite. Auch bei den praktischen und manchmal monotonen Laborarbeiten haben viele tatkräftige Hände zum Gelingen der Arbeit beigetragen. Genannt seien hier Yvonne Habenicht für ihre unzähligen Titrationen, Jens Berger für die Hilfe beim Bau des Versuchsbeckens und Thomas Hammerich, Dirk Wagenschein und Toni Wienrich für ihre Unterstützung bei der Probenahme in Labor und Feld.

Am Ende einer solchen Arbeit weiß man, dass die wahre Herausforderung erst beginnt, wenn die Daten gesammelt sind und man am Schreibtisch sitzt. Aber auch hier hatte ich großartige Unterstützung. Für viele fachliche und nicht fachliche Diskussionen, die weit über das Ende dieser Arbeit hinaus wirken werden, aber auch genauso zahlreiche kurze, aber äußerst vergnügliche Augenblicke möchte ich Antje Weitz, Astrid Hadeler und Kay Hamer sehr danken.

Neben den genannten haben viele weitere Menschen sowohl im wissenschaftlichen wie im privaten Bereich dazu beigetragen, dass ich diese Arbeit erfolgreich beenden konnte. Vor allem sei hier meine Familie genannt. Aber auch alle anderen Freunde sind nicht vergessen!

Inhalt

TEIL III

TEIL IV

TEIL V

GEOCHEMICAL PROCESSES IN THE SALT-FRESH WATER TRANSITION ZONE – COMPARING RESULTS OF A 2D-SAND-TANK-EXPERIMENT WITH FIELD DATA FROM THE COASTAL AQUIFER TEST FIELD AT THE GERMAN NORTH SEA COAST 80

ANHANG

Einleitung

Mehr als drei Viertel der Weltbevölkerung leben in Küstengebieten, wobei Regionen um Flussmündungen besonders attraktiv für die Siedlung sind. Den Grundwasserressourcen in diesen Gebieten kommt daher weltweit eine besondere Bedeutung zu. Die Veränderungen der Grundwasserqualität hat einen großen Einfluss auf die Qualität und Produktivität dieser Küstenregionen. Verursacht werden können solche Veränderungen durch Meeresspiegelschwankungen in Folge von Klimaveränderungen. Eine andere mögliche Ursache liegt in der Förderung von Grundwasser in Küstengebieten oder der Absenkung des Grundwasserspiegels durch Drainagemaßnahmen zur Landgewinnung. Unabhängig davon ob der Meeresspiegel oder der Grundwasserspiegel sich ändern ist eine Änderung des Gleichgewichtzustands zwischen Salz- und Süßwasser die Folge.

Der stabile Gleichgewichtszustand wurde quantitativ erstmals unabhängig von einander durch Badon-Ghyben (1889) und Herzberg (1901) beschrieben (BGH Prinzip, Abb.1). Dabei „schwimmt" das Süßwasser aufgrund seiner geringeren Dichte auf einem Salzwasserkeil. Die Mächtigkeit des Süßwasserkörpers nimmt vom Fuß des

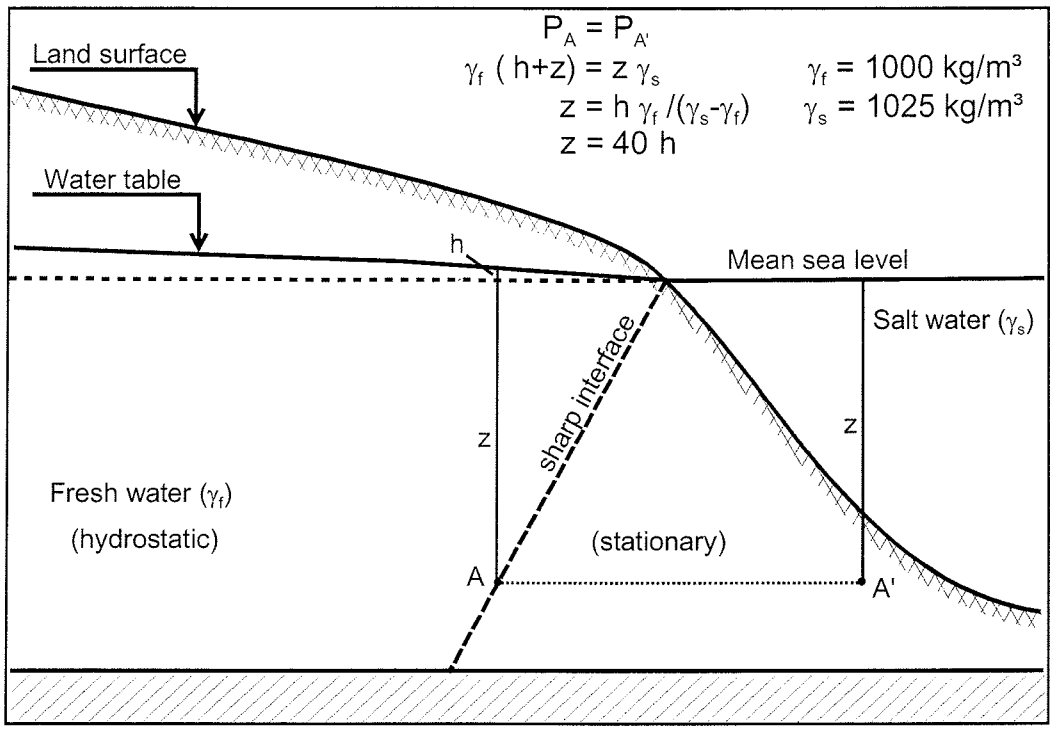

Abbildung 1: Erläuterung des Badon-Ghyben Herzberg Prinzips in einem idealisierten hydrostatischen Küstenaquifer. Eine scharfe Grenzfläche zwischen Süß- und Salzwasser wird angenommen. γ ist die Dichte; z die Tiefe unter dem mittleren Meeresspiegel (msl) und h die Höhe des Grundwasserspielgels über msl (Abb. verändert aus Custodio 1987).

Salzwasserkeils zum Meer hin ab. Diese Aussagen beruhen auf dem Prinzip des hydrostatischen Druckausgleichs auf beiden Seiten der Süß-Salzwassergrenzfläche. Die Position der Grenzfläche lässt sich demnach berechnen aus dem Dichteunterschied der beiden Wässer.

Mit dem BGH Prinzip lässt sich jedoch nur eine theoretische Tiefe der Grenzfläche berechnen. In der Natur ist selten eine scharfe Grenzfläche ausgebildet. Durch Mischung, Dispersion und Diffusion entwickelt sich eine Übergangszone mit mittleren Salzgehalten, deren Ausbreitung von den hydrodynamischen Charakteristiken des Aquifers abhängt (De Josselin de Jong and Van Duijn, 1986; Kohout, 1980). Dies hat zur Folge, dass je nach Mächtigkeit der Übergangszone, ein signifikanter Anstieg des Salzgehaltes schon oberhalb der dem BGH Prinzip entsprechenden Tiefe zu Beeinträchtigungen der Nutzbarkeit des Grundwassers führen kann. Schon durch eine Beimischung von ca. 1% Meerwasser wird die maximale akzeptable Chloridkonzentration für Trinkwasser von 0.2 g/l, bei einem Meerwasseranteil von ca. 3 % der

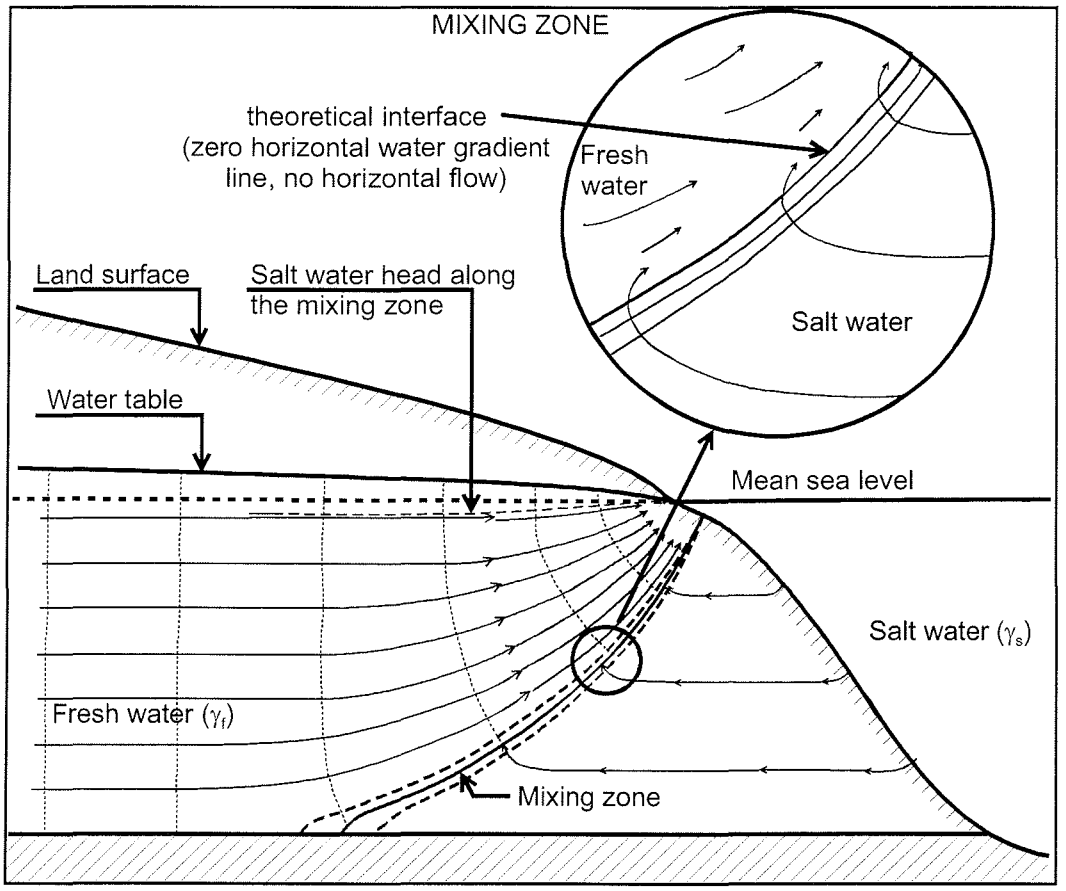

Abbildung 2: Ausbildung einer Übergangszone zwischen Süß- und Salzwasser. In der Übergangszone existiert ein seewärts gerichteter Fluss von Salzwasser. Um die Salzbilanz auszugleichen muss Salzwasser landeinwärts fließen, der Salzwasserspiegel in der Übergangszone nimmt also ab. Die Position der „Grenzfläche" liegt daher tiefer als nach dem BGH-Prinzip berechnet. (Abb. verändert aus Custodio 1987)

Trinkwassergrenzwert von 0.6 g/l überschritten (WHO, 1971). Durch die Ausbildung der Übergangszone wird die Druckspiegelhöhe des Salzwassers verringert, so dass in der Regel der natürliche Salz-Süßwasserübergang tiefer liegt als nach dem BGH Prinzip berechnet. Zum anderen ist der beim BGH Prinzip angenommene hydrostatische Zustand eine weitere wichtige Einschränkung für dessen Übertragbarkeit auf natürliche Verhältnisse. In der Natur wird es sich in der Regel um dynamische Systeme handeln. Viele Untersuchungen wurden durchgeführt, um über Variationen der in der BGH Gleichung benutzten Bezugswasserspiegel und durch Differentialgleichungen die genaue Lage des Salzwasserkeils im Untergrund unter natürlichen Gegebenheiten zu berechnen (Cooper, 1959; Henry, 1959; Hubbert, 1953; Santing, 1963; Wooding, 1972). Das Ergebnis ist ein deutlich komplizierterer Zusammenhang, der in Abbildung 2 skizziert ist. Grundsätzlich lässt sich jedoch feststellen, dass schon bei einer kleinen Verringerung der Differenz zwischen Süß- und Salzwasserspiegel die theoretischen Grenzfläche deutlich (etwa um den 40fachen Betrag) Ansteigen wird. Durch Mischung des vordringenden Salzwassers mit Süßwasser aus unterschiedlich zugänglichen Porenräumen weitet sich die Übergangszone dabei auf. Der gleiche Prozess führt dazu, dass wieder vordringendes Süßwasser durch in den Porenräumen zurückbleibendes Salzwasser noch für lange Zeiten verunreinigt wird.

Neben den rein physikalischen Mischungseffekten kommt es bei der Verlagerung der Übergangszone auch zum Ablauf verschiedener chemischer Prozesse. Am schnellsten reagieren Kationen, die vor allem an der Oberfläche von Tonmineralen adsorbiert sind, auf den verändernden Lösungsinhalt, da die Bindung der Ionen an die Minerale relativ labil ist. Die Spezieszusammensetzung der adsorbierten Kationen ist abhängig von den Substrateigenschaften, sie steht jedoch immer im Gleichgewicht mit der gelösten Phase. Ändert sich die Zusammensetzung der gelösten Phase, so werden die gebundenen Kationen entsprechend des Gleichgewichts ausgetauscht.

$$CaX_2 + 2Na^+ \leftrightarrow 2NaX + 2Ca^{2+} \qquad (1)$$

Die in der Gleichung beschriebene Reaktion läuft bei einer Intrusion von Salzwasser in den Aquifer ab. Da Kalzium von Natrium als dominierendes Kation im Porenwasser abgelöst wird, erfolgt ein entsprechender Austausch von Kalzium mit Natrium an den Austauscherplätzen (X). Anionen sind von Austauscherprozessen kaum

betroffen. So kommt es bei der Salzwasserintrusion zur Bildung eines Übergangswassertyps, der durch die Ionen Ca^{2+} und Cl^- charakterisiert ist. Durch den umgekehrten Prozess ist der Übergangstyp bei einem Vordringen des Süßwassers durch Na^+ und HCO_3^- Ionen charakterisiert.

Langsamer als die Austauscherprozesse reagieren Mineralphasen auf die Konzentrationsänderungen im Grundwasser. Neben den Konzentrationsänderungen kann sich hier auch die erhöhte Ionenstärke des Salzwassers bemerkbar machen. Diese verursacht nach der Debeye-Hückel-Theorie aufgrund der elektrostatischen Abschirmung durch entgegengesetzt geladene Ionen in der Lösung eine verringerte Aktivität der Ionen. In einem Salzwasser mit hoher Ionenstärke kann daher eine größere Menge eines Minerals gelöst werden als in einer verdünnten Lösung.

Komplexer sind die Zusammenhänge für das Karbonatgleichgewicht. Bei der Verschiebung der Süß-Salzwassergrenze werden zwei Wässer gemischt, die sich beide, jedoch bei unterschiedlichen CO_2 Partialdrücken, im Kalk-Kohlensäure - Gleichgewicht befanden. Je nach Ausgangsbedingungen und Mischungsverhältnis kann es so zu einer Über- oder Untersättigung der Lösung in Bezug auf Kalziumkarbonat kommen. Weiterhin Einflüsse auf das Karbonatsystem haben:

- freigesetztes Kalzium aus möglichen Austauscherprozessen,
- eine erhöhte Magnesiumkonzentration im Meerwasser, die einerseits die $CaCO_3$ Fällung hemmt (Berner, 1975), andererseits zur Ausfällung von Dolomit führen kann,
- ein erhöhter Sulfatgehalt, der zu verstärktem Abbau organischer Substanz führen und so den CO_2 Partialdruck beeinflussen, aber auch Kalzium als Kalziumsulfat (Gips) binden kann.

Grundsätzliche Aussagen über den Ablauf der Lösungs-Fällungsreaktionen bei einer Salzwasserintrusion, wie dies bei den Austauscherprozessen möglich war, lassen sich daher nicht treffen. Dies wird auch in Fallstudien widergespiegelt, in denen Beispiele für die Lösung von Karbonaten (Zilberbrand et al., 2001), Dolomitisierung (Ward and Halley, 1985), Bildung von Karbonaten (Magaritz et al., 1980) oder die Bildung von Gips (Gomis-Yagües et al., 2000) beschieben sind.

Neben den Karbonaten kann die Stabilität von Tonmineralen von höherem Interesse sein, da diese wieder Einfluss auf zuvor beschriebene Prozesse haben.

Zum einen kann sich das Austauscherverhalten des Sediments verändern, wenn sich als Folge der Salzwasserintrusion die Tonmineralzusammensetzung ändert. Zum anderen kann ein erhöhter Salzgehalt ein Aufquellen der Tonminerale bewirken. Dies hat ebenso wie die mögliche Neubildung von Mineralphasen Auswirkungen auf die hydraulische Durchlässigkeit des Aquifers (Goldenberg et al., 1984; Sanford and Konikow, 1989). Neben dem erwähnten Effekt des Residualwassers kann so das Ausspülen von einmal eingedrungenem Salzwasser erheblich erschwert werden.

Die ersten Untersuchungen zur Intrusion von Meerwasser in Küstenaquifere wurden von Badon-Ghyben und Herzberg Ende des 19. Jahrhunderts an der Nordseeküste durchgeführt. Dort war die Problematik aufgrund der intensiven Drainage der Niederlande und des hohen Süßwasserbedarfs in den touristisch erschlossenen Nordseebädern von besonderem Interesse. Heute gibt es zahlreiche Beispiele weltweit für Salzwasserintrusionen in Folge von direkten menschlichen Eingriffen in das natürliche Gleichgewicht. Ursache ist der erhöhte Süßwasserbedarf in ariden Urlaubsregionen (z.B. Mallorca (Kent et al., 2002); Zanzibar (Gössling, 2001)) oder von Küstenmetropolen (z.B. Los Angeles, (Thomas et al., 2001); Tel Aviv, (Zilberbrand et al., 2001); Dakar, Hanoi, Alexandria, Toronto, Venedig (Timmermann and White, 1997)). Sollten die Prognosen eines in der Zukunft steigenden globalen Meeresspiegels (ICCP, 2001) zutreffen, wird die Wichtigkeit dieses Themas weiter zunehmen. Um solche Szenarien zu verhindern ist daher ein verantwortungsvolles Management der Ressource Grundwasser von hoher Bedeutung. Voraussetzung hierfür ist eine genaue Kenntnis der Verfügbarkeit, Qualität und Bewegung des Grundwassers, sowie deren steuernde Prozesse. Erst aufgrund ausreichender Systemkenntnisse lassen sich Fragestellungen, die für die zeitlich-räumliche Grundwasserveränderung und damit für die Grundwassernutzung erhebliche Bedeutung haben, erfolgreich bearbeiten. Ein wichtiges Managementwerkzeug hierfür sind Grundwassermodelle, mit denen sich die Veränderungen des Grundwassers für verschiedene Szenarien berechnen lassen. Für eine erfolgreiche rechnerische Simulation ist die Identifikation der bestimmenden Parameter, sowie des vorhandenen Ausgangszustands essentiell.

Das Institut für Geowissenschaftliche Gemeinschaftsaufgaben, Hannover (GGA-Institut) befasst sich in seinem Forschungsschwerpunkt Grundwasser mit dieser Thematik. Als Untersuchungsgebiet wurde ein Coastal Aquifer Test Field (CAT-Field) bestimmt, in dem umfangreiche interdisziplinäre Untersuchungen durchgeführt

werden. Bei dieser Forschungsarbeit kooperiert das GGA-Institut mit verschiedenen Forschungseinrichtungen Deutschlands. Aus einer solchen Kooperation mit der Universität Bremen entstand die vorliegende Arbeit.

Ziel des Forschungsschwerpunktes Grundwasser im GGA-Institut ist die Entwicklung eines hydrogeochemischen Transportmodells, das realistische Aussagen zur Grundwassergüteentwicklung unter verschiedenen Nutzungsszenarien im Untersuchungsgebiet ermöglichen soll. Die Aufgabe der vorliegenden Arbeit war es, einen Beitrag zur Charakterisierung geochemischer Prozesse und der Identifikation geochemischer Milieus im CAT-Field als Eingangsparameter für das Modell zu leisten.

Eine Voraussetzung für die chemische Charakterisierung eines Küstenaquifers im Raum ist eine ausreichende Anzahl von Probenahmestellen. Daher musste das GGA-Institut das vorhandene Netz von Grundwassermessstellen ergänzen. Eine Besonderheit war in diesem Bereich die Durchführung einer Forschungsbohrung bis in 120 m Tiefe. Noch während der Bohrarbeiten wurden zwei Pumptests im Bohrloch durchgeführt. Der Einsatz einer mit Indikator versetzten Bohrspülung ermöglichte zum einen die Bestimmung hydraulischer Parameter (Dispersionslänge und Fliessgeschwindigkeit) in einem Einlochpumptest. Zum anderen konnte das Grundwasser in verschiedenen Stockwerken chemisch beprobt und eine Kontamination durch die Bohrspülung quantifiziert werden. Die Durchführung der Pumptests und deren Interpretation hinsichtlich hydraulischer Parameter sind Inhalt des ersten Teils dieser Arbeit *„Mud Tracer Test While Drilling“*. Herr Dr. W. Kessels hat diesen Teil durch die physikalische Dateninterpretation und die Modellierung des Pumptests ergänzt, während Herr Dr. F. Binot die geologische Interpretation der Bohrung durchgeführt hat.

Das erweiterte Messstellennetz ermöglichte die Probenahme an 80 Positionen in unterschiedlichen Tiefen und Küstenabständen innerhalb des CAT-Fields. Die Ergebnisse dieser Beprobung und ihre Interpretation werden im zweiten Teil *„Hydrochemical Characterisation of a Coastal Aquifer Testfield at the German North Sea Coast“* präsentiert. Dabei kann die Position der Süß- Salzwasser Übergangszone im CAT-Field festgelegt, sowie ihre Mächtigkeit bestimmt werden. Bei der Betrachtung von Ionenverhältnissen zeigt sich, dass neben dem einfachen Mischen zweier Wassertypen komplexere geochemische Prozesse im Grundwasserkörper des CAT-

Fields ablaufen. So lassen erhöhte Calcium/Chlorid Verhältnisse eine Lösung von im Sediment vorhandenen Kalzit vermuten. Letztendlich lassen sich diese Prozesse jedoch nicht eindeutig anhand der Felddaten identifizieren. Eine genauere Untersuchung der in der Übergangszone ablaufenden Prozesse fand daher anhand von Laborversuchen und deren geochemischer Modellierung statt.

Ein erster Schritt war die Durchführung von Säulenversuchen, die im dritten Teil *„Experimental Determination of Geochemical Prozesses Occuring During the Salinisation of a Coastal Aquifer"* beschrieben ist. In Säulenversuchen wurde ein dynamisches Vorrücken des Salzwassers in den Aquifer, sowie der umgekehrte Prozess, dessen Verdrängung durch Süßwasser, simuliert. Hierbei handelt es sich um eine Verschiebung der Salz- Süßwassergrenze. Wie erläutert dominieren Austauscherprozesse in diesem Stadium den Chemismus des Wassers. Andere Prozesse, wie etwa die Anpassung der Mineralphasen an das neue Milieu durch Lösungs- und Fällungsprozesse, laufen langsamer ab. Um die Auswirkungen beider Reaktionsmechanismen auf das Porenwasser voneinander zu unterscheiden, wurden die Austauscherprozesse mit dem Programm PHREEQC rechnerisch modelliert. Unterschiede zwischen den experimentellen und den berechneten Konzentrationen wurden als Effekte der in der Rechnung nicht berücksichtigten langsameren Prozesse interpretiert.

Um die Lösungs- und Fällungsprozesse auch im Labormaßstab unter definierten Bedingungen zu untersuchen, wurde ein zweidimensionaler Versuchsaufbau entwickelt. Dieser ermöglicht die Simulation einer in der Lage statischen Süß- Salzwasser Übergangszone, die sich jedoch in einem dynamischen Gleichgewicht befindet. Die neu entwickelte 2D Fliesszelle repräsentiert einen Schnitt durch den Küstenaquifer vom Meer ins Landesinnere. Da die Fliesszelle zunächst nur mit einem Wassertyp gefüllt sein kann und sich erst langsam ein natürliches Gleichgewicht einstellt, dominieren in dieser ersten Phase des Versuchs wieder die zuvor geschilderten Austauscherprozesse. Eine zweidimensionale Betrachtung dieser Prozesse, wiederum im Vergleich mit theoretischen Daten, findet sich im vierten Teil der Arbeit *„Geochemical Prozesses in the Salt Fresh Water Transition Zone – Exchanger Prozesses in a 2D Sand Tank Experiment"*. Als Betreuer und Initiatoren der Arbeit sind hier Prof. Dr. H.D. Schulz und Dr. W. Kessels als Koautoren genannt.

Im letzten Teil *„Geochemical Processes in the Salt Fresh Water Transition Zone – Comparing Results of a Sand Tank Experiment with Field Data from the Coastal Aquifer Test Field at the German North Sea Coast"* werden die langsameren Prozesse wie der Abbau organischer Substanz und Lösungs- und Fällungsprozesse in dem genannten Beckenversuch betrachtet. Den Ergebnissen des Laborversuchs werden Daten der Feldmessungen gegenübergestellt. Verschiedene Prozesse, die in den unterschiedlichen Bereichen des Aquifers ablaufen, konnten so identifiziert werden. Die Ergebnisse verdeutlichen jedoch auch die Grenzen des gewählten Versuchsaufbaus, da die natürlichen Redoxverhältnisse nur ungenügend abgebildet werden konnten.

Die wichtigsten Ergebnisse der Arbeit werden im Anschluss zusammengefasst dargestellt. Neben den durch diese Arbeit gewonnenen Erkenntnissen über die geochemischen Verhältnisse im CAT-Field wurde ein zweidimensionales Verfahren zur Laborsimulation entwickelt. Im Rahmen der Untersuchungen ergaben sich ergänzende Fragestellungen und Untersuchungsmöglichkeiten. Diese wünschenswerten zukünftigen Forschungsaufgaben im Bereich der Süß- Salzwasser Übergangszone und die spezielle regionalen Situation im CAT-Field werden abschließend skizziert.

Literaturnachweis

Badon-Ghyben W. (1889) Nota in verband met de voorgenomen put boring nabij Amsterdam. *Tijdschrift van het koninklijk Instituut voor Ingenieurs*, 21.

Berner R. A. (1975) The role of magnesium in the crystal growth of calcite and aragonite from sea water. *Geochimica Cosmochimica Acta* **39**(4), 489-504.

Cooper H. H. (1959) A hypothesis concerning the dynamic balance of fresh water and salt water in a coastal aquifer. *Journal of Geophysical Research* **64**(4), 461-467.

Custodio E. and Bruggeman G. A. (1987) *Groundwater Problems in Coastal Areas*. UNESCO.

De Josselin de Jong G. and Van Duijn C. J. (1986) Transverse dispersion from an originally sharp fresh-salt interface caused by shear flow. *J. Hydrol.* **84**, 55-79.

Goldenberg L. C., Magaritz M., Amiel A. J., and Mandel S. (1984) Changes in hydraulic conductivity of laboratory sand-clay mixtures caused by a seawater-freshwater interface. *Journal of Hydrology* **70**, 329-336.

Gomis-Yagües V., Boluda-Botella N., and Ruiz-Beviá F. (2000) Gypsum Precipitation/Dissolution as an Explanation of the Decrease of Sulphate Concentration during Seawater Intrusion. *J. Hydr.* **228**, 48-55.

Gössling S. (2001) The consequences of tourism for sustainable water use on a tropical island: Zanzibar, Tansania. *Journal of Enviromental Management* **61**, 179-191.

Henry H. R. (1959) Salt Intrusion into Fresh-Water Aquifers. *Journal of Geophysical Research* **64**(11), 1911 -1919.

Herzberg A. (1901) Die Wasserversorgung einiger Nordseebäder. *J. Gasbeleucht. Wasserversorg.* **44**, 815-819.

Hubbert M. K. (1953) The theory of groundwater motion. *Journal of Geology* **48**(8), 785-944.

ICCP. (2001) Third Assessment Report - Climate Change 2001. Intergovernmental Panel on Climate Change (IPCC).

Kent M., Newnham R., and Essex S. (2002) Tourism and sustainable water supply in Mallorca: a geographical analysis. *Applied Geography* **22**, 351-374.

Kohout F. A. (1980) Differing Positions of Saline Interfaces in Aquifers and Observation Boreholes: comments. *Journal of Hydrology* **48**, 191-195.

Magaritz M., Goldenberg L., Kafri U., and Arad A. (1980) Dolomite formation in the seawater-freshwater interface. *Nature* **287**, 622-624.

Sanford W. E. and Konikow L. F. (1989) Simulation of Calcite Dissolution and Porosity Changes in Saltwater Mixing Zones in Coastal Aquifers. *Water Resouces Research* **25**(4), 655-667.

Santing G. (1963) Salt water-fresh water relationships. In *The Development of Groundwater Resources with Special Reference to Deltaic Areas*, Vol. 24 (ed. ECAFE-Unesco), pp. 52-63.

Thomas S. T., Liles M. J., and Johnson T. A. (2001) Managing Seawater Intrusion in the Dominguez Gap Area of Los Angeles Country, California, USA. *SWICA-M3 Saltwater Intrusion and Coastal Aquifers.*

Timmermann P. and White R. (1997) Megahydropolis: coastal cities in the context of global environmental change. *Global Environmental Change* **7**(3), 205-234.

Ward W. C. and Halley R. B. (1985) Dolomitization in a Mixing Zone of Near-Seawater Composition, Late Pleistocene, Northeastern Yucatan Peninsula. *J. of Sedimentary Petrology* **55**(3), 407-420.

WHO. (1971) Normes européennes applicables a l'eau de boisson (european standart for potable water), pp. 62. World Health Organisation.

Wooding R. A. (1972) Groundwater problems of the intreaction of saline and fresh water. In *Salinity and Water Use* (ed. A. Talsma and J. R. Phillip), pp. 125-139. Australian Academy of Sciences, MacMillan.

Zilberbrand M., Rosenthal E., and Shachnai E. (2001) Impact of urbanization on hydrochemical evolution of groundwater and on unsaturated-zone gas composition in the coastal city of Tel Aviv, Israel. *Journal of Contaminant Hydrology* **50**, 175-208.

TEIL I Mud Tracer Test During Soft Rock Drilling

Mud Tracer Test During Soft Rock Drilling

Panteleit, B., Kessels, W., Binot, F.
Leibnitz Institute for Applied Geosciences, Stilleweg 2, 30655 Hannover, Germany

Abstract

Information on aquifer transport properties and the hydraulic and geochemical groundwater and aquifer conditions is essential for the understanding of groundwater systems. The sampling of fluids in boreholes using pumping methods is common practise to determine the natural geochemical groundwater and aquifer conditions. In general, any contamination of the sampled groundwater by the drilling process, the borehole and the sampling method itself should be avoided. The invasion of drilling mud is of special interest for groundwater sampling during and immediately after drilling.

The research borehole Cuxhaven Lüdingworth 1 (CAT-LUD 1) was drilled and logged in 2001. Two pump tests at the drilling depths of 53 m and 87 m were carried out using a new test design. High quality coring for geochemical analysis was important to obtain maximum chemical information on the sediments in the salt-fresh water transition zone. Drilling mud intrudes into the aquifer during drilling. The use of a uranine tracer in the drilling mud allowed to control for possible contamination of the core material. Likewise the contamination of hydrochemical samples from pump tests can be determined by tracer measurements.

The uranine concentration of the pumped water was monitored during the experiments. The total fluid loss in the test interval, as calculated afterwards from the pump test results, was in good agreement with the values calculated by the drilling operator during the drilling process. The uranine concentration decreased to 1% in the drilling mud after 10 invasion volumes were recovered. During the recovery, the uranine concentration decreased exponentially with increasing recovery volume. The mud tracer test described here is equivalent to a push pull test.

The experimental results are compared to 2D numerical calculations using the finite element program FEFLOW (WASY, 2001). The calculated breakthrough curves were fitted to the pump test data by varying the dispersion length α, and the effective groundwater velocity v_a. The best results are achieved for a dispersion length of α = 0.02 m and an effective groundwater velocity of v_a= 0.28 m/d. Both values are in

good agreement with the scale of the experiment and other determinations of the groundwater velocity.

1. Introduction

1.1. Contamination during soft rock drilling

Drilling operations affect natural groundwater by mixing of drilling mud with the groundwater, and through secondary effects associated with a disturbance of the geochemical environment (redox conditions, concentrations of dissolved ions, temperature) (Kloppmann et al., 2001). The drilling mud is required to transport the cuttings out of the borehole and to avoid instability and erosion of the borehole (Kessels, 1989). Clay particles or similar additives of the drilling mud accumulate on the borehole wall and form a mud cake up to a thickness of several millimeters. The liquid phase of the drilling mud intrudes into the aquifer during this process. Finally the build up of a mud cake seals the borehole wall. Mud loss normally affects the most recently drilled part of the borehole where the mud cake has not yet fully developed. The physically complicated intrusion of drilling mud into the aquifer is controlled by the fluid pressure, circulation rate, viscosity and the mud cake. The intrusion process itself is not discussed here in any more detail because the mud intrusion volume can be derived from the pump test result itself.

The uranine mud tracer test procedure is comparable to a push pull test, where a determined mass of tracer is injected into the aquifer and pumped back later. Since the natural groundwater flow velocity is disturbed during this test by pumping, the tracer breakthrough curve cannot be evaluated as described e.g. by Schulz (1992a). Leap and Kaplan (1988) describe a push pull test to determine the groundwater flow rate. Fried (1975) derives the dispersion length from such test. Flow rate and dispersion length are the main parameters to describe the results of this mud tracer test. Schroth et al. (2001) discuss the influence of tracer retardation on the break-through curves during the withdrawal phase and provide a useful review of the push pull technique.

1.2. The use of tracers in drilling mud

The influence of the drilling mud on the groundwater hydrochemistry depends on the amount of mixing between the different fluids and the concentration gradient of a given chemical ion between the two fluids. If the concentration of a species is known

in each of the original fluids, it is possible to quantify the mixing ratio of the two solutions by the measurement of the particular species. This is the case for species which are present in the drilling mud but absent in the formation water and which are not involved in chemical or physical reactions i.e. ideal tracers.

Tracers can be applied in two different ways to obtain representative results of the in situ water geochemistry. With a series of on-site tracer measurements during pumping, the evolution of the tracer concentration can be observed. The pumping continues until the final sample is considered representative of the formation water. If the pumping cannot be continued until a sufficient quantity of water is extracted to eliminate the contamination, or the on-site measurement is not possible, the contamination of the final sample has to be determined. Different correction methods are described for this case (Kloppmann et al., 2001). The linear-regression-based correction method cannot be applied to pH and E_H, which are affected non-linearly by drilling mud contamination.

A general overview of tracers used in hydrogeology is given by Käss (1992). Potential tracers for drilling are environmental species such as NO_3^- or ^3H if the formation water is of deep and/or old origin and therefore free of these species. Other possible tracers are Br^-, I^-, organic ions or Li^+, the later was used e.g. by Bath et al. (1996) in the Sellafield area investigations. Fluorescent tracers have the great advantage of being relatively easy and quick to measure in the field. A frequently used UV-fluorescent tracer is uranine (Disodiumfluoresceine), which was applied in Äspö, Sweden (Nilsson, 1989; Smellie and Laaksoharju, 1992). Uranine has a very low detection limit and low costs.

Käss (1992) discusses in detail the behaviour of uranine in groundwater. Only some aspects that have to be taken into account for the field analysis will be discussed here. There are different opinions concerning the adsorbtion of uranine to clay minerals: whilst Keil (1959) and Prinz (1923) assume an adsorption onto clay, silt and marl, batch tests performed by Käss (1992) did not show any loss of uranine. Continuous control of the uranine concentration in a filtered sample of the drilling mud allows to account for a possible reduction of the effective concentration. Uranine molecules possibly adsorbed on clay minerals of the aquifer could be partly desorbed during the extraction of groundwater, resulting in higher uranine concentrations in the extracted water. This desoption leads to an overestimation of the true contamination level and is therefore not further considered.

The organic structure of uranine is sensitive to UV light. On-site measurement is therefore recommended (Haug, 1985). Similarly, strong oxidisers may be harmful to the uranine structure. Since groundwater generally does not have a high oxidation potential this should not cause any problems. The sensivity of uranine to high temperatures must be taken into account in deep wells and/or wells drilled in hard rock. In acidic water, uranine may change to the cationic form and become sorptive. This might give rise to problems in peat layers. But even though these exist at the drilling location, the tested horizons lie below them as indicated by the measured pH of 8.5. Some natural substances have a fluorescent behaviour similar to that of uranine. This effect is higher in sedimentary aquifers and clay-rich drilling muds than in hard rock aquifers. Because such effect is hard to quantify, it is sometimes ignored and consequently true contamination may be overestimated. Since the structure and therefore the fluorescence of uranine depend on the pH (Foerster, 1982), it is important for a comparative analysis that the pH of all samples is constant.

Despite these limitations, uranine is widely used in hydrogeology and delivers good results. A combination of tracers can be used for quality control. For example, a combination with another organic tracer was used in the NAGRA (Nationale Gesellschaft für die Lagerung radioaktiver Abfälle) deep drilling programme (Haug, 1985). Because thermal instability is a problem for all organic ions, this could be circumvented by a combination of fluorescent tracers and inorganic I^-, as used in a hard rock deep drilling programme in France (Kloppmann et al., 2001). Mikulla et al. (2002) is the only publication we are aware of that is presenting tracer data from a soft rock borehole. They used a combination of two different fluorescent tracers.

The tests presented here were performed in the fresh water and the salt water zone of a coastal aquifer. The water used for the preparation of the drilling mud has an intermediate salt concentration. Thus, in addition to the artificial fluorescent tracer, the salt concentration can be regarded as a second environmental tracer once the original electrical conductivity (EC) of the groundwater has been measured.

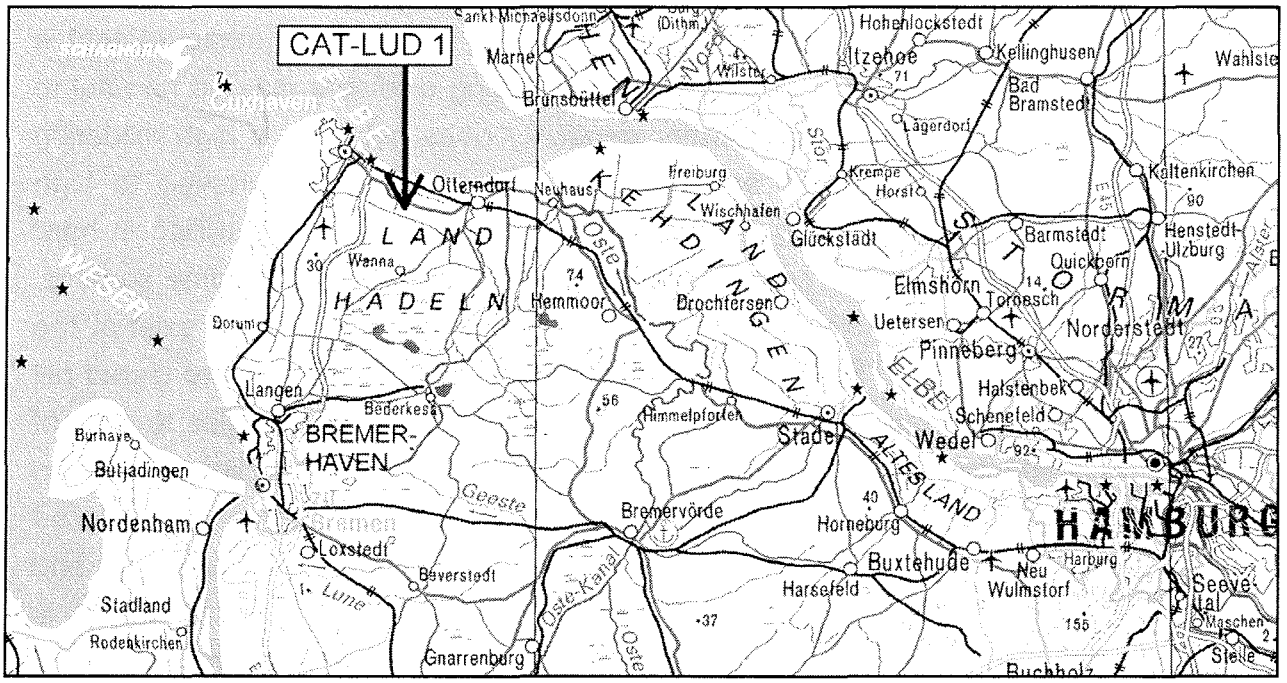

Figure 1: Geographic position of the scientific borehole CAT-LUD 1 at the German North Sea coast.

1.3. Site characterisation

The CAT-LUD 1 borehole examined in this study is a major well in the Coastal Aquifer Test Field (CAT-Field). Here the Leibnitz Institute for Applied Geosciences (GGA-Institute) examines the dynamics of the transition zone between salt and fresh water. The CAT-Field is bordered by the Elbe and Weser estuaries and the North Sea tidal flat coast. It is located between the coastal cities of Bremerhaven and Cuxhaven in the northwest of Germany (Fig.1).

The main hydrogeological horizon consists of Quaternary glacigene gravel and sand-rich onshore deposits. The sediments are remnants of the Elster and Saale glaciation. They are mostly characterised by a very good hydraulic permeability. At the well location itself this horizon is covered by 25 m of two interglacial transgressive tidal flat sediment sequences (Fig.2). These interfinger with muds of a brackish lagoonal type and with onshore peat deposits. The lower part of these covering sediments are Eemian in age, the upper part is Holocene in age. The Holocene sediments in this region are usually found beneath the flat marsh topography (Marsch). This sediment cover has poor to medium hydraulic permeability. Due to the fine grained material of the Holocene sediments and the extensive drainage for agricultural and land reclamation purposes, no recharge but upwelling groundwater is expected in the Marsch areas (Fulda, 2002).

Figure 2: the illustration presents a composition of 4 sections (from left to right): laterolog; cored sections (blocks) and pump test intervals; gamma ray log, geological profile.
Coincidence of the traces of deep (pink line in laterolog) and shallow (blue line) penetration resistance measurements in the borehole identify the transition zone from fresh to salt water.

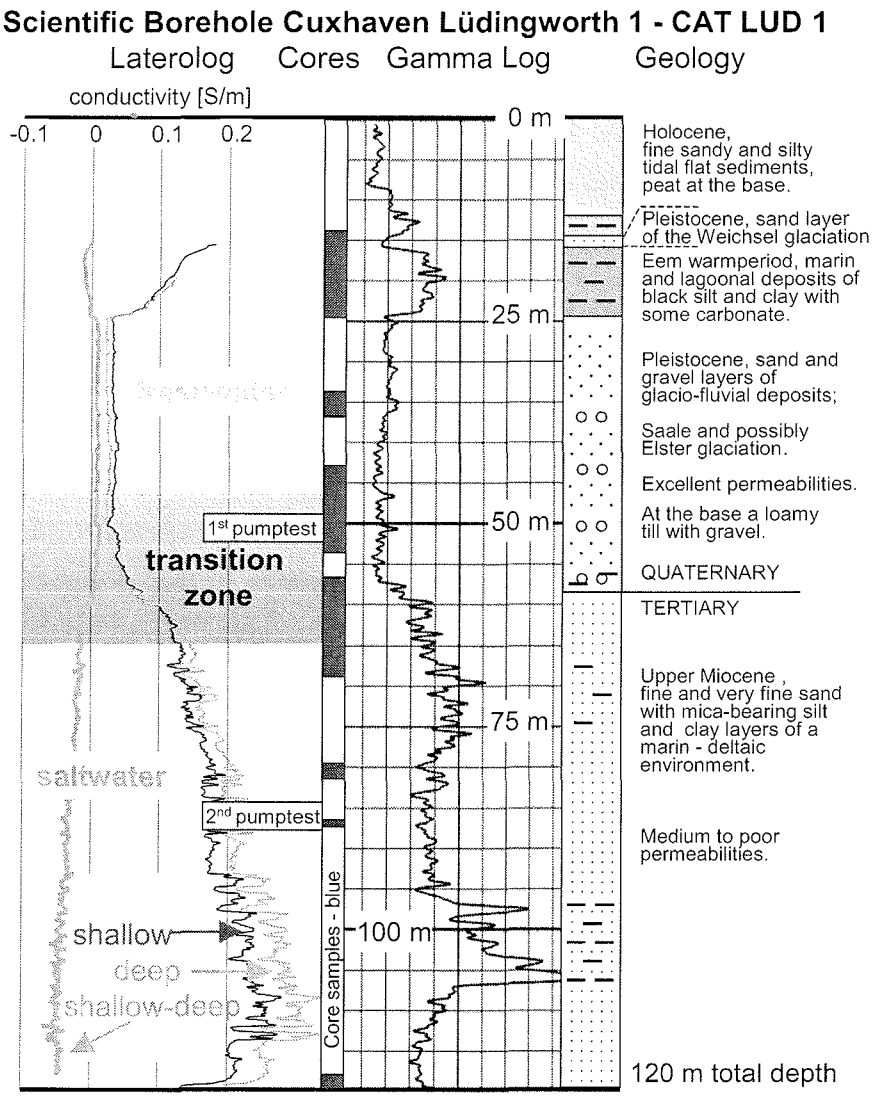

The glacigene sand-rich onshore deposits outcrop 3 - 4 km from the well and form slight ridges (Geest) of about 30 m hight, whereas the Marsch areas range in height from 1 m or less above NN. The Geest ridges are the most important groundwater recharge areas in the CAT-Field and must be considered as the motors of the hydraulic flow in the whole area.

Beneath the base of the glacigene gravel and sand-rich onshore deposits at a depth of 59 m, fine and very fine sands, silts and clays of the Upper Miocene are penetrated by the CAT-LUD 1 borehole (Fig.2). These sediments continue down to the total depth of 120 m. They are marine and deltaic in origin and are characterised by rather low permeabilities. Other boreholes in the neighbourhood and seismic data show that these and similar sediments continue down to more than 200 m.

Figure 2 presents the results of geophysical logging. A horizontal focussed conductivity measurement (laterolog (Serra, 1984)), consists of two different logs with

different penetrations depths (pink line and blue line). As the flushing water was taken from the transition zone, the salt-fresh water transition zone in the borehole can be determined by this method. This is the zone where the difference between both measurements (red line) is zero. At the depth of 58 m, conductivity of the used for the drilling mud in the borehole equals the groundwater conductivity.

The gamma ray log (Fig.2, black line) shows the natural gamma radiation of the rocks. Because natural gamma radiation is mainly associated with clay minerals, this log gives a good indication of the lithology. It therefore coincides with the independent sedimentary information from the cores. The low gamma ray values e.g. at the depth interval from 25 m to 55 m, correspond to the sand, coarse sand and gravel, whilst the Miocene clay layers in the deeper parts are marked by high gamma ray values.

Groundwater velocity in the completed well was measured using two different methods: observation of colloidal particle migration (Phrealog-method (Schöttler, 1997)) and spread of an injected salt tracer logged by multi-electrodes at the borehole wall (DMP-method (Kessels and Zoth, 1998)). At a depth of 86 m, the Phrealog method determined a velocity of 0.25 m/d (Schöttler, 2002), while the DMP method gives a higher velocity of 0.77 m/d (Kessels, 2002). The difference between the two velocities may be attributable to typical groundwater velocity determination problems as well as to artefacts caused by the well and density flow.

2. Methods

2.1. Drilling operations

Different drilling methods were used during the installation of the research borehole CAT-LUD 1. The first 12 m were cut with a diameter of 0.8 m. Below 10 m, the borehole has a diameter of 0.2 m. Between 10 m and 25 m no drilling mud was used for valve coring (10-13 m) and ram coring (13-25 m). From 25 m depth downwards, ram coring and flush drilling was alternated. The drilling operations started on 24.10.2001. The target depth of 120 m below surface was reached on 20.11.2001. The total length of core recovery was 40 m. Figure 2 shows the cored and the two pump test intervals. The well site became completed with the installation of the twin well CAT-LUD 1A in a distance of 3 meters. Both parallel wells were fitted with multiple filters down to the total depth of 120 m for further experiments not described

in this paper. The main reason for almost fully screening of the wells was the scientific requirement for future geophysical experiments.

To minimise the contamination of the groundwater by the drilling mud and to avoid pH effects on the tracer, water with a similar composition to the in situ water was used for the preparation of the drilling mud. This water originates from a well located 200 m from the drill site, that was screened between the depth of the two pump tests. The salt concentration of the drilling mud lies between that of the in situ water in the pump test horizons. The drilling mud had a specific electric conductivity of 5.6 mS/cm and a density of nearly 1010 kg/m³. The mud was conditioned using bentonite clay. To ensure the stability of the borehole, the bentonite content of the drilling mud was increased with depth. The total loss of fluid during the drilling of CAT-LUD 1 was 13.9 m^3. The drilling mud was spiked with uranine to measure the contamination associated with such loss. Traceing was done by adding a concentrated uranine solution to the drilling mud reservoir (8 m³). Because it is technically difficult to constantly maintain an exact tracer tracer concentration, the uranine concentration was held at a range of 5-10 ppm and permanently controlled during drilling.

2.2. Pump test operations

With regard to the borehole stability, classic test equipment such as straddle packer systems cannot be operated safely in the open hole section. For this reason

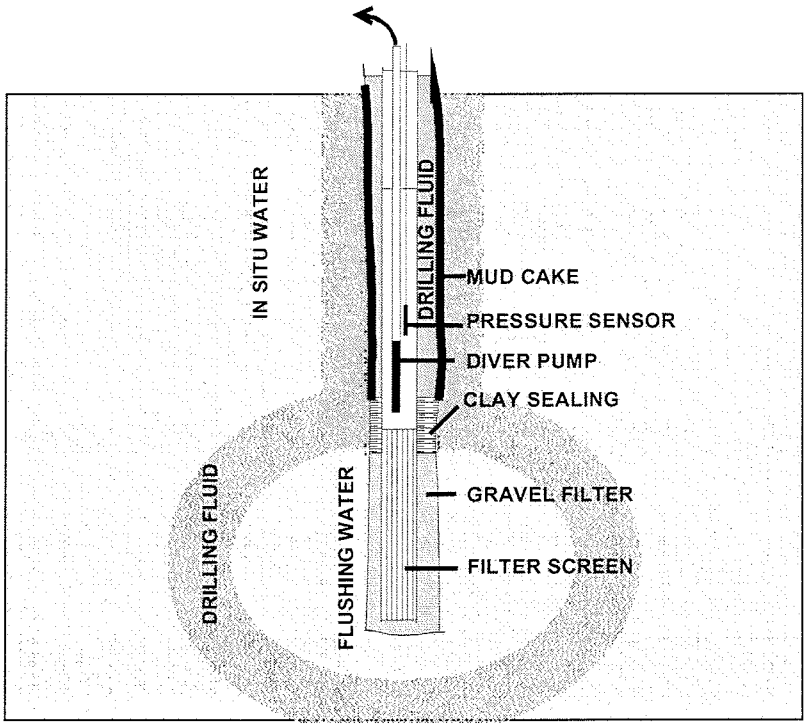

Figure 3: schematic test design (not to scale) for the pump tests performed during drilling of the borehole CAT-LUD 1

the new test design shown in Figure 3 was developed for sampling low contaminated groundwater while drilling through the Quaternary soft rock formation and to determine aquifer parameters.

The uranine mud tracer test discussed here can be divided into 3 test periods:

1 - uranine tracer injection into the test interval during drilling

2 - uranine tracer distribution by natural groundwater flow

3 - uranine tracer recovery by pumping

One important difference between push pull tests and the mud tracer test is the unspecific tracer injection quantity from fluid loss during drilling.

The first test was run at the beginning of the transition zone between salt and fresh water (51 m and 53 m depth, Fig.2). As outlined above, this zone appears to have relatively good hydraulic transmissivity. The deeper pumping test was performed at the depth interval from 85 m to 87 m.

To perform pump tests during drilling the drill strings were pulled out and a PVC filter with a 2 m screened zone (trench width 2 mm) was connected and installed at the base of the borehole. After installation of the filter, the clearance between the filter and the formation was filled with fine gravel over the whole filter length. The test interval was sealed from the upper, mud-filled borehole with a swelling clay, placed on top of the gravel (Fig.3). The proper performance of the clay seal was confirmed

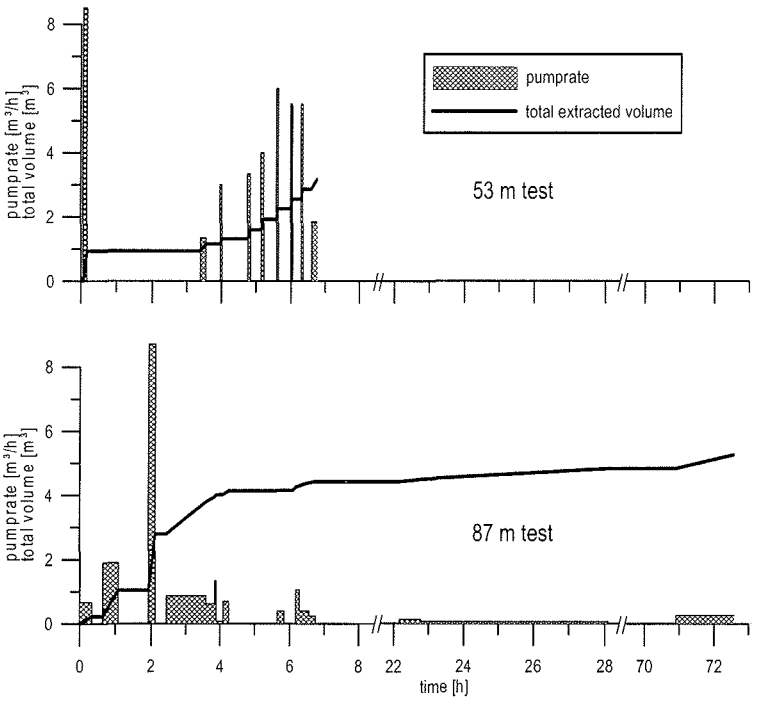

Figure 4: pump rate and cumulated extracted volume over time for the pump tests performed during drilling the borehole CAT-LUD 1

during the pumping tests by continuous measurements of the stable position of the water level in the drilling clearence.

24 hours after the end of the drilling operations, the filter zone was flushed to remove the mud cake from the borehole wall. The flushing water came from the same source as the drilling mud water but no bentonite and uranine were added. The pumping test started about 24 hours after flushing the filter zone.

The pump tests were performed using a submersible pump (Grundfos SP14A). No continuous pumping was possible because, in spite of the flushing, mud cake still effectively sealed parts of the test interval. Furthermore, the presence of fine sediments in the test interval limited the productivity of the test horizon. As a consequence, the tests were performed in a series of pumping cycles using different pumping rates (Fig.4). The pumping cycles were performed until the concentration of uranine in the extracted water was below the maximum target concentration of 1% of the injected concentration. This occurred after the extraction of 3.05 m^3 over a period lasting almost 7 hours during the 53 m test. For the deeper pumping test, it was necessary to continue the pumping cycles for more than 72 hours. The total extraction volume was 3.63 m^3 (Fig.4).

2.3. Sampling and Analysis

For the permanent control of the uranine concentration in the drilling mud, samples were taken periodically from the tanks of the borehole injection fluid. To remove clay particles, the samples were passed through a 45 µm cellulose filter. The uranine fluorescence at a wave length of 513 nm was measured with a Perkin Elmer LS-5B fluorescence spectrometer. The excitement wavelength was 485 nm, which showed maximum fluorescence. During the pump tests, samples were taken from the extracted water at the end of each pumping cycle and treated in the same way. The sensitive parameters (pH, E_H, electrical conductivity (EC) and O_2 saturation) were permanently measured in a flow chamber during the pumping cycles. The target concentration for hydrochemical sampling was determined at 1% drilling mud in the extracted groundwater. Upon reaching this target uranine concentration, samples were taken for different purposes. For geochemical analysis, the samples were filtered at 45 µm and acidified with HNO_3 for cation analysis. Untreated samples were stored at 3 °C for the subsequent analysis of anions and nutrients. Alkalinity was also determined in the field by titration with HCl (Cook and Miles, 1980).

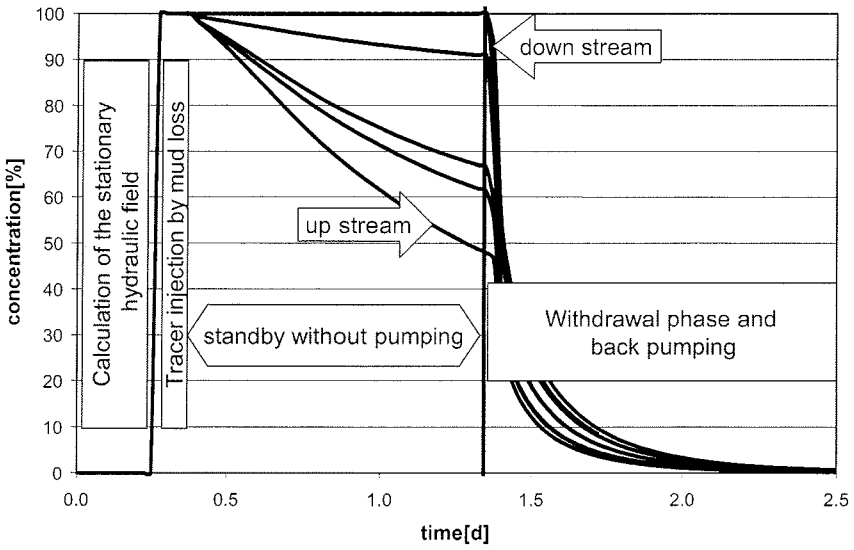

Figure 5: pump operation phases for the mud tracer test with calculated concentrations in back pumped water around the borehole. Calculated for v_a= 0.28 m/d.

2.4. Numerical calculations

To understand the invasion process, numerical calculations were carried out with the finite element program FEFLOW (WASY, 2001). The 2D model consists of a horizontal square mesh of 4 m side length. The well is located in the centre of the model area and has a diameter of 0.1 m. The mesh consists of 19141 nodes and 37720 three-noded triangular elements, while the central square meter is mesh refined. Coupled hydraulic and tracer transport is calculated with a uniform hydraulic conductivity of k= 10^{-4} m/s. Time-dependent concentrations in the well are collected during each run using the mean value from eight observation points around the borehole. For the borehole wall, a time-dependent flow and tracer mass boundary is set to calculate the different drilling and pumping operations (Fig.5). For the outer hydraulic boundary, a constant hydraulic head is set and adapted to the different groundwater flow scenarios. During the injection phase, a constant tracer concentration of 100 g/m^3 is used, while the concentration is set to zero for the outer boundary. Sensitivity tests regarding the model size show no significant influence by the outer tracer mass boundary on the pumped concentrations.

3. Results and Discussion

3.1. Experimental breakthrough curves

In Figure 6, the uranine breakthrough curve is displayed against the total pumped volume for the 53 m pumping test (above) and the 87 m pumping test (below). The figure shows the uranine concentration related to the initial mud concentration and the EC of the recovery water. At the beginning of both tests, the delivered water was

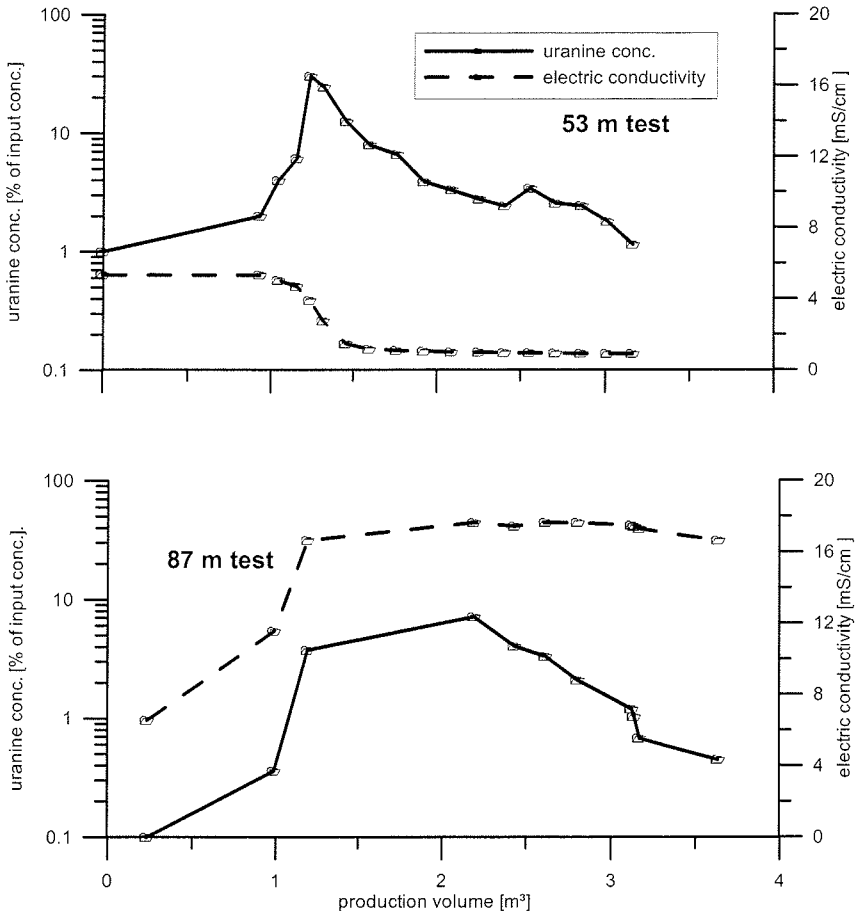

Figure 6: breakthrough of the uranine concentration and electric conductivity with progressing pump tests performed during drilling of the borehole CAT-LUD 1

characterised by a low uranine concentration and an EC of about 5.5 mS/cm. After this initial stage, the behaviour changed in both tests corresponding to the different hydraulic permeabilities of the formation and the different test schedules: In the shallow 53 m test, the uranine concentration rises to a maximum of about 30% of the drilling mud concentration after approximately 1.15 m^3 water was extracted. Synchronous with the maximum uranine concentration, the EC drops rapidly to a value of about 1 mS/cm. After this steep change, the EC stayed constant, while the uranine concentration decreased slowly to the target value of 1%, where the test was terminated. This target concentration was reached after the extraction of another 2 m^3 after the maximum uranine concentration was reached. For this 53 m test interval, a mud loss of 1 m^3 during the last 5 m of drilling was reported by the drilling operator.

For the deeper, 87 m pumping test, the maximum uranine concentration reached about 7% of the original concentration and was measured after the extraction of 2.2 m^3 water. The effective maximum concentration seems to be higher but might be undetected during sampling because of the major change in the delivery volume (Fig.4). However, the maximum concentration is reached later than in the upper test. Instead of a decrease of the EC corresponding to the point of the highest tracer

concentration, a rise to the final stable value of 17.4 mS/cm was observed during the deeper pump test. The following decrease of the uranine concentration down to the target value occurred within the following 68 hours, during which another 1.4 m^3 water were extracted. The decrease in uranine concentration from the maximum value down to the target value was thus steeper with respect to the extraction volume than in the upper test. Similar to the shallow test, 0.2 m^3 of drilling mud were lost in the last meter above the 87 m test interval.

3.2. Specific mud loss derived from the breakthrough curves

In contrast to the push pull test, the mud tracer test requires the determination of the fluid loss. In addition to measurements made while drilling, the fluid loss can be obtained from the breakthrough curves of the tracer during the test. The uranine concentration during the pump test shows a exponential decrease over the production volume (Fig.6). For low groundwater flow velocities, this is in good agreement with the numerical results shown in the next chapter. The theoretical uranine concentration in the pumped groundwater is shown in Figure 7. For a piston flow model (no dispersion) the sharp tracer front results in a rectangular concentration function. The total tracer mass can be derived by the integration of the rectangle. The rectangular piston flow function is smoothed (Fig.7, left) if dispersion and a slow groundwater flow rate are also considered. To estimate the total extracted tracer mass *m*, the integration over the withdrawn volume is divided into piston flow and an exponential decrease (eq.1):

$$m = \int_0^\infty C(V)\,dV = m_{piston} + m_{\ln} \qquad (1)$$

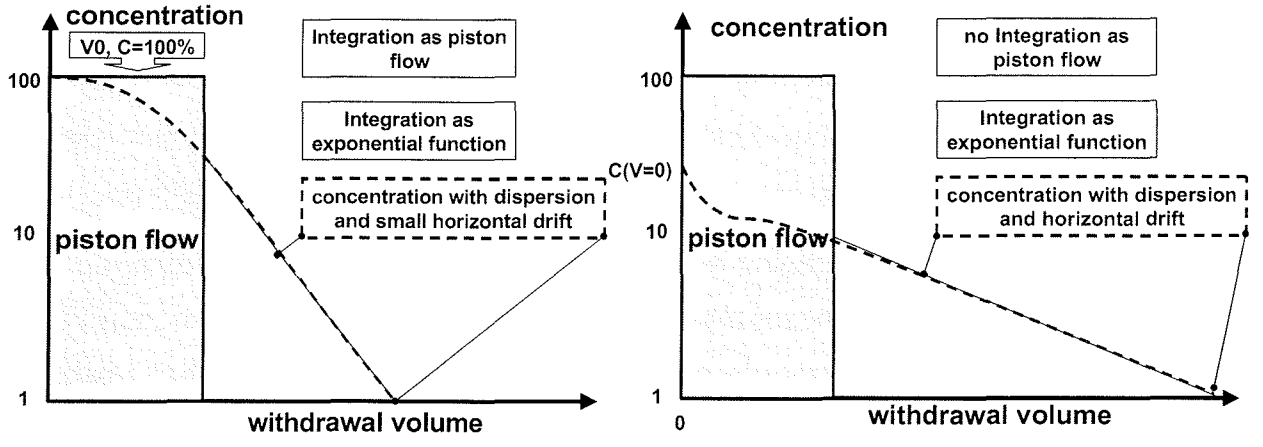

Figure 7: theoretical tracer concentration during a push pull test

A higher groundwater flow rate and a time delay between injection and withdrawal delivers an exponentially decreasing concentration function (Fig.7, right). Consequently, the uranine concentration *C* as a function of the production volume *V* and the dispersion length α is given by equation 2, where C(0) is the concentration at the start of pumping.

$$C(V) = C(0) \cdot e^{-\alpha V} \tag{2}$$

The total tracer mass *m* lost in the filtered borehole section can then be calculated by integration over an infinite production volume (eq.3).

$$m_{\ln} = \int_0^\infty C(V)dV = C(0) \cdot \int_0^\infty e^{-\alpha V} dV = \frac{C(0)}{\alpha} \tag{3}$$

This model is restricted to low groundwater velocities, as the injected tracer plume should not be moved far away from the hole. Also, for very low concentrations (below 1% of the initial tracer concentration) the validity of this rough calculation is no longer given.

Because these equations are only an approximation, their validity is evaluated by the numerical results given in the next chapter. The results of the integration method are given for different combinations of α and v_a compared to the calculated results of the FEFLOW (WASY, 2001) model (Tab.1). The error is in the range 20% to 30%. The method fails only if the tracer plume is moved too far away from the borehole. This is reflected in the calculation results with a groundwater velocity of 1.12 m/d, where the difference between the methods is about 88%.

The time-dependent tracer recovery for the different combinations of α and v_a are displayed in Figure 8. According to the nearly exponential function, over 90% of the injected tracer mass is recovered with the first 1 to 2 m^3 of produced water if the groundwater velocity and the standby time between injection and withdrawal are small enough. For higher groundwater velocities, i.e. greater than 0.5 m/d, the pump volume applied here is too low for full recovery of the tracer after transport during the standby time (Fig.8). Similarly, full recovery becomes impossible if the tracer plume is

dispersion length [m]	0.01	0.04	0.08	0.16	0.02	0.02	0.02	0.02
pore velocity [m/d]	0	0	0	0	0.07	0.28	0.56	1.12
estimated extr. mass / calculated inj. mass	1.12	1.23	1.25	0.89	1.19	1.16	1.07	0.12

Table 1: comparison of the extracted tracer mass from integration of equation 3 with the extracted tracer mass calculated by a finite element model, for different scenarios of dispersion length and groundwater velocity.

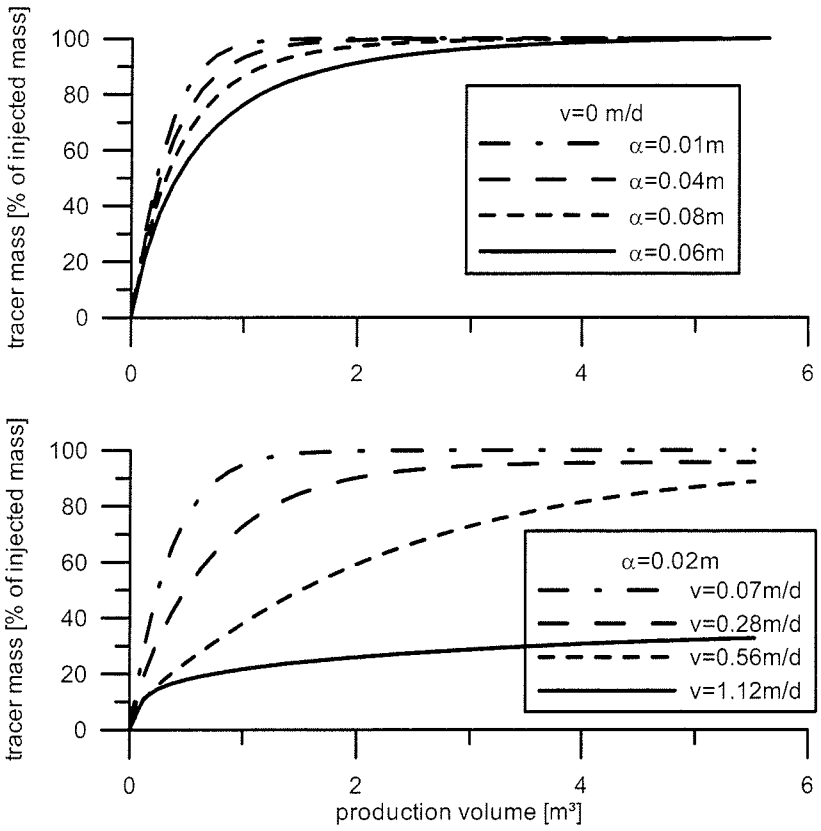

Figure 8: time dependent tracer recovery calculated from the integration of equation 3 for different combinations of dispersion length (α) and pore velocity (V). Full recovery becomes impossible for higher V, because the tracer plume is moved to far away from the borehole.

moved too far during the standby time to reverse the natural groundwater velocity through the pump rate. The total extracted tracer mass was calculated using the previously discussed method. The measured concentration, and the best fit line for both tests are shown in Figure 9.

The 53 m test shows a high derivation from the calculated straight line, while the 87 m test corresponds better with the assumed exponential decrease (Fig.9). The parameter for the best fit function and the derived uranine mass are shown in Table 2. Because the time schedule and the mud conditions during drilling were very

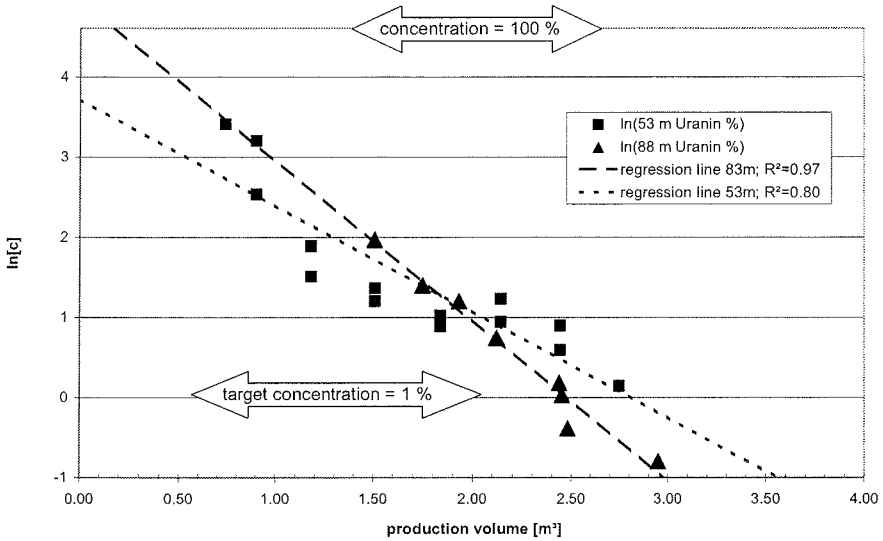

Figure 9: measured concentration and best linear fit to the data to be used for integrating the tracer mass

pump test		53 m	87 m
log regression parameter	A	3.71	4.95
ln(C)=A+B*V	B	-1.33	-2.00
theoretical initial exponential concentration	C(0) [%]	41.05	141.67
theoretical injection volume	V(100)[m³]	-0.67	0.17
piston phase concentration	tracer mass [%m³]	0.00	0.02
exponential phase concentration	tracer mass [%m³]	30.96	49.97
injected tracer mass during experiment	[g]	2.94	4.75
experimental initial uranine concentration	[ppm]	9.5	9.5

Table 2: theoretical result from integration of the uranine breakthrough curves

similar in both tests, the differences must be explained by different aquifer transmissivities and mud pressure conditions during drilling: On the one hand, the geophysical investigations and sedimentary analysis of the cores show a higher clay content which most probably influences the hydraulic conductivity in the 87 m test interval. This should reduce the invasion of drilling mud. On the other hand, the higher mud density gives rise to a higher overpressure during drilling in the deeper test interval, resulting in increased fluid invasion. Because the calculated uranine loss in the deeper test interval is higher, the overpressure must be the dominant factor for mud intrusion rather than the lower permeability of sediment layers.

The higher permeability in the 51 m to 53 m test interval causes a higher groundwater velocity. Consequently, the tracer has to be pumped back from a greater distance. This is in agreement with the lower slope of the concentration curve in Figure 9. The influence of groundwater velocity and dispersion length is discussed in the next chapter based on numerical calculations. With the initial uranine concentration, a fluid loss of 0.15 m^3/m is calculated for the 53 m test and 0.25 m^3/m for the 87 m test can be calculated. This correlates well with the mean fluid loss of 0.20 m^3/m reported by the drilling operator for this drilling depth. The fact that the fluid loss was about the same at each of the two test intervals during drilling supports the assumption that the loss only occurred in the deepest part of the borehole. Otherwise, the larger borehole wall surface should result in an increasing loss with increasing depth of the borehole.

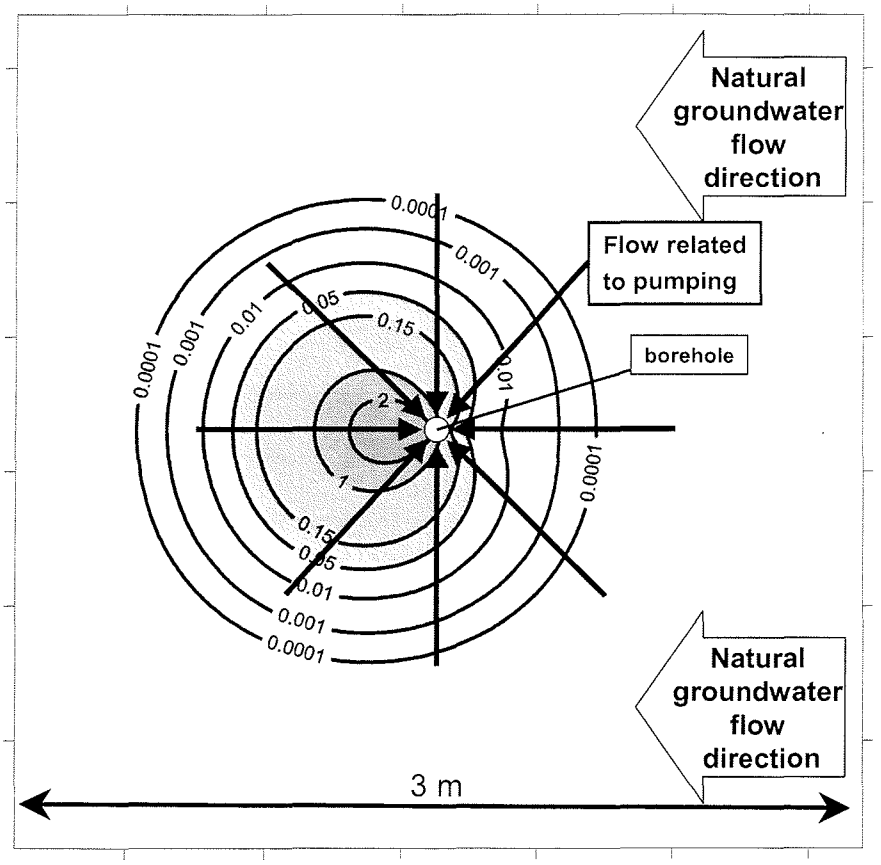

Figure 10: tracer cloud around the borehole six hours after the start of back pumping as calculated by a finite element model. (v_a= 0.28 m/d). Isolines indicate uranine concentrations

3.3. Numerical calculations

In a first calculation phase (Fig.5) the stationary hydraulic flow field around the borehole is calculated (Drost et al., 1968). The second phase represents the tracer injection and is followed by the standby time. During the standby time, the tracer plume is moved away from the borehole with the groundwater flow. Through the last phase the tracer is pumped back. Figure 10 shows the tracer concentration around the borehole 6 hours after the start of back pumping. The following calculations are run with 53 m test data. The measured concentrations of this test are plotted together with the calculated curves for different scenarios (Fig.11-13).

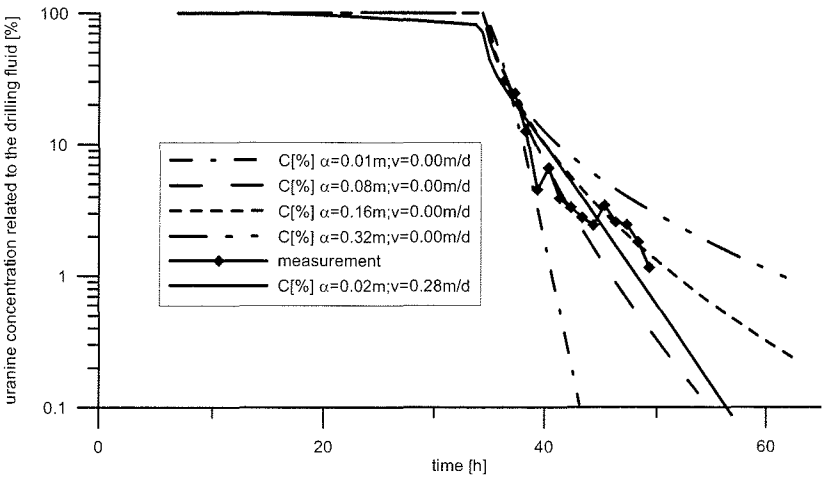

Figure 11: modeled uranine decrease during the 53 m pump test for different dispersion lengths assuming no groundwater flow, compared to measured data. For comparison the final choice of best fit is also shown (solid line)

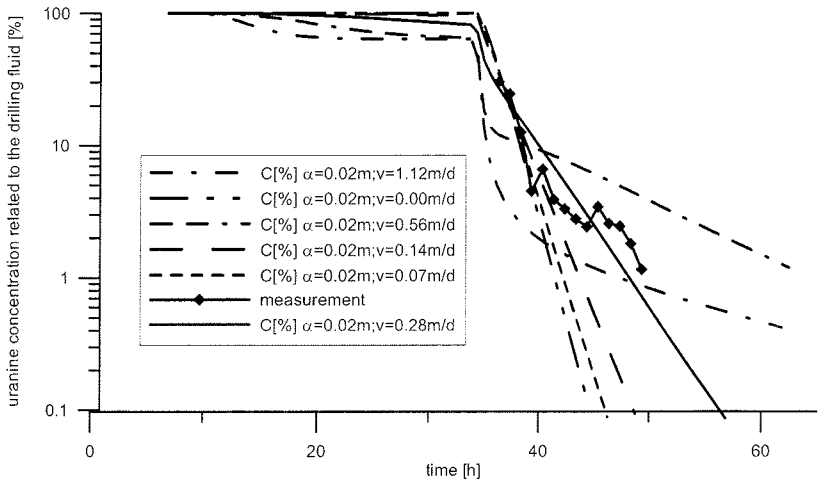

Figure 12: modeled uranine decrease during the 53 m pump test for different groundwater velocities compared to measured data. The final choice of best fit is also shown (solid line)

In a first step, the sensitivity with respect to the aquifer dispersivity is tested. The increase in the dispersion length results in a shorter slope of the concentration curve (Fig.11). With decreasing dispersion length, the concentration curve approaches a vertical line, which would result without dispersion (α=0.0 m). This is the case for the theoretical piston flow model. However, in the finite element program, numerical dispersion is always present (Diersch, 1998). As shown in Figure 8, the approximation of an exponential decrease of the tracer concentration becomes weaker for greater dispersion lengths and with shorter pumping times.

The best fit of the measured data is reached using a dispersion length between α=0.08 m and α=0.16 m. This value lies in the upper range compared to values from the literature (Kinzelbach and Rausch, 1995; Klotz, 1973; Schulz, 1992b). These studies show that a dispersion length of α=0.02 m can be expected for a scale length of 1 m. For comparison, the final choice of best fit is also presented in Figure 11.

Figure 12 shows the effect of groundwater velocity variation for a dispersion length of α=0.02 m. The steep decrease in the tracer concentration with a large groundwater velocity is caused by the rapid movement of the tracer plume during the standby phase. As a result of the plume migration the borehole is located at the margin of the tracer plume at the start of back pumping. Again, the strongly nonlinear results for higher groundwater velocities v_a=1.12 m/d and v_a=0.56 m/d demonstrate the limits of the exponential concentration decrease model. The best match to the measured data is reached using a groundwater velocity of v_a=0.28 m/d. This correlates well with the groundwater velocities measured with the phrealog system (Schöttler, 2002) and the multi-electrode double-wall packer (Kessels, 2002).

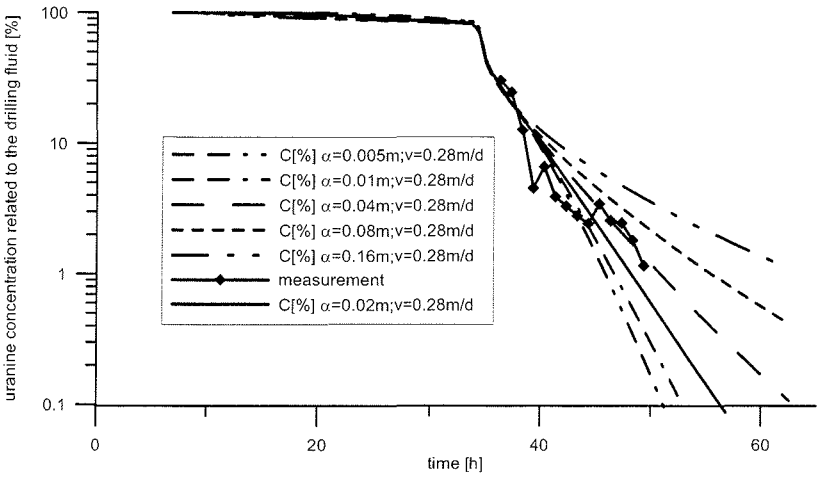

Figure 13: modeled uranine decrease during the 53 m pump test for different dispersion lengths, using the "best fit" groundwater velocity of v_a= 0.28 m/d together with measured data. The combination of α=0.02 m and v_a=0.28 m/d shows the lowest standard deviation of the calculated curves

Finally, different scenarios using the best fit groundwater velocity of 0.28 m/d are calculated. Figure 13 presents the results of these calculations, showing a good fit of the reasonable combination of α=0.02 m and v_a=0.28 m/d.

4. Conclusions

The use of uranine as a tracer in pumping tests during drilling proved to be a sensitive method for the determination of the contamination of the groundwater with drilling mud. The tracer method allows to detect even small amounts of drilling mud in the extracted water. Standard hydrochemical analysis methods do not identify such small hydrochemical differences between drilling mud and groundwater.

The constant rate of mud loss as borehole depth increases and the derived mud loss from a separate test interval reveal that the mud loss during drilling is mainly attributable to the freshly drilled borehole section. The mud recovery during the pump test can be quantified, in addition to groundwater velocity and dispersion length, if the mud is spiked with a tracer and data integration of the tracer breakthrough curves is applied as shown here. A proper quantification of the mud loss volume during drilling the test interval is essential.

A new and cheap way for the stepwise testing and sampling of a sedimentary aquifer at different depths was presented. Hydraulic tests are performed in the deepest (most recently drilled part) of the borehole after the section is isolated from the upper layers through a clay seal. The presented technique reduces problems common to open hole testing that are associated with borehole instability, and avoids hydraulic short cuts behind the casing or in long filter screens connecting discrete aquifers. In addition to the technical advantages, the test described here also

provides information on dispersion length and groundwater velocity of the local flow field if it is combined with a finite element model.

Acknowledgment

The authors would like to thank Mr. Tran Vied for his specification during the tendering procedure and the crew of the drilling company "Bohr und Brunnenbau Steden" for their support and good work. Haifa Rifai from the GGA-Institute and Thomas Hammerich from the University of Bremen are thanked for their support during analysis and measurements at the drilling location.

References

Bath A. H., McCartney R. A., Richards H. G., Metcalfe R., and Crawford M. B. (1996) Groundwater chemistry in the Sellafield area: a preliminary interpretation. *Quarterly Journal of Engineering Geology* **29**, 39-57.

Cook J. M. and Miles D. L. (1980) *Methods for the chemical analysis of groundwater.* Reports of the Institute of Geological Sciences, Hydrogeology Unit.

Diersch H. J. (1998) Interactive, Graphics Based Finite Element Simulation System FEFLOW for Modeling Groundwater Flow Contaminant Mass and Heat Transport.

Drost W., Klotz D., Koch A., Moser H., Neumaier F., and Rauer W. (1968) Point Dilution Method of Investigating Ground Water Flow by Means of Radioisotopes. *Water Resouces Research* **4**(1), 125-146.

Foerster T. (1982) *Fluoreszenz organischer Verbindungen.*315 pp Vandenhoeck & Ruprecht, ISBN: 3525423128.

Fried J. J. (1975) *Groundwater Pollution Theory, Methodology, Modelling and Practical Rules.* 346 pp, Elsevier, ISBN: 0444413162.

Fulda C. (2002) Numerische Studie zur Salz-/Süßwasserverteilung im Rahmen der Cuxhavener Forschungsbohrung. *Mitteilungen der Deutschen Geophysikalischen Gesellschaft* **Sonderband II**, 10-26.

Haug A. (1985) Feldmethoden zur Grundwasserentnahme aus Tiefbohrungen und zur Hydrochemischen Überwachung der Bohrspülung, pp. 71. NAGRA.

Käss W. (1992) *Geohydrologische Markierungstechnik.* Gebr. Bornträger. ISBN: 344301013X

Keil K. (1959) *Ingenieurgeologie und Geotechnik.*1065 pp, Knapp; ISBN B0000BK1VH

Kessels W. (1989) Observation and interpretation of time-dependent behaviour of borehole stability in the Continental Deep Drilling pilot borehole. *Scientific Drilling* **1**, 127-134.

Kessels W. (2002) Multi Electrode Geoelectric on the Borehole Wall- Determination of Groundwater Velocity and Dispersion Parameters. *AGU Spring Meeting.*

Kessels W. and Zoth G. (1998) Doppelmantel - Packers mit geoelektrischer Meßtechnik zur Bestimmung der Abstandsgeschwindigkeit des Grundwassers. In *Patent Az:19855048.0.*

Kinzelbach W. and Rausch R. (1995) *Grundwassermodellierung - Eine Einführung mit Übungen.* Gebr. Bornträger, ISBN 3443010326.

Kloppmann W., Matray J. M., and Aranyossy J. F. (2001) Contamination of deep formation waters by drilling fluids: correction of the chemical and isotopic composition and evaluation of errors. *Applied Geochemistry* **16**, 1083-1096.

Klotz D. (1973) Untersuchungen zur Dispersion in porösen Medien. *Zeitschrift der deutschen Geologischen Gesellschaft* **124**, 35-39.

Leap D. I. and Kaplan P. G. (1988) A Single-Well Tracing Method for Estimating Regional Advective Velocity in a Confined Aquifer: Theory and Preliminary Laboratory Verification. *Water Resources Research* **24**(7), 993-998.

Mikulla C., Büttner G., Fleischmann F., Fritzer T., and Wrobel J.-P. (2002) Forschungsbohrung Altdorf bei Landshut/Niederbayern - Repräsentative Grundwasserbeprobung von Lockergesteinsaquiferen im Zuge einer Kernbohrung. *Grundwasser* **7**(1), 25-30.

Nilsson A.-C. (1989) Chemical Characterisation of Deep Groundwater on Äspö, pp. 11. Royal Institute of Technology.

Prinz E. (1923) *Handbuch der Hydrogeologie*. Springer.

Schöttler M. (1997) Meßbarkeit der Grundwasserbewegung durch Visualisierung der Strömung in Bohrbrunnen. Dissertation, Universität Köln.

Schöttler M. (2002) Grundwasser Strömungsmessungen in den Forschungsbohrungen LUD1 und LUD1A in Cuxhaven Lüdingworth. Leibnitz Institute for Applied Geosciences.

Schroth M. H., Istok J. D., and Haggerty R. (2001) In Situ Evaluation of Solute Retardation Using Single-Well Push-Pull Tests. *Advances in Water Resources* **24**, 105-117.

Schulz H. D. (1992a) Auswertung von Durchgangskurven. In *Geohydrologische Markierungstechnik*, Vol. 9 (ed. W. Käss), pp. 347-355. Gebr. Bornträger.

Schulz H. D. (1992b) Physikalische Grundlagen des Stofftransports im Untergrund. In *Geohydrologische Markierungstechnik* (ed. W. Käss), pp. 325-337. Gebr. Bornträger.

Serra O. (1984) The Laterologs - LL. In *Fundamentals of well-log interpretation*, Vol. 1, pp. 64-76. Elsevier.

Smellie J. and Laaksoharju M. (1992) The Äpsö Hard Rock Laboratory: Final evaluation of the hydrogeochemical pre-investigations in relation to existing geologic and hydraulic conditions, pp. 239. Svensk Kärnbränslehantering AB.

WASY. (2001) FEFLOW 4.9. Finite Element Subsurface Flow & Transport Simulation System, Institute for Water Resources and Systems Research, Berlin, Germany.

TEIL II Hydrochemical Characterisation of a Coastal Aquifer Test Field at the German North Sea Coast

Hydrochemical Characterisation of a Coastal Aquifer Test Field at the German North Sea Coast

Panteleit, B.

Abstract

A Coastal Aquifer Test Field (CAT-Field) was established at the German North Sea coast with the aim to develop a numerical flow and transport model for a representative coastal aquifer. As an important input to the model the present day geochemical system was investigated. Groundwater samples were taken from a network of wells, screened in depths between 5 and 190 m. Geochemical data were used to determine the position of the transition zone from fresh to seawater, and to proof the marine origin of the salinisation. Ion chloride ratios of Li^+, Fe^{2+}, Ca^{2+}, Sr^{2+} and Mn^{2+} show evidences of interactions with the solid phase besides conservative mixing of the two water types.

1. Introduction

1.1. Motivation

The Coastal Aquifer Test Field is a representative region for the continental European North Sea coast. It is located in the north of Germany in the vicinity of the city of Cuxhaven, bordered by the estuaries of the rivers Weser and Elbe (Fig.1). Intense interdisciplinary research was performed and is planned to study the groundwater dynamics in the CAT-Field area (Friedhoff, 2001; Fulda et al., 2001; Kessels et al., 2000; Kessels et al., 2001; Siemon et al., 2001; Wagenschein, 2002; Willert et al., 2001). Aim is the numerical simulation of flow and transport in the multi layered aquifer system for different scenarios of large area salt water intrusions (Gräsle et al., 2001). Essential for the simulation of future scenarios is the understanding of the present day situation of the hydraulic and geochemical system in the CAT-Field. While hydraulic data and first modeling results are published by Fulda (2002) this paper focuses on the geochemical situation.

1.2. Geological site description

In the studied area permian salt structures are present in the subsurface beneath 900 m below sea level (bsl), their position and depth are well known from

hydrocarbon exploration (Baldschuhn, 2000). The evaporitic layers are overlain by cretaceous clay, marl and chalk sediments and – much more important for the hydrogeologic understanding – by some hundred meters of eocene clays. In places the transgression of the Oligocene is preserved and represented by a few meters of marine clays.

Transgressive Miocene covers the eocene and/or oligocene clays in about 200 m – 350 m bsl. Fine sands and silts of a marine, prodelta and deltaic-fluviatile regime are characteristic sediments of the miocene to upper pliocene deposits. Some re- and transgressive stages, additionally influenced complicated by salt movement in the subsurface, can be determined (Kuster, 1989). A speciality of the pliocene sequence is the presence of heavy-mineral deposits in its upper part (Elsner and Simon, 1994). These layers can be found in sediments all along the North Sea coast (Bonka, 1980; De Meijer et al., 1987).

In North Germany the overlying quaternary horizons are dominated by glacial and periglacial sedimentation and erosion processes. In the underground a characteristic

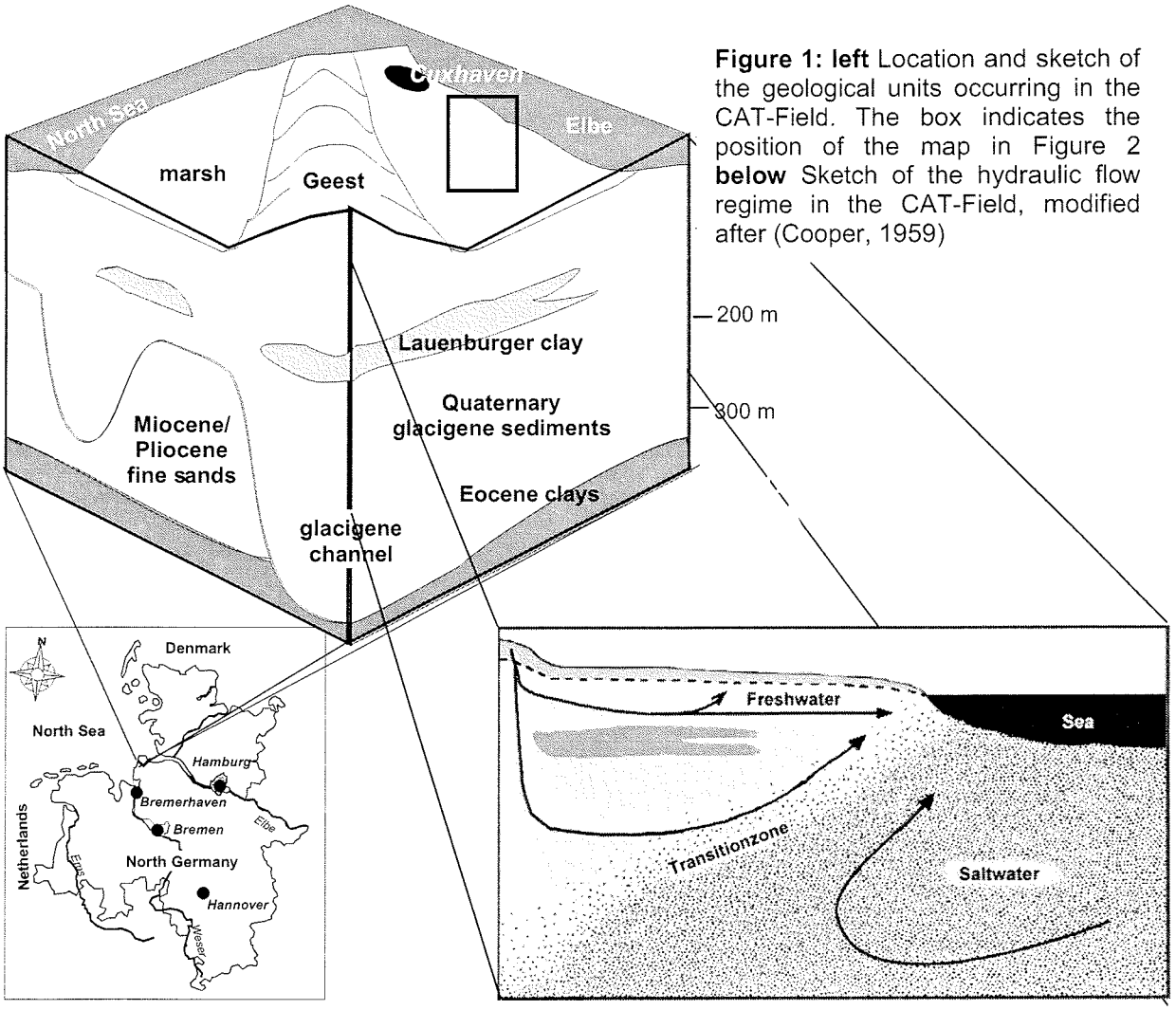

Figure 1: left Location and sketch of the geological units occurring in the CAT-Field. The box indicates the position of the map in Figure 2 **below** Sketch of the hydraulic flow regime in the CAT-Field, modified after (Cooper, 1959)

system of glacigene channels can be found. The glacial channels cut down deeply through the pliocene and miocene sediments into the eocene clays. They reach depths of more then 350 m bsl whereas the width is only 1 or 2 km. The glacial channels were refilled at the end of the Elster ice age (Kuster and Meyer, 1979). Also the CAT-Field is crossed from north to south by one of these channels. The channel filling consists of coarse grained material of the Elster glaciation, which is mostly covered by a thick (100 m) clay layer (Lauenburg Clay). Intercalations into the clay of more than 10 m of sands are common. In places the Lauenburg Clay is thin or absent. Coarse grained sediments of younger glaciations (Saale) are found above the Lauenburg Clay or above the pliocene fine sands in depths of about 50 m. Lacustrine carbonates and marine clays of the Eem interglacial (Höfle, 1985) are locally found in depths between 7 and 25 m bsl. The last glaciation is locally recorded by sand layers above the Eem sediments. In the centre of the CAT-Field the glacigene sand rich deposits form slight ridges (Geest), where these sediments are found at the surface. East and west of the Geest, in the topographically flat areas of the marsh, they are covered by several meters of holocene sediments.

The holocene sedimentation normally starts with a basal peat horizon, followed by brackish lagoonal or tidal flat sediments, interfingered with muds that developed in a brackish lagoonal environment. Different regression phases can be derived from intercalated peat horizons (Streif, 1982). Cut and fill structures of moving tidal channels generate fast lateral grain size variations. Some also younger tidal channels eroded the holocene sediments and cut down into the basal peat.

The Geest ridges are the main groundwater recharge areas in the CAT-Field, while the eocene and oligocene clay formations build the rather impermeable hydraulic base. Due to the fine grained material of the holocene sediments in the marsh, and an extensive artificial drainage system installed for agricultural and land saving purposes, no recharge but upconing groundwater is expected in these areas (Fulda, 2002).

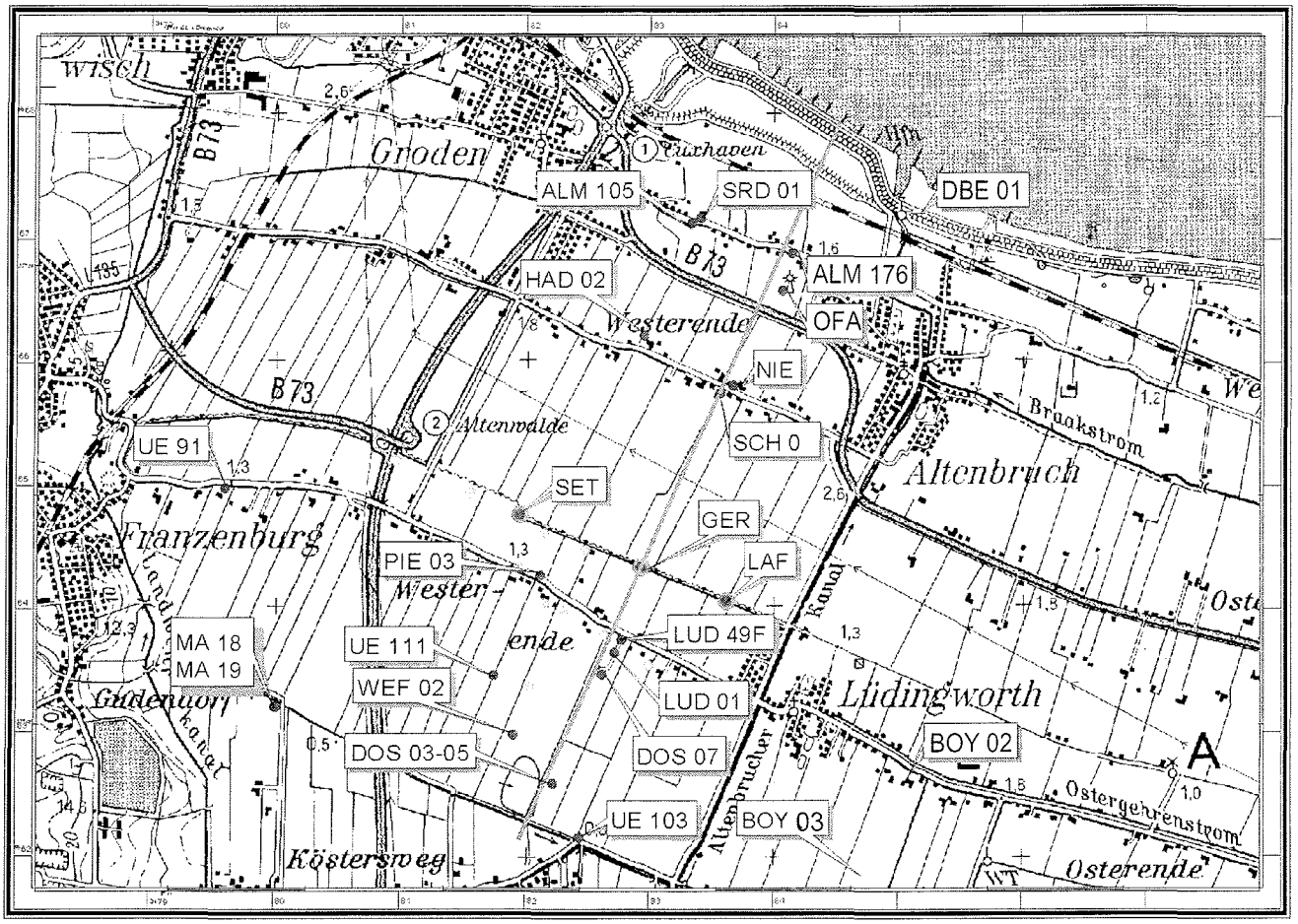

Figure 2: map of a section from the CAT-Field with locations of sampled wells (blue); geological drills (green); multi level wells (red/blue) and the position of the transect of Figure 4 (red line).

2. Methods

Since summer 2000 a number of wells have been installed in the CAT-Field (Fig.2), among them three multi level well clusters in a distance to the coast of about 4 km. Geological drills went down to 90 m below surface (mbs) and were screened between 5 and 50 m below surface, filters have a length of 1 or 2 m. During the installation of the multi level wells the drilled aquifer material was sampled every 5 m; additional samples of the aquifer material were taken in the filter regions between 40 and 50 mbs. This sandy material was used for column experiments (Panteleit et al., 2001). The groundwater sampling net was completed by a series of existing wells of various origin (irrigation wells, fire brigade and research wells from earlier investigations). Filters of existing wells reach down to 190 mbs.

Groundwater samples were taken at different times of the year, but showed no seasonal variation. For the sampling of groundwater a vertical flow-through cell was used which accommodates probes for the simultaneous determination of sensitive parameters (pH, E_H, dissolved O_2, temperature and electric conductivity (EC)). The chamber has a small diameter tubing inlet at the bottom and an outlet port at the top. From the top into which they were sealed, the probes protruded into the centre of the cell. The chamber was flooded from below using a peristaltic pump (Grundfos MP1). The fluid was allowed to exit from the outlet port at the top of the cell, resulting in the movement of fluid past the probes. A WTW model pH192 meter was used with model pHsentix sur and E_H sentix96 probes for pH and E_H measurements; a WTW LF 191 meter with a LS1/T probe for EC and an EOT 190 probe for the measurement of dissolved oxygen. Final measurements were recorded after the equilibration of the measuring probes. For the analysis of alkalinity a water sample of 100 ml that passed a 40 µm filter was titrated with 0.1 n hydrochloric acid to a pH of 4.3 (Cook and Miles, 1980). Two samples for laboratory analysis were passed through a 40 µm cellulose filter, one subsample was acidified for cation analysis the other one untreated but stored cool for anion analysis. Standard laboratory analyses were performed of about 40 components. Inductive coupled plasma atom emission spectroscopy (ICP-AES; Perkin Elmer, Optima 3000) was used for the measurement of the cations Na^+, Ca^{2+}, K^+, Mg^{2+}, Li^+, Sr^{2+}, Ba^{2+}, Mn^{2+}, Fe^{2+} as well as for the anions BO_3^- and SO_4^{2-} and further rare elements. Chloride was determined by high pressure liquid chromatography (HPLC;tpp P100 with a Kratos Spectroflow 773 absobance spectrometer).

3. Results and Discussion

The results of the chemical analyses of the major components in groundwater samples taken from the multi level wells are given in the appendix.

3.1. Salt content in the underground

In Figure 3 the chloride concentrations measured over depth through the multi level wells are displayed. In their position at a distance of 4 km to the coast the chloride concentration increases with depth, starting at about 35 m below surface. The transition from fresh to salt water does not occur in a sharp interface but in a

Figure 3: chloride and electric conductivity (EC) versus depth for multi level well clusters (4 km from the coast line; for location of sampled wells see Fig.1)

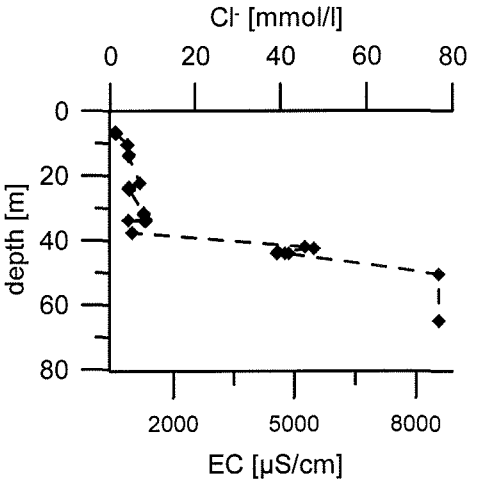

transition zone of several meters which is characterised by a rising salt content with depth.

Measured chloride concentrations from wells located on a transect perpendicular to the coast line (Fig.2) confirm data from recent airborne geophysical investigations (Siemon et al., 2001; Willert et al., 2001) which are shown in Figure 4. While close to the coast line high salt concentrations can be found at the surface, transition zone declines with distance from the shore line. The position determined by this study is

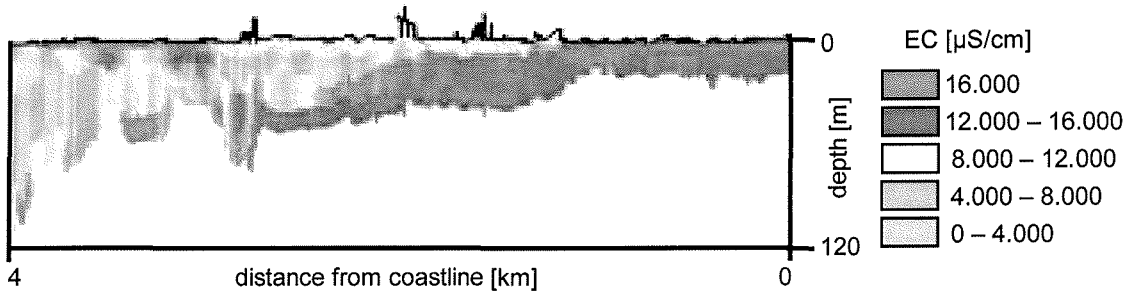

Figure 4: Depth profile of the electric conductivity (EC) as measured on the transect indicated in Figure1 by airborne sounding using an 1D inversion algorythm (Sieman et al., 2001)

also in agreement with geoelectric soundings (Repsold, 1990) and older hydrological observations (Sindowski, 1969).

3.2. Origin of salt content

Three different sources can be discussed for the origin of the salt content measured in the CAT-Field groundwater.

- The most likely source might be the marine influence of the nearby North Sea. Salt water would intrude into the fresh water aquifer based on density

effects (Badon-Ghyben, 1889; Herzberg, 1901). Thus, the position of the transition zone could reflect the recent equilibrium situation. However, in a non steady state situation it could be a remnant from an ancient seawater intrusion. Such was demonstrated for the Wittmund area west of the river Weser by Hahn (1991) and related to climatic changes.

- A second source to discuss is residual water of marine origin mobilized from deeper layers by dispersion processes. As demonstrated by Meinardi (1991) this is the source for salt in Dutch brackish groundwaters.
- The dissolution of halite from the underlying permian salt dome, as well as the weathering of minerals would represent a non marine, but mineral source of the salt content of the CAT-Field groundwater.

Information about the origin of the salt content can be obtained from the Br^-/Cl^- ratio. If evaporitic minerals would be the source, chloride should be enriched due to the lower solubility of chloride minerals compared to bromide (McCaffrey et al., 1987). Different sources, e.g. the degradation of marine organic matter (Manheim, 1972), anthropogenic pollution (Davis et al., 1998) or the release of interstitial water from silicate minerals (Stober and Bucher, 2000) could cause an enrichment of bromide and thus a higher Br^-/Cl^- ratio. Figure 5 compares the Br^-/Cl^- ratio and the Li^+/Cl^- ratio from the CAT-Field to the seawater ratios. Since measured Br^-/Cl^- ratios

Figure 5: Ion ratios of Br^- and Li^+ versus Cl^- from sampled wells in the CAT-Field (Fig.1); lines represent seawater ratio

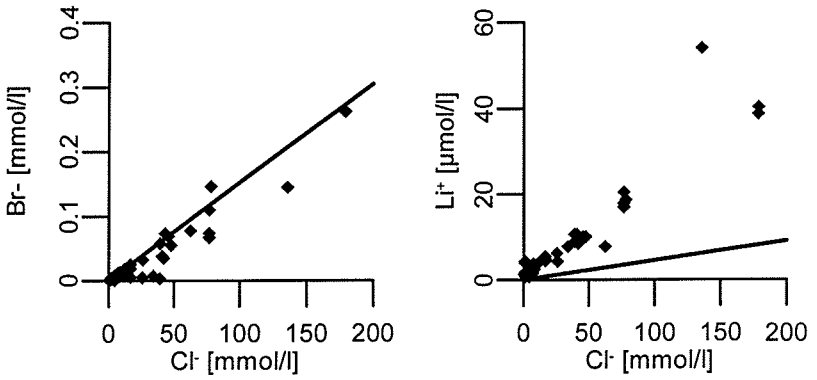

are in a very good agreement with the seawater ratio, a marine origin can be assumed.

The Li^+/Cl^- ratio explains whether the source of the salt content is a recent seawater intrusion or the dispersion from relict water originating from underlying layers. Lithium may be released from mineral lattices of clayey minerals or from exchanger places of organic matter after of the salt content or temperature changed. Once lithium is dissolved, there is no process that is able to separate it from water

again. Thus, lithium can be used as indicator for the residence time of water in the aquifer (Gimernez and Morell, 1997). There is a positive correlation between the salinity and the lithium content of the samples, although the groundwater samples show a steeper slope than the line of conservative mixing (seawater ratio). Thus the saline water had some time to react with the solid phase of the aquifer. The presence of residual water seems to be excluded through results from isotope hydrological investigations. Estimated time scales for groundwater flow in the CAT-Field are between several centuries to a few millennia (Suckow et al., 2003), showing the weakness of isotope dating methods in this time window. This time scale seems to be reasonable for a steady state flow as proposed by Cooper (1959) for the dynamic balance of fresh water and salt water in a coastal aquifer (compare to Fig.1).

3.3. Other chemical properties

The lithium concentrations show that, besides to mixing of fresh and seawater, the groundwater of the CAT-Field is influenced by interactions with the solid phase of the aquifer. Similar to lithium the concentrations of calcium, manganese and iron differ from the concentrations expected from conservative mixing of fresh and seawater (Fig.6).

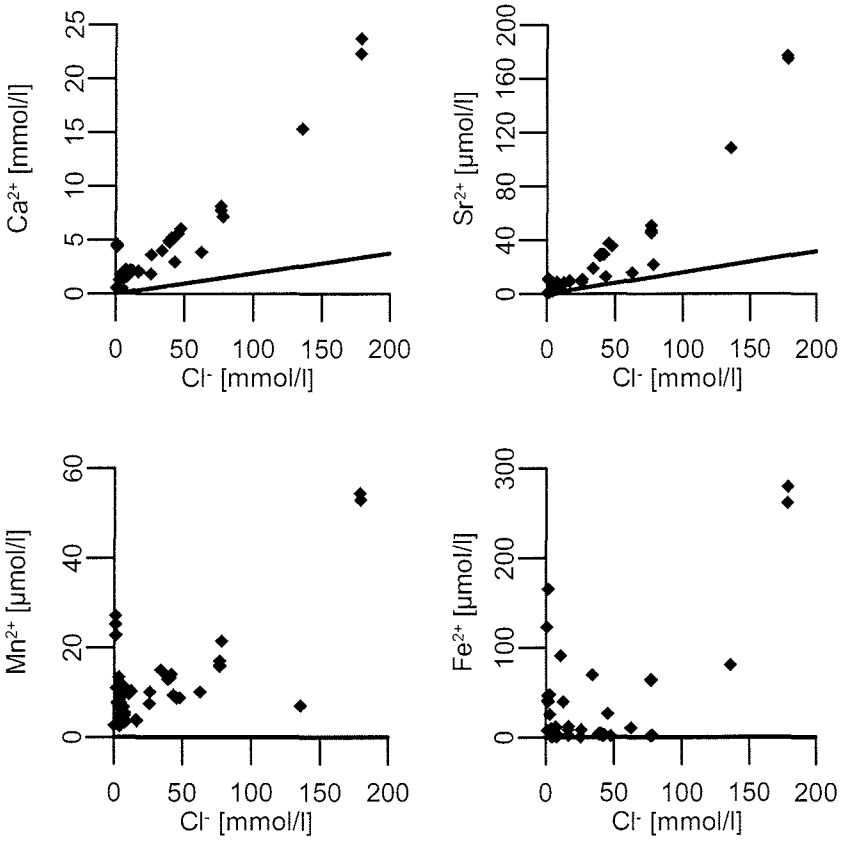

Figure 6: Ion ratios of Ca^{2+}, Sr^{2+}, $Fe^{2+}$and Mn^{2+} versus Cl^- from sampled wells in the CAT-Field (Fig.1); lines represent seawater ratio

The lithium, calcium and strontium concentrations depend on the chloride content, while iron and manganese are more independent of it. Therefore iron and manganese must have a different source of enrichment. Calcium and strontium might be affected by exchanger processes, commonly occurring when the salt content of the water changes (Appelo and Postma, 1996; Jones et al., 1999). Iron and manganese are by redox processes during the degradation of organic matter. For all elements an additional influence towards dissolution and precipitation of minerals induced by the mixing of two water types with different saturation indices and ionic strength must be assumed.

4. Conclusion

Geochemical field investigations and geophysical data were combined to determine the position of the transition from fresh to salt water in the underground of the CAT-Field. The transition zone was identified to be several meters of width. It declines from near surface at the coastline to 35 m depth at about 4 km land inwards. The results suggest that the slow salt water intrusion is in a dynamic balance with the discharge of fresh water through ground water flow.

Measured Br^-/Cl^- and Li^+/Cl^- ratios excluded an underlying salt dome or interstitial water as potential source of the salt content in the groundwater. Mixing of fresh and salt water induces several geochemical processes as indicated by the concentrations of lithium, strontium, calcium, manganese and iron. The identification of the geochemical processes occurring in the transition zone from fresh to seawater will be the subject to future studies.

References

Appelo C. A. J. and Postma D. (1996) *Geochemistry, Groundwater and Pollution*. Balkema.

Badon-Ghyben W. (1889) Nota in verband met de voorgenomen put boring nabij Amsterdam. *Tijdschrift van het koninklijk Instituut voor Ingenieurs*, 21.

Baldschuhn R., Binot, F., Frisch, U. & Kockel, F. (2000) *Geotektonischer Atlas von Nordwest-Deutschland und dem deutschen Nordsee-Sektor.*

Bonka H. (1980) Erhöhte natürliche Strahlenexposition durch Schwermineralanreicherungen an der Küste Norddeutschlands. *Atomenergie- Kerntechnik* **35**(1), 5-11.

Cook J. M. and Miles D. L. (1980) *Methods for the chemical analysis of groundwater*. Institute of Geological Sciences, Hydrogeology Unit.

Cooper H. H. (1959) A hypothesis concerning the dynamic balance of fresh water and salt water in a coastal aquifer. *Journal of Geophysical Research* **64**(4), 461-467.

Davis S. N., Whittermore D. O., and Fabryka-Martin J. (1998) Uses of Chloride/Bromide Ratios in Studies of Potable Water. *Ground Water* **36**(2), 338-350.

De Meijer R. J., Put L. W., Schuling R. D., De Reus J. H., and Wiersma J. (1987) Natural radioactive heavy minerals in sediments along the dutch coast. *KNGMG Symposium "Coastal Lowlands, Geology and Geotechnology"*, 355-361.

Elsner H. and Simon P. (1994) Midlum-Holssel Heavy Metal Deposit in Northwestern Germany. *Angewandte Geologie* **40**(1), 25-30.

Friedhoff T. (2001) Wasserhaushaltsuntersuchungen im tiedebeeinflussten Einzugsgebiet der Medem (Land Hadeln). Diplomarbeit, Hochschule Bremen.

Fulda C. (2002) Numerische Studie zur Salz-/Süßwasserverteilung im Rahmen der Cuxhavener Forschungsbohrung. *Mitteilungen der Deutschen Geophysikalischen Gesellschaft* **Sonderband II**, 10-26.

Fulda C., Kessels W., and Wonik T. (2001) Fluidlogging with cartridge salting in the Coastal Aquifer Test Field (CAT-Field) between Bremerhaven and Cuxhaven, Germany. *SWICA-M³ 2001.*

Gimernez E. and Morell I. (1997) Hydrogeochemical analysis of salinization processes in the coastal aquifer of Oropesa (Castellon, Spain). *Environmental Geology* **29**(1/2), 118-131.

Gräsle W., Willert T., Fulda C., and Kessels W. (2001) The MOWIN concept in hydraulic and transport modeling in the Coastal Aquifer Test Field (CAT-Filed) between Bremerhaven and Cuxhaven, Germany. *SWICA-M³ 2001.*

Hahn J. (1991) Aspects of Groundwater Salinization in the Wittmund (east Friesland) Coastal Area. In *Hydrogeology of Salt Water Intrusion - A Selection of SWIM Papers* (ed. W. D. Breuck), pp. 251-269. Heise.

Herzberg A. (1901) Die Wasserversorgung einiger Nordseebäder. *J. Gasbeleucht. Wasserversorg.* **44**, 815-819.

Höfle H. C., Merkt, J. & Müller, H. (1985) Die Ausbreitung des Eem-Meeres in Norddeutschland. *Eiszeitalter und Gegenwart* **35**, 49-59.

Jones B. F., Vengosh A., Rosenthal E., and Yechieli Y. (1999) Geochemical Investigations. In *Seawater intrusion in Coastal Aquifers - Concepts, Methods and Practices*, Vol. Vol. 14 (ed. J. Bear, A. H.-D. Cheng, S. Sorek, D. Ouazar, and I. Herrera), pp. 51 - 71. Kluwer Academic Publishers.

Kessels W., Dörhöfer G., Fritz J., and Fulda C. (2000) Das Forschungsprojekt "Bremerhaven-Cuxhavener Rinne" zur Beurteilung von Grundwasservorkommen in Rinnensystemen. *Arbeitshefte Wasser* **2000**(1), 189-203.

Kessels W., Fulda C., Binot F., Dörhöfer G., and Fritz J. (2001) Monitoring and Modeling in the Coastal Aquifer Test Field (CAT-Field) between Bremerhaven and Cuxhaven in the Northern Part of Germany. *SWICA-M³ 2001.*

Kuster H. (1989) Bemerkungen zur Lithostratigraphie des Jungtertiär in der Forschungsbohrung Wursterheide. *Geol. Jahrb.* **A111**, 21-31.

Kuster H. and Meyer K.-D. (1979) Glaziäre Rinnen im mittleren und nordöstlichen Niedersachsen. *Eiszeitalter u. Gegenw.* **29**, 135-156.

Manheim F. T. (1972) Interstitial waters in sediments. In *The encyclopedia of geochemistry and environmental sciences* (ed. F. R.W.), pp. 764-769. Van Nostrand Reinhold Co.

McCaffrey M. A., Lazar B., and Holland H. D. (1987) The evaporation path of seawater and the coprecipitation of Br- abd K+ with halite. *Journal of Sedimentary Petrology* **57**(5), 928-937.

Meinardi C. R. (1991) The Origin of Brackish Water in the Lower Parts of the Netherlands. In *Hydrogeology of Salt Water Intrusion - A Selection of SWIM Papers* (ed. W. De Breuck), pp. 271-289. Heise.

Panteleit B., Binot F., Kessels W., Schulz H. D., and Kantor W. (2001) Geological and geochemical characteristics of a salinization-zone in a Coastal Aquifer. In *New Approaches Characterising Goundwater Flow*, Vol. 2 (ed. K.-P. Seiler and S. Wohnlich), pp. 1237-1241. A.A.Balkema.

Repsold H. (1990) Geoelektrische Untersuchungen zur Bestimmung der Süßwasser-/Salzwasser-Grenze im Gebiet zwischen Cuxhaven und Stade. *Geologisches Jahrbuch* **C**(56), 3-37.

Siemon B., Sengpiel K.-P., Rehli H.-J., Röttger B., and Eberle D. (2001) Identification of Saltwater Intrusions and Coastal Aquifers Using the BGR Helicopter-borne Geophysical System. *SWICA-M³ 2001.*

Sindowski K.-H. (1969) Erläuterungen zu Blatt Cuxhaven Nr. 2118. NLfB.

Stober I. and Bucher K. (2000) Herkunft der Salinität in Tiefenwässern des Grundgebirges unter besonderer Berücksichtigung der Kristallinwässer des Schwarzwaldes. *Grundwasser* **5**(3), 125-140.

Streif H. (1982) The occurence and significance of peat in the Holocene deposits of the German North Sea coast. *Symposium on peat lands below sea level*, 31-41.

Suckow A., Bayer R., Binot F., Brost E., Fulda C., Gröning M., Kessels W., Loosli H., Noell U., Oster H., Panteleit B., Purtschert R., Schellschmidt R., Siemon B., Sültenfuß J., Wiederholt H., and Willert T. (2003) CAT: an Integrated Geological, Geophysical, Geochemical and Isotope Hydrological Approach to Study the Marine - Ground Water Interaction. *International Symposium on Isotope Hydrology and Integrated Water Resources Management.*

Wagenschein D. (2002) Zur Unterscheidung toniger und salzwasserführender Sedimente mit dem Verfahren der spektralen induzierten Polarisation (SIP). Diplomthesis, Universität Bremen (Germany).

Willert T., Behain D., Fulda C., Worzyk P., and Kessels W. (2001) Regional saltwater distribution in the Coastal Aquifer Test Field (CAT-Field) between Bremerhaven and Cuxhaven, Germany, by DC-geoelectric measurements. *SWICA-M³ 2001.*

TEIL III Experimental Determination of Geochemical Processes Occurring During the Salinisation of a Coastal Aquifer

Experimental Determination of Geochemical Processes Occurring During the Salinisation of a Coastal Aquifer

B.Panteleit

Abstract

Geochemical processes occurring in the transition zone between salt and fresh water in a coastal aquifer were studied through laboratory column experiments and numerical simulations using PHREEQC (Parkhurst and Appelo, 1999). In both experiments a salinisation followed by a refreshening of the aquifer was simulated. Rapid exchange of adsorbed ions was distinguished from slower dissolution and precipitation processes through the comparison of experimental and simulation results. The numerical model simulation of the experiment considered exchanger reactions only. Experimental breakthrough curves of major ions are in good agreement with data from the numerical simulation. Differences between experimental and modeled data suggest the dissolution of $CaCO_3$, $FeCO_3$ and $MnCO_3$, while $MgCa(CO_3)_2$ seems to be precipitated. Interactions with clay minerals seems to be reflected in a release of Li^+ and an enhanced adsorption of K^+.

1. Introduction

1.1. Motivation

This publication presents first results from a geochemical characterisation of a coastal aquifer at the German North Sea coast. The investigations are a contribution to an interdisciplinary project with the aim to develop a numerical model of the transport and flow processes in a coastal aquifer. First results from hydrochemical field investigations served to determine the origin and position of a transition zone from fresh to seawater. Panteleit et al. (2001) concluded that processes other than conservative mixing must occur in this zone, since measured ion/chloride ratios deviate from the seawater ratio. Because a process study in the field is rather difficult to realise, these

processes were simulated in laboratory experiments. In a first step column experiments were performed, their results are presented here.

1.2. Geochemical introduction

1.2.1. Geochemistry of saltwater intrusion

In a coastal aquifer two types of water merge, which usually are separated in space. One type is seawater, which is characterised by a high ion content, mainly Na^+ and Cl^-. The other one is fresh water, characterised by a low ion content, mainly Ca^{2+} and HCO_3^-. Between these two end-members a dispersion induced transition zone will develop. Its shape and position depends on the salt content and the groundwater flow, and is strongly affected by soil and climatic parameters (Reilly and Goodman, 1985).

Changes in the salt content will induce geochemical processes, resulting in a new equilibrium between solid and liquid phase. Possible processes are cation exchange, precipitation and dissolution of minerals (mainly gypsum, calcite, dolomite), ion sorption and desorption, and oxidation of organic matter. All these processes have individual reaction kinetics, resulting in different time periods needed until a new equilibrium establishes. In any case, a water composition deviating from simple conservative mixing of the end members is the result of these processes.

1.2.2. Exchanger reactions

Exchanger reactions occur almost immediately when the ion composition of the pore water changes. Therefore they are dominating the pore water chemistry during the first phase of a salt water intrusion, when the salt content changes. Exchanger reactions occur at the surface of minerals, where negative charges are located due to ion substitutions in the mineral lattice (Vaughan and Pattrick, 1995). These negative charges are balanced by weakly bound cations from the groundwater. The adsorbed ions are in equilibrium with the ions in solution. Thus, a changing composition of the solution also changes the occupation of the exchanger sites e.g.:

$$Na^+ + KX \rightarrow NaX + K^+ \qquad \mathrm{K}_{Na/K} = \frac{[NaX][K^+]}{[KX][Na^+]} \qquad (1),$$

where X indicates the exchanger site on the solid surface and brackets the "activity" of the species. If the law of mass action is applied formally, the affinity of the different ions can be expressed by the selectivity coefficient K. Since the selectivity coefficient depends on the characteristics of the adsorbing material, it does not represent a constant in a thermodynamical sense (Sposito, 1984). Even though they are depending on the material and solution composition, the coefficients generally follow the lyotrophic series. Considering two cations of the same charge, the one covered by a smaller hydration shell of water molecules is bound stronger to the mineral surface (Appelo and Postma, 1996).

Uncertainties about the exchanger structure on the mineral surface result in two different model assumptions to describe heterovalent exchange. Corresponding to the "Gaines & Thomas convention" (Gaines and Thomas, 1953) the activities of the adsorbed ions are assumed to be proportional to the number of exchanged cations:

$$CaX_2 + 2Na^+ \rightarrow 2NaX + Ca^{2+} \qquad K^{GT}_{Na/Ca} = \frac{[NaX]^2[Ca^{2+}]}{[CaX_2][Na^+]^2} \qquad (2),$$

while the "Gapon convention" (Gapon, 1933) refers to the number of exchanger sites (Appelo and Postma, 1996).

$$Ca_{0.5}X + Na^+ \rightarrow NaX + 0.5Ca^{2+} \qquad K^{G}_{Na/Ca} = \frac{[NaX][Ca^{2+}]^{0.5}}{[Ca_{0.5}X][Na]} \qquad (3)$$

The choice of a given convention is prompted primarily by the best fit that can be obtained when applied to experimental data. For the simulations of the column experiments, both results of models are presented and compared to the experimental data.

2. Method

2.1. Strategy

To identify reactions that are occurring in coastal aquifers during salt water intrusion, the following strategy was applied. Column experiments were used to separate changes of the water composition due to exchanger reactions from slower geochemical reactions. At the same time a numerical modeling using PHREEQC (Parkhurst and Appelo, 1999) was carried out, considering

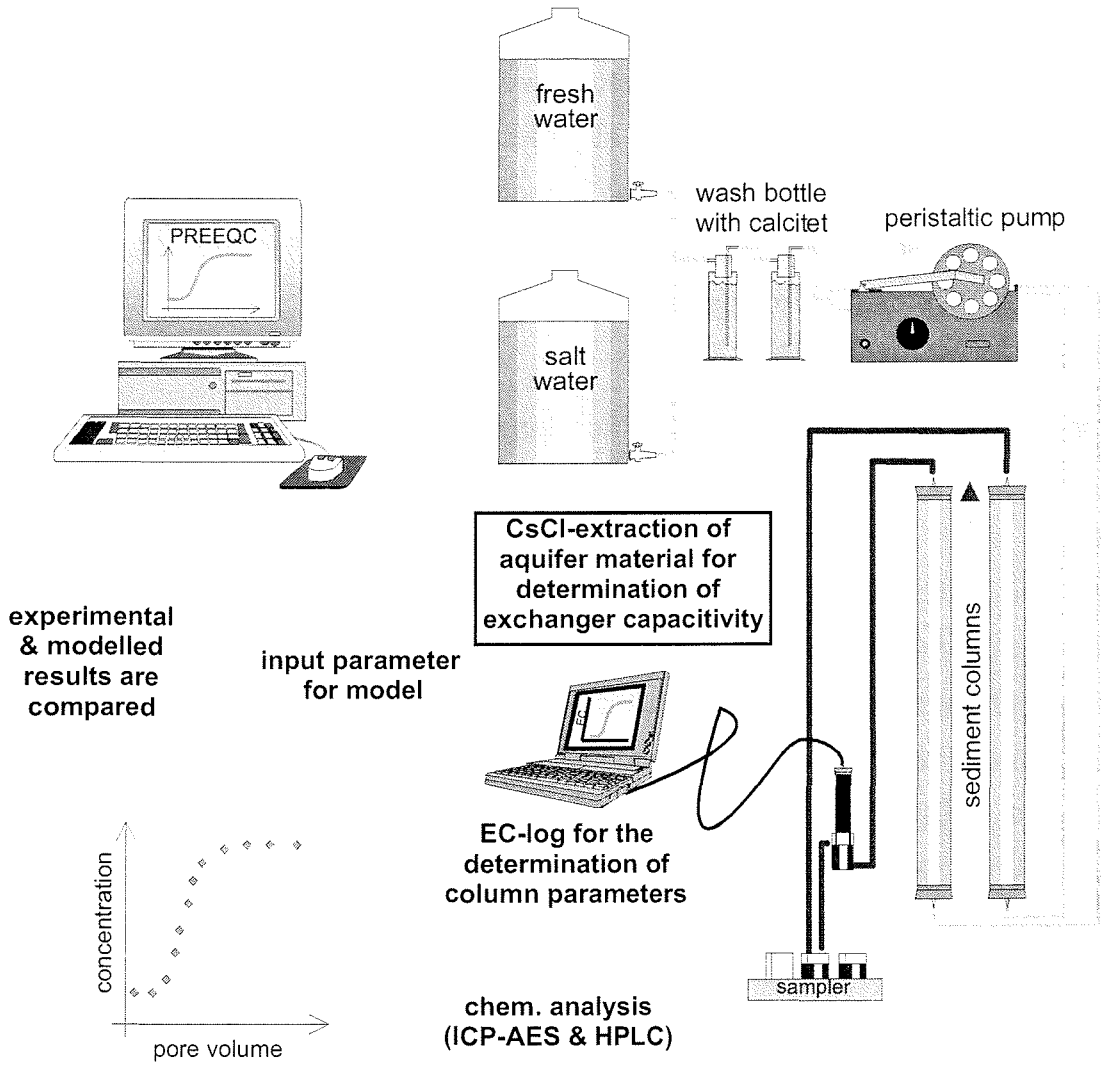

Figure 1: Sketch of the experimental set-up

exchanger reactions only (Fig.1). Differences between results from the laboratory experiment to those from the numerical model should originate from reactions not considered in the model.

2.2. Column Experiments

For the column experiment glaciofluviatile sands were used. The material was sampled from a coastal aquifer at the German North Sea coast in a depth of about 45 m during a drilling campaign in the summer of 2000 (Panteleit et al., 2001) and stored meanwhile at 3° C in closed bottles. Two acryl columns (each of 50 cm length and 5 cm diameter) were successively filled with the stored sediment. Packing of the columns occurred through a water layer of 2 cm to avoid inhomogeneities and embedding of air gaps.

During the conditioning phase of the experiment the sediment was flushed with artificial groundwater. The water was synthesised to match the chemistry of the groundwater sampled at the point of origin of the sediment. Subsequently it was saturated with respect to calcite by passing it through two 200 cm^3 wash bottles filled with calcite sand (Fig.1). The two columns were flushed from bottom to top at a flow rate of 0.6 ml/min, corresponding to a hydraulic slope of 0.05.

Electrical conductivity (EC) was measured continuously in a flow through cell located at the outflow of the columns. Samples of effluent water were taken every 4 hours by a self constructed autosampler, and immediately acidified with nitric acid. During the first salinisation experiment problems with the autosampler lead to a lower sampling rate, manually taken twice per day. Hydrochemical analyses of major elements were carried out by Inductive Coupled Plasma Atom Emission Spectroscopy (ICP-AES, Perkin Elmer, optima 3000). Mineral equilibrium was assumed after a constant EC was measured for over 100 hours, which commonly established after one week. Geochemical analyses showed no significant differences between the input and the effluent water at the end of the conditioning phase.

After the conditioning phase the column was flushed with diluted (20%) artificial seawater (Grasshoff et al., 1999), which was also equilibrated with respect to calcite. Sampling and EC measurement were performed as before. This first salinisation experiment was followed by a desalinisation phase, flushing with artificial groundwater again. Equilibrium conditions after the desalinisation phase were documented again through geochemical analysis of the input and outflow water. When analysis results were similar, the salinisation was repeated at a higher sampling rate, in order to control for the reproductivity of the first results.

For the numerical simulation, column and sediment parameters were required as input parameter. Column parameters (K_f and dispersivity) were determined by fitting the transport equation to the measured electrical conductivity at the column outflow during breakthrough of the saltwater. Sediment porosity was determined by weight loss after heat drying of water saturated samples at 105 °C over 24 hours. The cation exchange capacity

(CEC) and exchange coefficients were derived from analysis of a CsCl-extraction (Reardon et al., 1983) of the sediment used in the column experiment. For the CsCl-extraction 100 g of moist sediment were mixed with 20 ml of 0.5 mol/l CsCl solution and immediately centrifuged to separate the liquid phase from the mineral phase. The high concentration of the CsCl solution results in the exchange of all adsorbed ions, while the limited exposure time restricted further reactions. The separated fluid was analysed by ICP-AES.

2.3. Numerical simulation

Using the computer program PHREEQC (Parkhurst and Appelo, 1999), the results of the column experiments were modeled. For the transport simulation the column length was discretised into 50 cells each of 1 cm length (see input code in appendix). Input parameter for the transport module, which are displayed in Table 1, were determined as described in the experimental section. Exchanger processes were considered only. For the calculation of selectivity coefficients equilibrium of the exchanger occupation with the artificial groundwater used for the condition phase was assumed. Selectivity coefficients were then calculated for monovalent ions using equation 1. For bivalent ions the equations 2 and 3, representing the "Gaines & Thomas convention" (Gaines and Thomas, 1953) and the "Gapon convention" (Gapon, 1933), respectively were used in separated model runs. All calculated selectivity coefficients are also displayed in Table 1.

parameter		column A	column B
Kf	**m/s**	9.50E-05	7.25E-05
Porosity		0.36	0.29
dispersivity	**m**	0.017	0.013
length	**m**	0.48	
area	**m²**	1.96E-03	
slope		0.05	
CEC	**meq/ kg**	5.56	

Ion	log $K_{I/Na}$	log $K^G_{I/Na}$
Na^+	-	
K^+	0.42	
Li^+	1.62	
Ca^{2+}	1.35	1.21
Mg^{2+}	1.16	0.68
Sr^{2+}	1.29	-0.03
Mn^{2+}	1.33	-0.24

Table 1: Experimentally determined column parameters and selectivity coefficients that were used as input parameter for numerical simulations; selectivity coefficients for bivalent ions were calculated for the Gapon model (K^G; eq.3) and the Gaines & Thomas model (K; eq.2)

3. Results and Discussion

As shown in Figure 1 two columns were operated parallel serving as replicates. Beside slight differences in the hydraulic column parameters (Tab.1) the geochemical results were identical (detailed data is given in appendix C), therefore only results from one column are presented and discussed sequential for major and minor elements.

3.1. Major Elements

3.1.1. Chloride

Considering a higher measurement error for Cl^- analysis compared to techniques used for the other ions, the measured Cl^- concentrations are in good agreement with the modeled data (Fig.2). Thus chloride behaves as an ideal tracer. During the first salinisation experiment the measured chloride concentration rises and reaches the salt water concentration after one porevolume was flushed. The concentration increase for the second salinisation phase after a refreshening in between. However a slightly higher chloride concentration in the outflow water after the refreshening suggests a certain amount of interstitial water, which is successively flushed out.

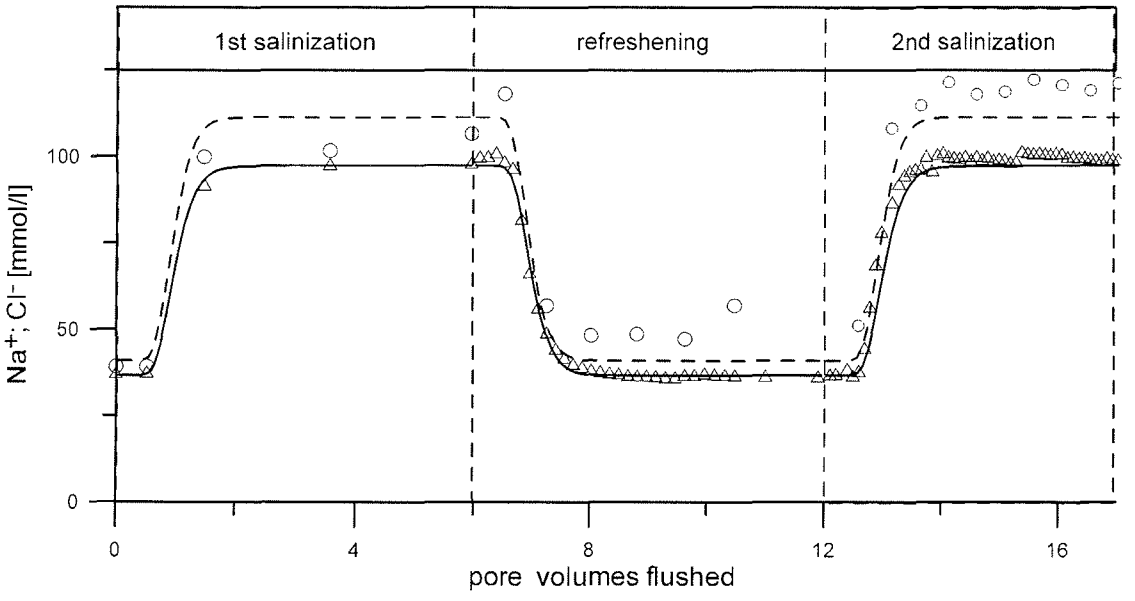

Figure 2: Simulated (lines) and experimental (marks) data of the column transport experiment for Cl (dashed line, circles) and Na^+ (solid line; triangles). Salinisation experiments range from 0-6 and 12-17 pore volumes, refreshening phase from 6-12 pore volumes flushed. Equilibration phases in between are not displayed

3.1.2. Sodium

The sodium concentration shows an almost identical behaviour (Fig.2). The experimental data and the modeled data from the transport/exchange simulation with the computer program PHREEQC (Parkhurst and Appelo, 1999) match very well. Simulation results using the "Gapon convention" (Gapon, 1933) and the "Gaines & Thomas convention" (Gaines and Thomas, 1953) showed no differences. Compared to chloride a delayed concentration increase would be expected for Na^+. Ion concentration changes result in rapid replacement of adsorbed cations, e.g. Ca^{2+} by Na^+, delaying the increase of Na^+ in the solution. This delay is neither reflected in the experimental data nor in the modeled data. The reason for this deviation from expected results is the high Na^+ concentration in the salt water compared to the CEC. Consequently ion exchange reactions do not have a significant effect on the concentration breakthrough.

3.1.3. Calcium

Due to the long sampling interval used during the first salinisation experiment it can only be said that the results do not contradict the modeled data (Fig.3). Since the first experimental results were reproduced by the

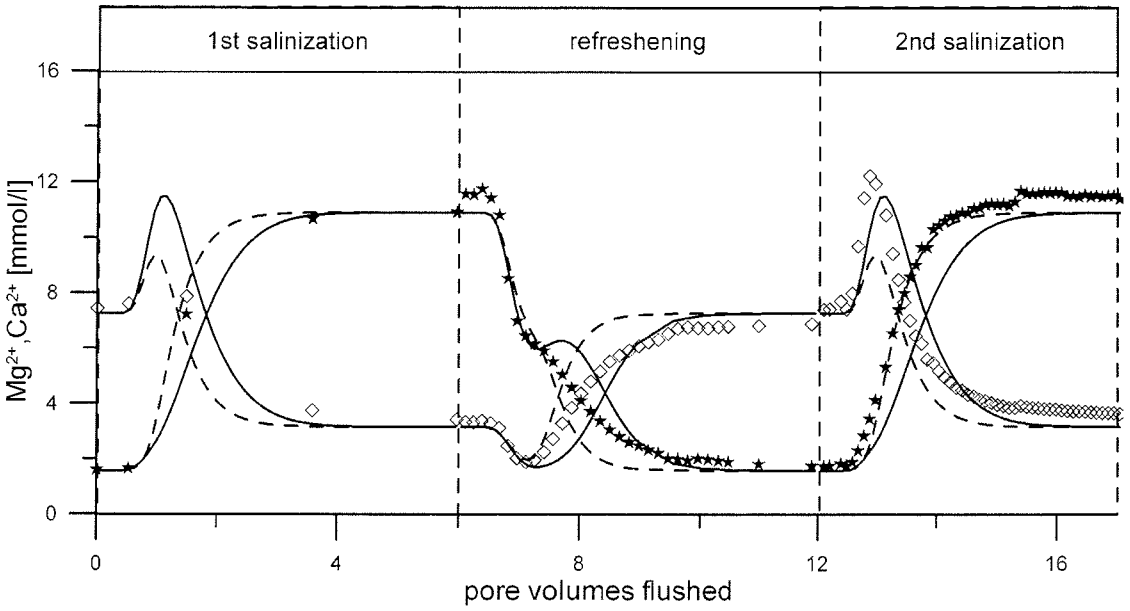

Figure 3: Experimental data of column transport of Ca^{2+} (open rhombs) and Mg^{2+} (stars). Solid lines represent modeled data using the "Gaines & Thomas" convention, dashed lines using the "Gapon" convention (see text). Salinisation experiments range from 0-6 and 12-17 pore volumes, refreshening from 6-12 pore volumes flushed. Equilibration phases in between are not displayed.

second salinisation experiment, the following statements are based upon the results of the later only. Even before the Cl^- concentration reaches that of the input water, the Ca^{2+} concentration rises to a maximum value of 12.2 mmol/l, which is well above the concentration of the local groundwater (7.2 mmol/l). After five pore volumes were flushed the Ca^{2+} concentration is still slightly above that of the flow water. It remains more or less constant until the end of the salinisation experiment. The first Ca^{2+} peak at the beginning of the salinisation phase is caused by the release of exchanger site bound Ca^{2+} (equations 2 and 3) due to the high Na^+ concentration of the intruding salt water. This behaviour is also known and described from other experiments (Beekmann and Appelo, 1990; Gomis-Yagües et al., 1997).

The geochemical exchange reaction is reversed at the beginning of the refreshening. Subsequently to the start of flushing the column with fresh water, the calcium concentration decreases first to a minimum concentration of 1.9 mmol/l, before it rises back to the fresh water value. The experimental data are for both experiments in between the results of the two simulation runs. However, experimental data tend towards the "Gaines-Thomas" model data, which result in higher peak concentrations.

At the end of the salinisation experiment the calcium concentration in the effluent water is still slightly above the salt water concentration of 3.1 mmol/l. This might be an indication for calcite dissolution or dolomitisation within the column. Such process was also observed elsewhere (Magaritz et al., 1980; Magaritz and Luzier, 1985). The assumption of dolomitisation is supported by thermodynamic calculations of field water analyses using PHREEQC (Parkhurst and Appelo, 1999). They result in an increasing saturation index (SI=log(ion activities in water sample/ion activities in equilibrium)) for dolomite, while the SI of calcite decreases with higher salt content of the flushing water. The effluent water of the column experiment shows a SI of –0.4 for calcite, while it seems to be saturated with respect to dolomite. Another support for this assumption is given by the Ca^{2+}/Cl^- ratios of 0.12 mol/mol measured from field samples, which lie clearly above the seawater ratio of 0.02 mol/mol (Panteleit et al., 2001). Such high ratios also suggest a calcium releasing process.

3.1.4. Magnesium

Magnesium concentrations are higher for salt water (10.9 mmol/l) than for fresh water (1.6 mmol/l). Accordingly, the Mg^{2+} concentration increases at the beginning of the salinisation experiments, but is delayed compared to the steep increase of the Na^{+} and the Cl^{-} concentration. This is due to the replacement of Ca^{2+} on the exchanger sites and agrees with the modeled data. Due to the lower Mg^{2+} concentration and a higher affinity to the exchanger sites (see Tab.2) compared to Na^{+}, the effect of this reaction can be seen more clearly in the magnesium concentration. Likewise, the exchanger reactions are reflected in the pattern of the concentration curves during the refreshening phase. Here the release of the adsorbed magnesium leads to a temporary maximum.

In contrast to Ca^{2+}, for Mg^{2+} experimental data are matched better using the "Gapon" model than the "Gaines-Thomas" model. The differences reflect the uncertainties about the structure of the exchanger sites. Beekmann and Appelo (1990) preferred the "Gapon" convention for multi component transport modeling. They relate observed differences between experimental and modeled data to changing selectivity coefficients of Ca^{2+} over Mg^{2+} during the breakthrough. Such changes are still not completely understood and consequently hardly to insert into a model.

3.1.5. Strontium

Principally Sr^{2+} shows the same exchange behaviour as Ca^{2+}, consequently the breakthrough curves show the same characteristics for both species (Fig.4). Similar to Ca^{2+}, Sr^{2+} seems to be better described by the "Gaines & Thomas" model run than by the "Gapon" model. Analysis of groundwater samples from the investigation area result in a Sr^{2+}/Cl^{-} ratio of about $7 \cdot 10^{-4}$ mol/mol, which is well above the seawater value of $1.6 \cdot 10^{-4}$ mol/mol. Based on these field data analysis Panteleit et al. (2001) suggest a dissolution process occurring in the field aquifer. In contrast to Ca^{2+}, the Sr^{2+} results from the column experiments do not support this conclusion, since the Sr^{2+} concentration in the effluent does not exceed the input water concentration of 0.017 mmol/l. Since this difference in behaviour may be due

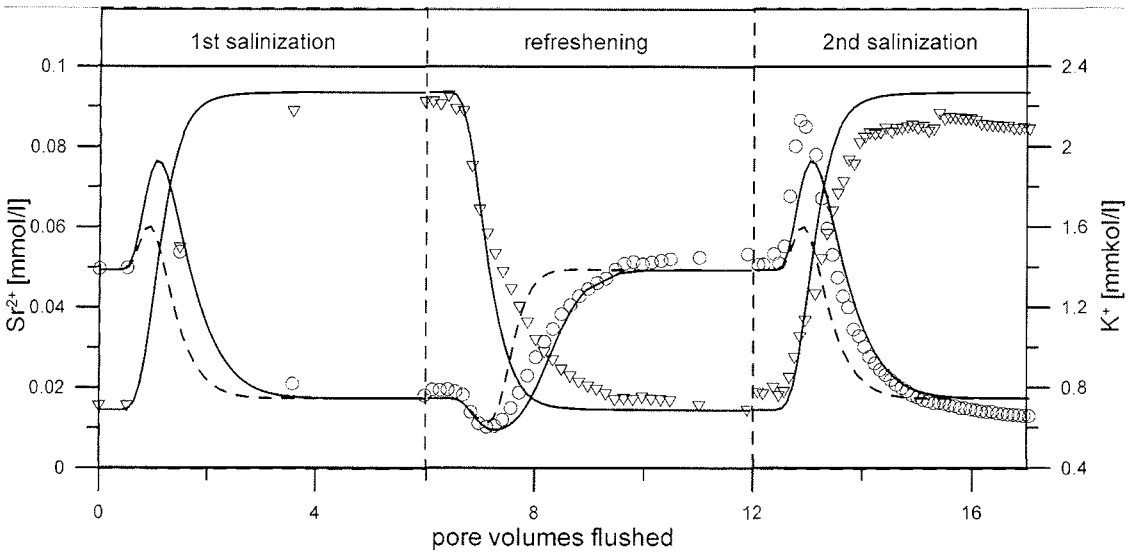

Figure 4: Experimental data of column transport of Sr^{2+} (circles) and K^+ (triangles). Solid lines represent modeled data using the "Gaines & Thomas" convention, dashed line using the "Gapon" convention for (see text). Salinisation experiments range from 0-6 and 12-17 pore volumes, refreshening from 6-12 pore volumes flushed. Equilibration phases in between are not displayed

to the limited reaction time during the column experiments. Thus this result does not contradict the overal results of our investigation

3.1.6. Potassium

During salinisation the modeled potassium reaches maximum values after 2 pore volumes are flushed. This is only a slightly delayed increase compared to that of chloride (maximum after 1.5 pore volumes flushed). In contrast, the experimental data clearly show such a delay (Fig.4, maximum is reached after 3.3 pore volumes flushed). This observation is confirmed by results of a likewise experiment by Beekmann and Appelo, (1990). A delay of the potassium concentration decrease during the refreshening of the column was also observed. Experimental K^+ concentrations stayed slightly higher than modeled ones. The delay of the K^+ breakthrough curves might have two reasons:

First, as pointed out before, the selectivity coefficients are not constant, but depend among other parameters on the concentration of the solution. In higher concentrated solutions the ions show a lower selectivity with respect to the exchanger sites (Stumm and Morgan, 1995), resulting in preferred K^+ adsorption. Since the exchanger occupation was determined from fresh water samples, the modeled data might overestimate the actual selectivity during

the intrusion of higher saline water. Thus, in the experiment the preferential adsorption of alkaline earth metals to exchanger sites probably was less than estimated by the model, while alkali metals show a higher adsorption than modeled.

Second, a part of the potassium might be adsorbed tightly to a different type of exchanger site (Merkel and Sperling, 1996). Evidences for this assumption are also present in data from groundwater, that was sampled during the collection of the sediment used for the column experiment. The K^+/Cl^- ratio of the deeper groundwater is 0.015 mol/mol, which is slightly below the seawater ratio of 0.019 mol/mol (Panteleit et al., 2001), suggesting a potassium sink. Due to the slow reaction, this exchanger site type can not be characterised through the CsCl extraction, consequently it is also not incorporated in the model simulation.

The slow reaction suggests a strong adsorption site, which could be build up by clay minerals. In general, clay minerals are known to have a high capability for the adsorption of potassium. Due to its ion radius, potassium is known to form inner sphere complexes with clay minerals. Once incorporated into clay complexes, K^+ ions are not readily exchanged (Sposito, 1989). Additionally, clay minerals swell under the influence of salt water, which may enhance their adsorption potential with respect to potassium (Goldenberg et al., 1984; Magaritz and Luzier, 1985).

3.2. Minor Elements

Due to the low concentrations of the minor ions, experimental data show a noticeable variation. However, for some of these species interesting observations were made, which are presented here qualitatively.

3.2.1. Manganese

For Mn^{2+} the results of the first salinisation could not be reproduced in the second salinisation phase (Fig.5). In the first salinisation run Mn^{2+} shows a concentration peak of 23 µmol/l, which is well above the simulated peak concentration of 15.7 µmol/l. Subsequently, the concentration decrease down to the very low salt water values of 0.1 µmol/l occurs much slower than estimated by the model. During refreshening the Mn^{2+} concentration increases

much later and less high than expected. In fact the concentration rose in the equilibration phase after the end of sampling. Already during the initial condition phase at the beginning of the experiment manganese needed very long to decrease down to a constant value. In the second salinisation experiment a concentration peak can clearly be observed, but this time it lies well below that one of the modeled data. The decrease again is slower than modeled and thus closer to the result of the "Gapon" model run.

The behaviour of manganese might be explained by a dissolution process. In contact with salt water a mineral compound holding Mn^{2+} dissolves, resulting in a measured Mn^{2+} concentration above that one expected from exchanger release only. During refreshening the mineral is precipitated again resulting in a delayed concentration rise with respect to modeled data. In the second salinisation experiment the small amounts of the precipitated mineral redissolve, resulting in a smaller concentration peak then during the first experiment. Actually, it is even less pronounced than the modeled one, because the labile mineral phase also partly dissolves during the CsCl extraction. Consequently the exchanger bound manganese was overestimated by the CsCl extraction. This hypothesis is supported by field

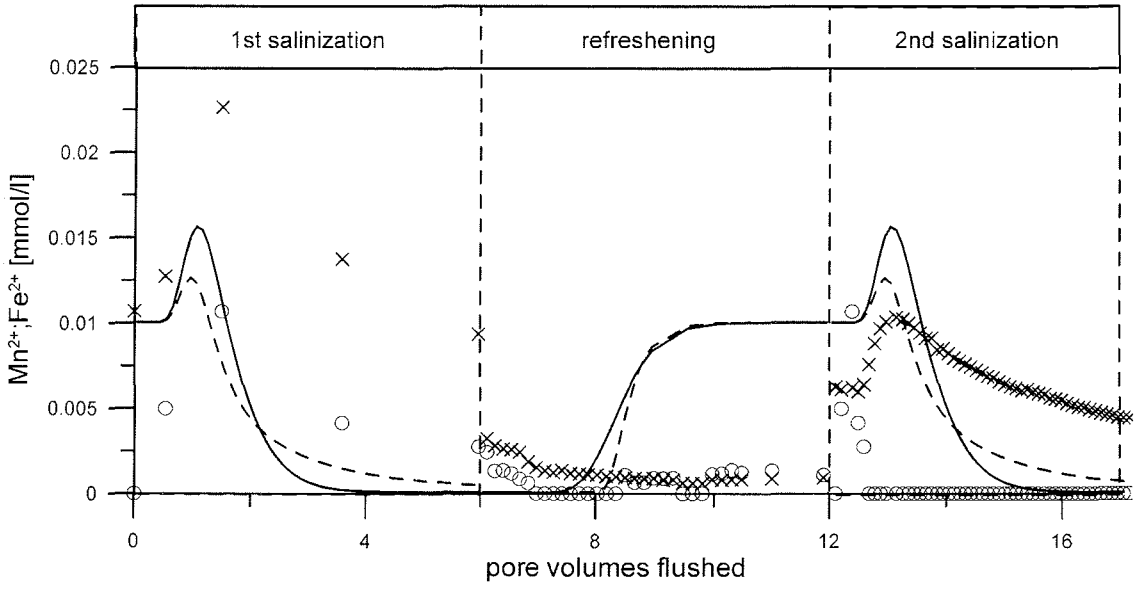

Figure 5: Experimental data of column transport of Mn^{2+} (crosses) and Fe^{2+} (cirles). lines represent modeled data of Mn^{2+}: solid line using the "Gaines & Thomas" convention, dashed line using the "Gapon" convention for (see text). Salinisation experiments range from 0-6 and 12-17 pore volumes, refreshening from 6-12 pore volumes flushed. Equilibration phases in between are not displayed; data below the detection limit were set to zero

data of groundwater samples, gathered when collecting sediment material for the column experiment. The Mn^{2+}/Cl^- ratio of $2.2 \cdot 10^{-4}$ mol/mol (in the anoxic surface layer even higher) in groundwater samples under the influence of salt water are above the seawater ratio of $1.0 * 10^{-8}$ mol/mol (Panteleit et al., 2001). Additionally thermodynamic calculations using PREEQC deliver a positive saturation index for rhodochrosite ($MnCO_3$) in the upper part of the aquifer, while the deeper part with rising salt concentrations is at equilibrium (SI = 0). The same calculations for the salt water used in column experiments result in a negative saturation index, which indicates $MnCO_3$ dissolution during the column experiments. Further information concerning the manganese source could be obtained by mineral analysis, however such were not subject of this investigation.

3.2.2. Iron

The distribution of iron in water is primarily controlled by the redox conditions. Due to the oxidising conditions of the CsCl extract no dissolved iron was detectable. Consequently only experimental data are presented (Fig.5). During the initial condition phase no iron could be detected in the effluent. However, during the first salinisation experiment iron shows a concentration peak. As for manganese, the concentration decrease occurs much slower than expected from an exchanger process. The concentration peak seems to be too high to be explained by exchanger processes only,

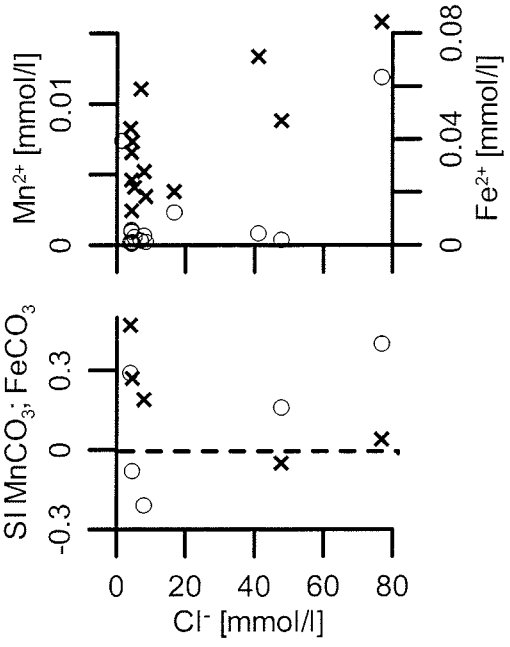

Figure 6: above: concentration of Mn^{2+} (crosses) and Fe^{2+} (circles) vs. Cl^- from field samples (Panteleit et al., 2001)
below: Saturation indices (SI) of MnCO3 (crosses) and FeCO3 (circles) vs. Cl^- concentration for field samples calculated with PHREEQC (Parkhurst and Appelo, 1999)

even model results would not serve as reference. The breakthrough characteristics seem to be better explained assuming an additional mineral dissolution process. This assumption is supported by thermodynamic calculations using field data. An undersaturation with respect to siderite ($FeCO_3$) was calculated for water samples with intermediate salt concentrations between 2 and 45 mmol/l Cl^- (Fig.6). Ironcarbonate might be present in the sediment, possibly even in combination with manganese-carbonate. But in contrast to what was discussed for Mn^{2+} siderite is not precipitated again during the refreshening, since iron is only present in very low concentrations in the fresh water of the column experiments. Consequently the concentration peak in the second salinisation experiment is less pronounced than in the first one.

3.2.3. Lithium

The analysed concentrations of lithium shows a broad scattering. Thus, the poor precision (analytical error of about 20%) of the measurements has to be taken into account while discussing the results. As a consequence of the analytical error the selectivity coefficient presented in Table 1 gives only an estimation. However, in relation to the selectivity coefficients of other ions,

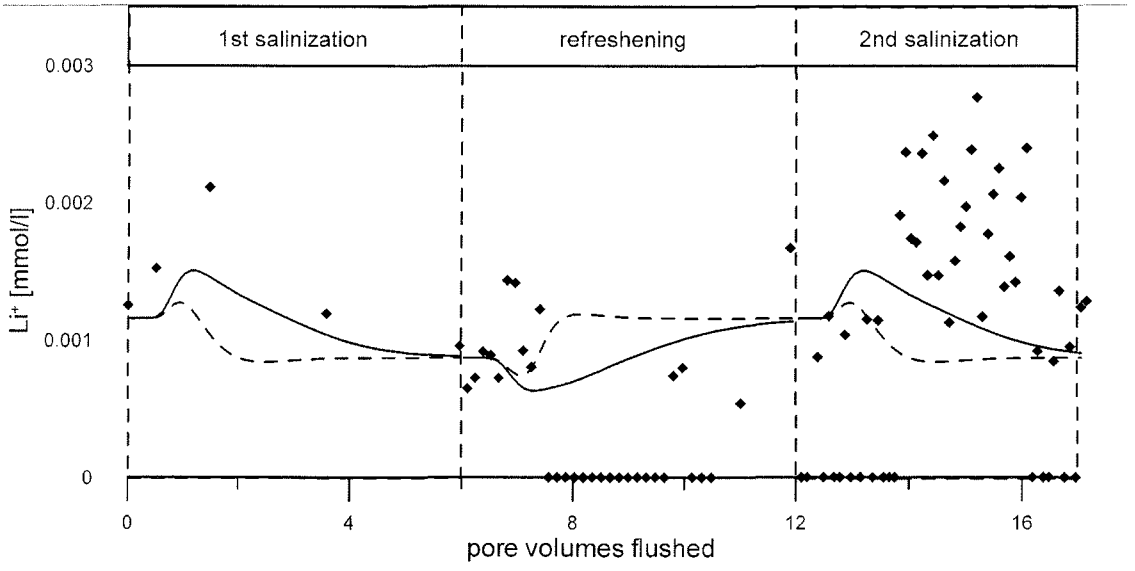

Figure 7: Experimental (diamonds) and modeled (lines) data of column transport of Li^+. Solid line represent data according to the Gaines & Thomas convention, dashed line according to the Gapon convention (see text). Salinisation experiments range from 0-6 & 12-17 pore volumes, refreshening from 6-12 pore volumes flushed. Equilibration phases in between are not displayed; concentrations below the detection limit of 0.0005 mmol/l) were set to zero

lithium follows the theory of the lyotrophic series, as Li^+ should have the highest selectivity coefficient due to its small ion radius.

For both salinisation experiments Li^+ concentrations are clearly higher than modeled values (Fig.7). Under the influence of fresh water the Li^+ concentrations seem to be below the modeled ones. Again this might be explained by a releasing process. In contrast to manganese and iron, the releasing mineral source seems to be still present during the second salinisation phase, because the high concentration was reproduced. Again the Li^+/Cl^- ratio from field samples of $2.4 \cdot 10^{-4}$ mol/mol support this assumption, as the ratio lies significantly above the seawater value of $5 \cdot 10^{-5}$ mol/mol. Also in the literature it is documented that Li^+ may be released from clay minerals under the influence of changing salinity (Gimernez and Morell, 1997). Due to this effect lithium can be used as tracer for seawater residence times in aquifers (Tulipano and Fidelibus, 1984).

4. Conclusions

In a laboratory column experiment sediment, sampled from a coastal aquifer, was exposed to salinisation and refreshening. For major ions the resulting breakthrough curves were generally in good agreement with numerical simulations reflecting exchanger reactions. Slower geochemical processes seem to be masked during the movement of a salt water front. Dolomitisation was indicated by a slight excess of calcite combined with a simultaneous depletion of magnesium in the effluent.

Results for selected minor elements showed differences between experimental and modeled data. Combined with data from a field investigation published earlier, evidence is given for the following processes:

- Dissolution of manganese- and ironcarbonate (siderite, rhodochrosite)
- Release of lithium from clay minerals
- Enhanced adsorption of potassium by clay minerals

For verification and a better understanding of these processes a detailed examination of the transition zone in a stable position without the influence of exchanger reactions would be helpful. These conditions would be available in

a 2D flow experiment with a stable position of the transition zone. This experiment is projected for the future.

References

Appelo C. A. J. and Postma D. (1996) *Geochemistry, Groundwater and Pollution*. Balkema.

Beekmann H. E. and Appelo C. A. J. (1990) Ion chromatography of fresh- and salt-water displacement: Laboratory experiments and multicomponent transport modelling. *Journal of Contaminant Hydrology* **7**, 21-37.

Gaines G. L. and Thomas H. C. (1953) Adsorption studies on clay minerals. II. A formulation of the thermodynamics of exchange adsorption. *J. Chem. Phys.* **21**, 714-718.

Gapon E. N. (1933) Theory of Exchange Adsorption.V. *(in Russian). J. Gen. Chem. (USSR)* **3**, 667-669.

Gimernez E. and Morell I. (1997) Hydrogeochemical analysis of salinization processes in the coastal aquifer of Oropesa (Castellon, Spain). *Environmental Geology* **29**(1/2), 118-131.

Goldenberg L. C., Magaritz M., Amiel A. J., and Mandel S. (1984) Changes in hydraulic conductivity of laboratory sand-clay mixtures caused by a seawater-freshwater interface. *Journal of Hydrology* **70**, 329-336.

Gomis-Yagües V., Boluda-Botella N., and Ruiz-Beviá F. (1997) Column displacement experiments to validate hydrogeochemical models of seawater intrusions. *J. Cont. Hydrol.* **29**, 81-91.

Grasshoff K., Ehrhardt M., and Kremling K. (1999) Methods of Seawater Analysis, pp. 600. Wiley-VCH.

Magaritz M., Goldenberg L., Kafri U., and Arad A. (1980) Dolomite formation in the seawater-freshwater interface. *Nature* **287**, 622-624.

Magaritz M. and Luzier J. E. (1985) Water-Rock Interactions and Seawater-Freshwater Mixing Effects in the coastal dunes aquifer, Coos Bay, Oregon. *Geochimica Cosmochimica Acta* **49**, 2515-2525.

Merkel B. and Sperling M. (1996) *Hydrogeochemische Stoffsysteme, Teil 1.* DVWK-Fachausschuß "Grundwaserchemie".

Panteleit B., Kessels W., Kantor W., and Schulz H. D. (2001) Geochemical characteristics of salinization-zones in the Coastal Aquifer Test Field (CAT-Field) in North Germany. *SWICA-M3 Saltwater Intrusion and Coastal Aquifers.*

Parkhurst D. L. and Appelo C. A. J. (1999) PHREEQC for Windows - A Hydrogeochemical Transport Model. U.S.G.S.

Reardon E. J., Dance J. T., and Lolcama J. L. (1983) Field Determination of Cation Exchange Properties for Calcareous Sand. *Ground Water* **21**(4), 421-428.

Reilly T. E. and Goodman A. S. (1985) Quantitative Analysis of Saltwater-Freshwater Relationships in Groundwater Systems - A Historical Perspective. *Journal of Hydrology* **80**, 125-160.

Sposito G. (1984) *The Surface Chemistry of Soils*. Oxford University Press.

Sposito G. (1989) *The Chemistry of Soils*. Oxford University Press.

Stumm W. and Morgan J. J. (1995) *Aquatic Chemistry*. Wiley Interscience.

Tulipano L. and Fidelibus M. D. (1984) Geochemical charateristics of Apulian coastal springs (Southern Italy) related to mixing processes of ground waters with seawater having different residence time in to the aquifer. *5th interntaional conference on Water Ressources Planning and Management. Water in the year 2000.*

Vaughan D. J. and Pattrick R. A. D. (1995) *Mineral Surfaces*. Chapman & Hall.

TEIL IV Geochemical Processes in the Salt-Fresh Water Transition Zone – Exchanger Reactions in a 2D-Sand-Tank Experiment

Geochemical Processes in the Salt-Fresh Water Transition Zone – Exchanger Reactions in a 2D-Sand-Tank Experiment

B. Panteleit[1,2], W. Kessels[2], H. D. Schulz[1]
[1]University of Bremen, Klagenfurter Str., 28359 Bremen, Germany, pan@uni-bremen.de
[2]Leibnitz Institute for Applied Geosciences (GGA), Stilleweg 2, 30655 Hannover, Germany

Abstract

Most investigations concerning the subject of salt water intrusion into aquifers look mainly on either the physical density flow system or the geochemical aspects. The aim of a joint project at the Leibnitz Institute for Applied Geosciences is to combine both, geochemical processes and hydraulic aspects of seawater intrusion into a porous coastal aquifer system. For this purpose a Coastal Aquifer Test Field (CAT-Field) was established at the German North Sea coast. This study focuses on well known exchanger reactions during salt water intrusion. A 2D-sand-tank was build for the laboratory scale simulation of a density driven salt water intrusion into an aquifer system. As expected from previous investigations, products of exchanger reactions overlap and mask slower reactions, such as mineral dissolution and precipitation during the intrusion of salt water. Thus, the geochemistry of the porewater is characterised by the resulting salt concentration and the products of the exchanger processes. These results are compared and agree well with results of former column experiments using the same aquifer material and data of a computer simulation using PHREEQC (Parkhurst and Appelo, 1999).

1. Introduction

1.1. Salt water intrusion

Coastal regions all over the world are characterised by a high density of human settlements and their related industrial and agricultural activities. This is one reason for the high importance of coastal aquifers as a source for fresh water. The distribution of salt- and fresh water under natural conditions depends on soil parameters (mainly hydraulic permeability) as well as on climatic parameters (mainly precipitation) (Cooper, 1959; Oude Essink, 2001; Reilly and Goodman, 1985). In many regions excessive pumping as well as global mean sea level rise disturb the

natural equilibrium between salt and fresh water and lead to salt water intrusion (El-Baruni, 1995; Steinich et al., 1998).

From the chemical point of view the salt water intrusion represents a mixing of a high-salinity solution (seawater) and a dilute solution (fresh water) in a medium with many reactive solids (e.g. calcite, organic matter, clay minerals). In a detrital sedimentary aquifer, cation exchange is one of the most important geochemical processes taking place during salinisation (Appelo and Willemsen, 1987; Appelo et al., 1990; Panteleit et al., 2001b). Sometimes it is difficult to distinguish between exchanger and dissolution or precipitation processes like the reaction of carbonate minerals, sulfate reduction, etc. (Sposito, 1989). In any case these processes have a minor influence on the porewater chemistry during the beginning of the salt water intrusion, but are getting more important with increasing time and decreasing change of the salt concentration.

1.2. Exchanger Reactions

Electrical charges on the solid surface of the aquifer material are balanced by adsorbed ions from the aqueous phase. The occupation of the exchanger sites may be changed through substitution of one ion by another. Characteristic cation exchange reactions that are taking place during seawater intrusion are:

$$Mg^{2+} + CaX_2 \Leftrightarrow Ca^{2+} + MgX_2, \qquad K_{Mg/Ca} = \frac{[MgX_2][Ca^{2+}]}{[Mg^{2+}][CaX_2]} \tag{1},$$

$$K^{+} + 0{,}5\ CaX_2 \Leftrightarrow KX + 0{,}5\ Ca^{2+}, \qquad K_{K/Ca} = \frac{[KX][Ca^{2+}]^{0,5}}{[K^{+}][CaX_2]^{0,5}} \tag{2},$$

where X indicates the exchanging, electrically charged solid surface. Only the Gaines & Thomas notation of heterovalent exchange (Gaines and Thomas, 1953) is considered here, since previous investigations (Panteleit et al., 2001b) have shown its good validity for the CAT-Field study area. If the mass law is applied formally the affinity of the different ions can be expressed by the selectivity coefficient K. It must be pointed out that the selectivity coefficient represents not a constant value in a thermodynamic sense, but depends on the adsorbing material. As it can be seen from the equation 1 and 2 the occupation of the exchanger sites of a certain material depends mainly on the composition of the porewater. This is the reason for the

importance of the cation exchange process when the salt content of the liquid phase changes, for example during the intrusion of higher saline waters.

Besides the higher content of dissolved solids due to mixing effects, products of the exchanger reactions may effect the quality of the fresh water during a salt water intrusion (Appelo and Greinaert, 1991; Beekmann and Appelo, 1990; Martinez and Bocanegra, 2002). As described above the exchanger reactions depend on the composition of the solid phase. Even though the investigation area is considered representative for detrital coastal aquifers it shows some special features which effect the hydrological and chemical processes.

1.3. Investigation area

A sketch of the location and the geological setting of the CAT-Field is shown in Figure 1. The water conductive layers are mainly build up by fine sands and reach down to a depth of 200 m - 350 m below sea level (bsl). A speciality is a heavy

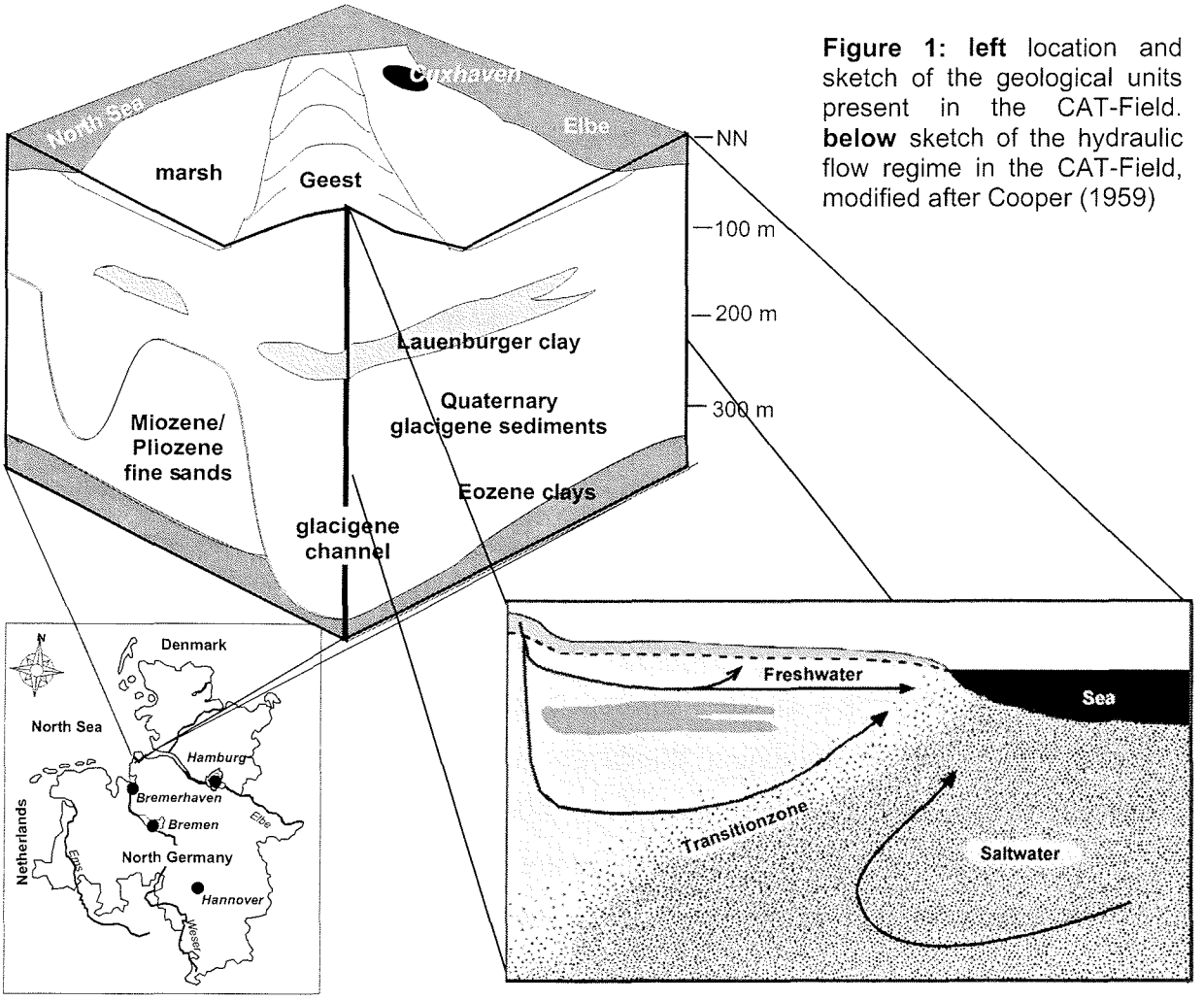

Figure 1: left location and sketch of the geological units present in the CAT-Field. **below** sketch of the hydraulic flow regime in the CAT-Field, modified after Cooper (1959)

mineral deposit in the pliocene layers (Besenecker et al., 1981; Elsner and Simon, 1994). Deep glacial erosion channels cut down to the aquifer base (Kuster and Meyer, 1979). They are refilled with partly coarse grained quaternary material from the Elster and Saale glaciations. The high hydraulic permeability of those coarse textured sediments will lead to a quicker change in the salt-fresh water distribution during a salinisation or freshening scenario (Vandenbohede and Lebbe, 2002). In most parts a low permeable layer (Lauenburger Clay) covers, or is intercalated into the galcigene series. In the flat topography of the marsh areas holocene terrestrial and tidal flat sediments can be found at the surface. These sediments have a higher content of clay, calcite and organic material (peat). Therefore they will affect the chemical reactions during a salinisation scenario by intensified exchanger processes due to a higher cation exchange capacity (CEC) and a possible calcite dissolution.

A sketch of the groundwater flow pattern in an orthogonal transect from the coast is shown in Figure 1. Slight ridges (the so called Geest) build up by glacigene-sandy deposits are the important groundwater recharge areas in the CAT-Field. From there the flow is directed towards the coast line. A natural salt water intrusion can be observed below the marsh areas (Siemon et al., 2001) and results in a groundwater flow pattern according to the typical Henry Problem (Henry, 1959). Dispersion and advection processes create a transition zone between salt- and fresh water with intermediate salt concentrations (Panteleit et al., 2001a). Due to the low permeable holocene sediments and to extensive drainage for agricultural and land saving purposes in the marsh areas no recharge, but upconing groundwater is found, as documented by a negative water balance (Friedhoff, 2001) and increasing hydraulic pressure heads with depth (Rifai, pers.comm.). For this reason in the CAT-Field the transition zone shows a lower inclination than expected under static conditions in this region (Fulda, 2002; Hahn, 1982).

2. Methods

2.1. Hydraulic simulation

A 2D sand tank experiment was developed, which simulates the hydraulic flow field in a laboratory scale and allows for the first time geochemical sampling in the salt-fresh water transition zone at the same time (Fig.2). The Plexiglas box (200 x 50 x 5 cm) consists of a sediment filled flow chamber with a storage chamber on each

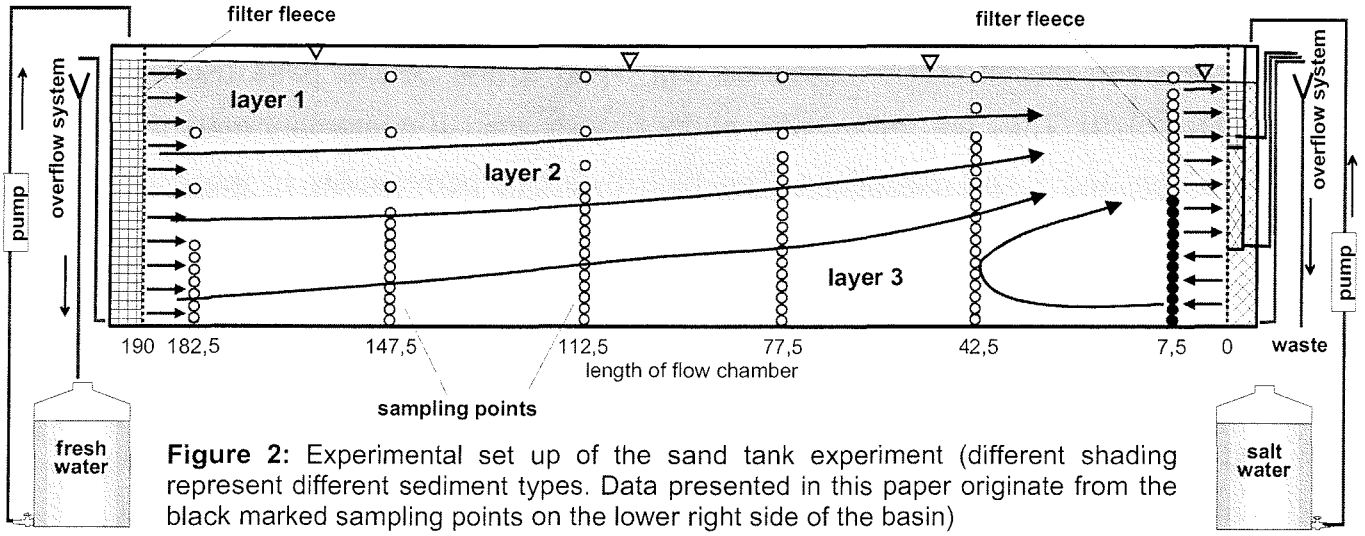

Figure 2: Experimental set up of the sand tank experiment (different shading represent different sediment types. Data presented in this paper originate from the black marked sampling points on the lower right side of the basin)

side. Two dimensionality is guaranteed by the flow chamber dimensions, the hydraulic gradient and homogenate packing of the sediment over the chamber thickness. The three compartments are separated by a filter fleece, which prevents the sediment from entering the storage chambers and also guarantees hydraulic contact. The flow chamber was filled with natural sediments recovered during the research drilling project in the CAT-Field (part 1; Binot et al., 2002). To minimise the odds to create inhomogeneities and air gaps in the repacked sediment, the chamber was filled in layers through a water column of about 2 - 3 cm. However, inhomogeneities could not be avoided totally. Similar to the natural setting of the aquifer system sediments from different layers of the quaternary deposits were build in (see part 1 and 5). The uppermost layer (layer 1) with a thickness of 0.15 m consisted of eemian and holocene tidal flat and marsh sediments. These are characterised by a high content of calcite and organic compounds. The lithogene component consist of silt and clay with only very small amounts of fine sand. The deeper part of the chamber (layer 3) was filled to 0.25 m with glacifluviatile sands from the Drenthe stage. The texture of these sediments ranges from fine sand to fine gravel. Almost no or very low amounts of fine mineral textures, organic or carbonate fractions are present. The intermediate layer (layer 2) is a mixture of the material from layer 1 and 3. It has a thickness of 0.10 m. In agreement of the physical properties of the different sediment types, the hydraulic conductivity should increase with depth. The flow chamber was covered with Plexiglas to minimise evaporation. Cation exchange capacity (CEC) and ion exchange coefficients of the sediment were

determined by CsCl-extraction (Reardon et al., 1983). The specific surface of the sediment was determined via the BET-method (Brunauer et al., 1938). Artificial water, prepared to match the chemical composition of the groundwater at the field site and equilibrated with calcite, was used as input water on the fresh water side. On the "seaside" artificial seawater synthesised according to Grasshoff et al. (1999) was used. It was spiked with uranine (disodiumfluoresceine) to provide a quick observation of the salt water intrusion. The water level in all chambers can be controlled separately by an overflow system. Two outflow chambers in the upper part of the salt water storage chamber avoid the intrusion of mixed water and guarantee a constant salt concentration of the intrusion water. The position of the intrusion zone depends on the hydraulic gradient. After a conditioning phase with artificial groundwater the level of the fresh water chamber was held constant, while the salt water level was raised stepwise through the adjustment of the overflow height of the salt water until a sufficient salt water intrusion appears. The fresh water flow follows the induced hydraulic gradient towards the "seaside" of the chamber, while the salt water intrudes mainly into in the lower part of the chamber due to it's higher density (Thorenz et al., in print).

2.2. Geochemical sampling

100 sampling sites are arranged in six lines at different intrusion lengths with up to 25 sample points at different depths (Fig.2). The sampling points consist of a soil moisture sampler, a porous polymer tube (diameter 2,5 mm) with a pore width of 1,1 µm which penetrates the whole chamber width of 5 cm. Because of the relative high sampling surface of almost 4 cm^2 the risk of sealing of the sampling sites due to fine material is minimised, while the small diameter keeps the disturbance of the hydraulic system low. For the same reason samples were taken permanently using a peristalitic pump and a self constructed auto-sampler. At the beginning of the experiment samples were taken simultaneously from 24 sites. After the transition zone developed only 12 points, lying in the transition from fresh- to salt water, were sampled. The position of the transition zone was controlled through the measurement of the uranine content in the samples. Samples were acidified immediately after sampling and later analysed by inductive coupled plasma atom emission spectroscopy (ICP-AES) for major cations (Na^+, Ca^{2+}, K^+, Mg^{2+}), for Li^+, Sr^{2+}, Ba^{2+},

K_f	m/s	7.25E -05
Porosity		0.25
Dispersivity	m	0.008
CEC	meq/kg	5.56

Table 1: Hydraulic parameters and CEC as used as input for the PHREEQC model

Ion	$K_{l/Ca}$ Determined by CsCl extraction	$K_{l/Ca}$ Medium as compiled by (Appelo and Postma, 1996)
Na^+	0.06	0.40
K^+	0.16	0.50
Mg^{2+}	0.73	0.64
Ca^{2+}	1	1

Table 2: Selectivity coefficients for the exchange of adsorbed Ca^{2+} by different ions (equation 1 & 2).

Mn^{2+}, Fe^{2+}, and for the anions sulfate and borate. Due to problems caused by interactions of the analysis system with the UV active tracer in the samples the chloride concentration has not been determined. Alkalinity (as described by Grasshoff et al. (1999)), pH and E_H were determined periodically from extra samples and in a final sampling event at all points immediately after sampling.

2.3. Numerical modeling

To quantify the resulting concentrations from exchanger reactions under idealised conditions a 1D numerical modeling was done using PHREEQC (Parkhurst and Appelo, 1999). For simulations no other reactions than the exchange between sodium, calcium, magnesium, potassium and lithium on the exchanger sites, a single exchanger site, horizontal flow and a homogeneous material was presumed. In a first step the exchanger processes for the deeper part of the flow chamber were modeled as a horizontal one dimensional intrusion into an isolated soil layer. Sediment depending input parameters stem from the modeling of column experiments with material of the similar origin (part 3; Panteleit et al., 2001a) and are displayed in table 1 and 2. The hydraulic slope changes with depth and depends on the position of the corresponding sampling point.

3. Results and Discussion

From the experimental salinisation of sediment columns it is known that exchanger processes determine the composition of the porewater (Appelo and Willemsen, 1987; Beekmann and Appelo, 1990). In a first step this conclusion will be evaluated for the present chamber experiment. The intrusion of salt water into the

flow chamber is documented by the sodium concentration. Also Na^+ is expected to be involved into the exchanger reactions. Comparing the CEC (5.6 µmol/g) with the Na^+ concentration of the intruding salt water (475 mmol/l) the error due to the amount of Na^+ attached to the exchanger sites seems to be negligible. This finding is supported by results and modeling of column experiments with diluted (20%) seawater (Panteleit et al., 2001b) and by the simulation of a horizontal intrusion into the sand tank. No significant differences between the modeled chloride and Na^+ concentration curves can be seen (Fig.3a). Furthermore the Na^+ concentration correspond well with the theoretical total cation equivalent concentration (TEC) indicating a conservative mixing of fresh- and seawater (Fig.3c). A slightly negative deviation at medium salt concentrations might be caused by the mentioned Na^+ depletion due to exchanger processes, but in general an almost linear curve with a regression coefficient of 0,9993 results. This shows that chemical processes result at

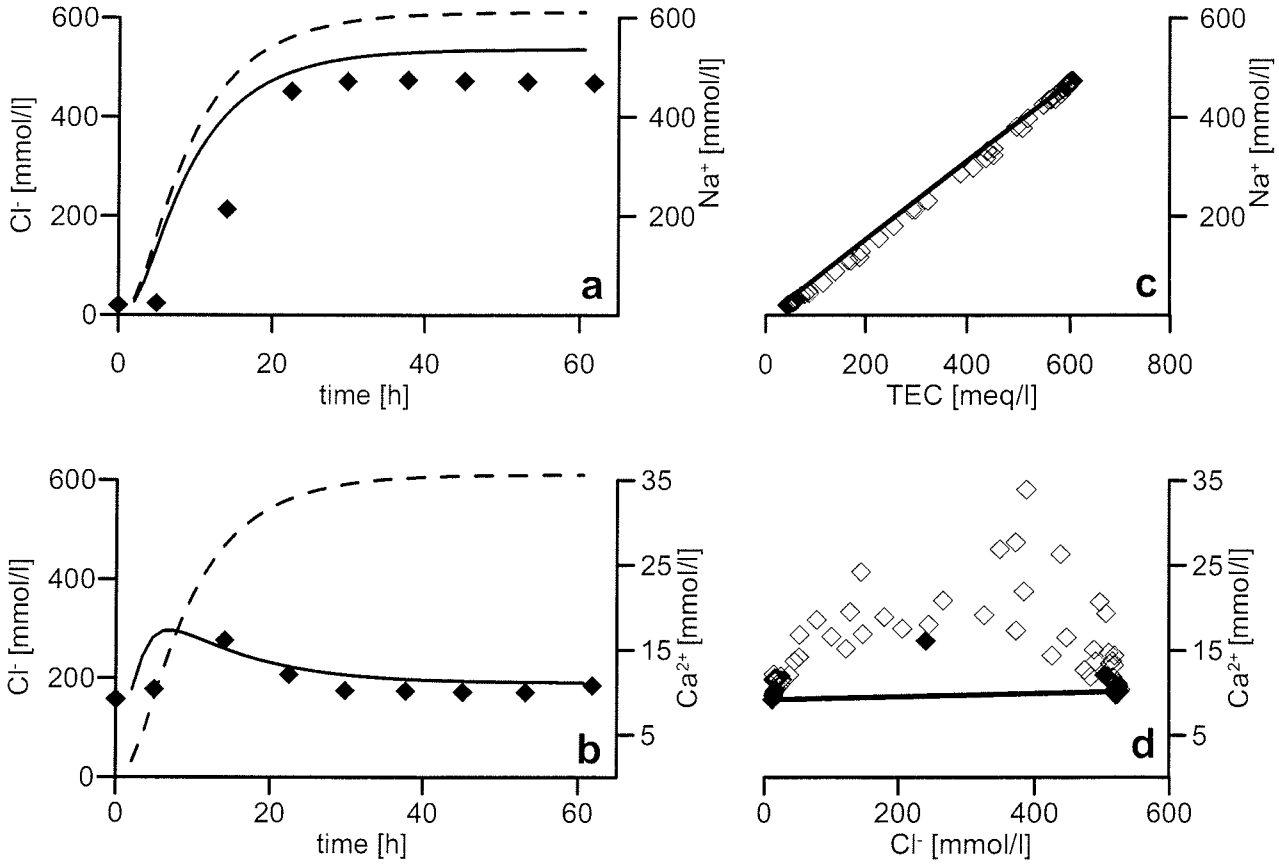

Figure 3: a,b Concentration changes during a horizontal salt water intrusion into the chamber measured at depth of 41 cm (diamonds = measured data of Na^+ (a) and Ca^{2+} (b), resp.; lines = modeled data, dashed line for Cl^-, solid lines for Na^+ and Ca^{2+}, resp.) **c,d** Na^+ (c) and Ca^{2+} (d) vs. Cl^- (calculated) concentrations for all sampled depths (diamonds, filled symbols represent data from Fig.4a,b) and theoretical conservative mixing concentrations (line)

most in a qualitative change of the TEC. Since precipitation or dissolution processes would cause a quantitative change of the TEC, which is not apparent in our data, it is concluded that these processes are of minor importance, while ion exchange dominate during the salt water intrusion. For the following discussion of the exchange of major cations a theoretical Cl^- concentration, calculated by the charge difference between the analysed TEC and the anions (sulfate and alkalinity) is used.

$$[Cl^-_{calc}] = TEC - 2 * [SO_4^{2-}] - [HCO_3^-] \quad (3)$$

Figure 4a displays the change of the concentration of Na^+ in the bottom section as measured at the first sampling profile (see black marked sampling points in Fig.2) over the experimental time. Salt water intrudes from the right side and is indicated by high Na^+ concentrations (red). In general the level of the salt water rises continuously up to a certain level that represents equilibrium. Based on a higher content of fine material and the corresponding lower hydraulic permeability at about 45 cm, the salt water increase is delayed.

The exchanger reactions occurring during the intrusion of the salt water are evident in the concentration behaviour of calcium (Fig.4b). Assuming that the Na^+ distribution reflects the salt water intrusion, it is obvious that the Ca^{2+} concentration increases initially, it drops down after about 25 hours and reaches the salt water concentration at about 35 hours. Ca^{2+} is the dominating cation (42,6 meq%) in the fresh water. The selectivity coefficients from literature and the CsCl-extraction (Tab.2) reflect a high affinity of Ca^{2+} for the exchanger sites. Consequently the negative surface charges of the sediment particles are predominantly occupied by Ca^{2+} ions. With increasing salt contend the Ca^{2+} ratio in the porewater decreases down to 3.3 meq%. As the occupation of the exchanger sites is always in balance with the porewater composition, Ca^{2+} is released from the exchanger sites during salinisation although it shows a greater affinity than the ions which are to be adsorbed (K^+, Na^+, Mg^{2+}). The release of Ca^{2+} results in a temporal maximum in the Ca^{2+} concentration between 10 and 20 hours of the experiment (Fig.4b).

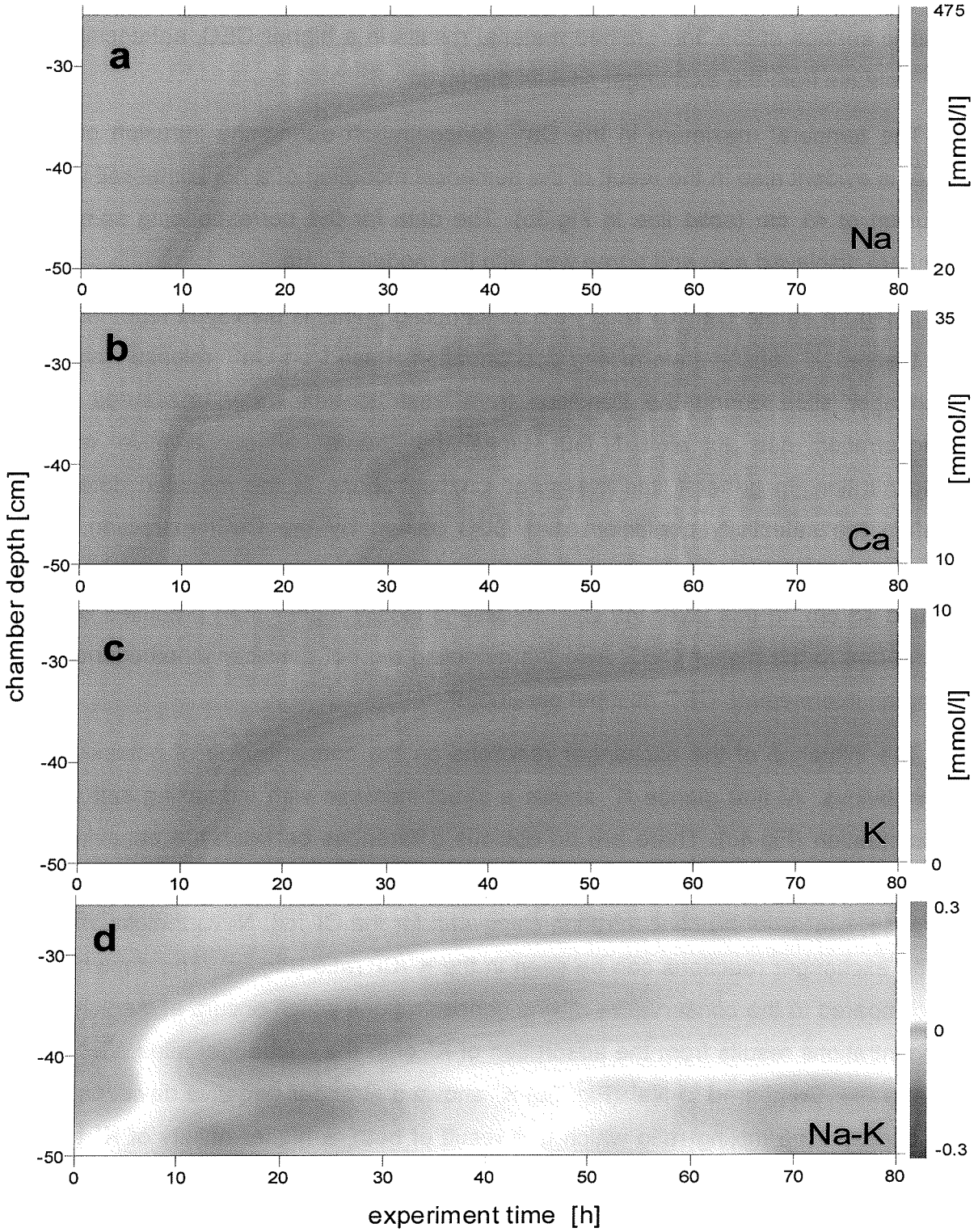

Figure 4: a-c Change of concentrations of different ions with depth and time for the sampling points highlighted in Fig.3; **d** Difference between the normative concentrations of Na^+ and K^+; displayed are changes with depth and time.

A peak concentration was measured at about 45 cm depth. As mentioned above, a higher content of fine materials, respectively clay, is present in this layer. The higher specific surface of the fine grained material results in a higher CEC, enhancing the Ca^{2+} release from the exchanger sites in this layer.

The temporal maximum in the Ca^{2+} concentration during the intrusion of salt water is evident also in the result of the numerical modeling of a horizontal salt water intrusion at 41 cm (solid line in Fig.3b). The data for the corresponding sampling point are displayed also and agree well with the modeled data.

In Figure 3d the Ca^{2+}/Cl^- ratio from all sampling points is displayed together with the theoretical conservative mixing concentration. Based on Ca^{2+} release from the exchanger sites during the transition from fresh to salt water, measured Ca^{2+} concentration rise to almost four times the theoretical conservative mixing concentration. In general, the measured concentrations fit the modeled data and confirm the selectivity coefficient and CEC gained by the CsCl extraction. The measured data in Figure 3d originate from the sampling points at a chamber depth of around 45 cm. In this layer the Ca^{2+} release is locally higher than predicted by the model due to the higher CEC. Also the modeling did not consider inhomogeneities, using an intermediate CEC as input parameter.

The influence of the exchanger reactions on the concentration of potassium is less obvious. At first glance K^+ shows a direct increase with increasing salt water concentration (Fig.4c). There are no obvious differences between the behaviour of Na^+ and that of K^+. Also the modeled concentration (Fig.5a) shows an immediate increase, similar to the concentration calculated for the Cl^- ion. Nevertheless, effects of the exchanger reactions can be seen in the K^+/Cl^- ratio (Fig.5c). The depletion of K^+ compared to the conservative mixing concentrations which occurs at medium salt concentrations results from the adsorption of K^+ onto the exchanger sites after Ca^{2+} is released. Compared to Na^+ (Fig. 3c) K^+ shows a stronger negative deviation from the conservative mixing ratio which is a result of both, a higher affinity of K^+ to the exchanger sites, and a higher influence of this process on the lower K^+ concentration. This can also be seen by a comparison of the two dimensional data of Na^+ and K^+ (Fig.4d). For this figure, the maximum concentrations of the ions were set to one, while the minimum concentrations were set to zero. The difference

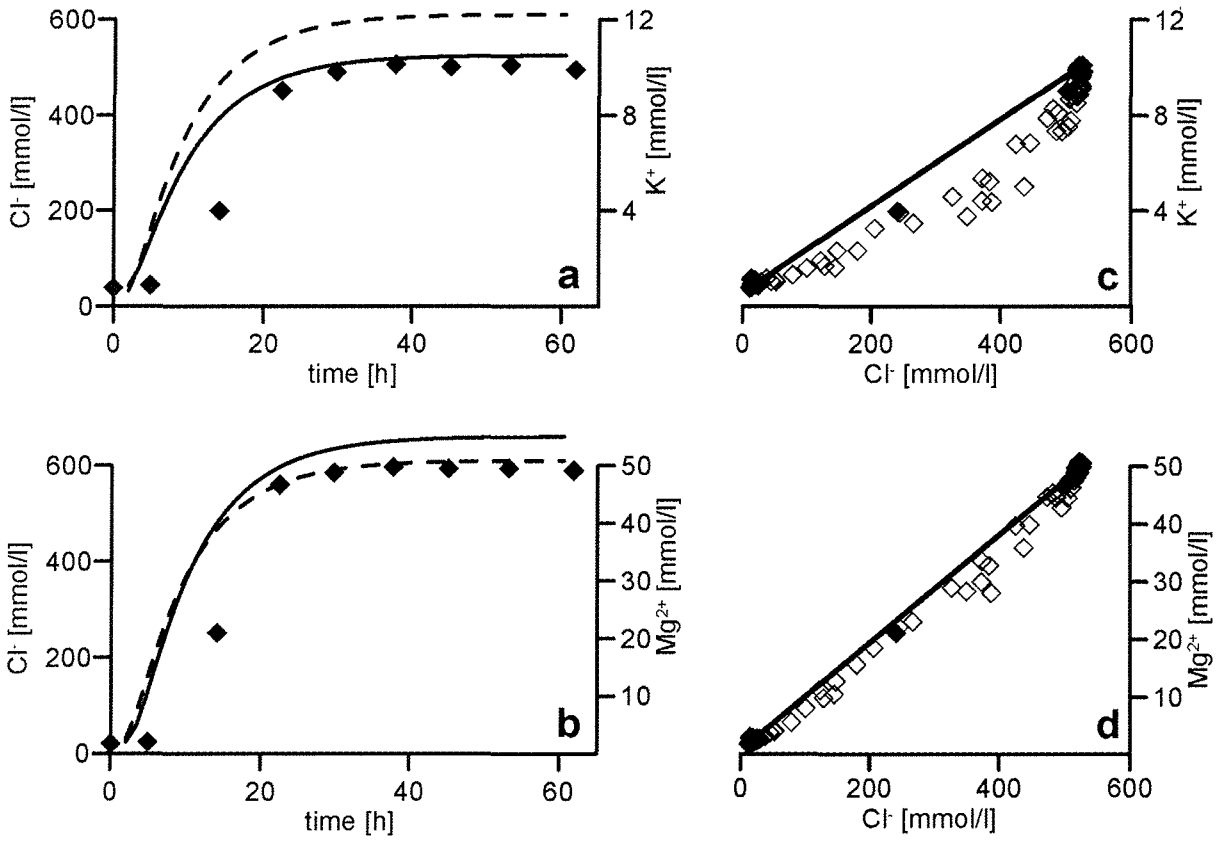

Figure 5a,b:Concentration changes during a horizontal salt water intrusion into a chamber, measured at depth of 41 cm (diamonds = measured data of K^+ (a) and Mg^{2+} (b),resp.; lines = modeled data; dashed line = Cl^- solid line K^+ and Mg^{2+}, resp.) **c,d**: K^+ (c) and Mg^{2+} (d), resp. vs. Cl^- (calculated) concentrations for all sampled depths (diamonds, filled symbols represent identical data as in Figure 6a,b) lines represent the theoretical conservative mixing concentrations (line)

between the normative Na^+ and K^+ concentrations, clearly shows that during salt water intrusion the increase of K^+ is retarded compared to that of Na^+ (red and yellow colours in Fig.4d). The K^+/Na^+ ratio reflects conservative mixing only before (green between zero and 10 hours) and after (green after 70 hours) the influence of exchanger processes dominate.

The higher affinity of K^+ compared to Na^+ results from a smaller hydration shell of water molecules that stick to the K^+ ion. The higher affinity is also expressed in published exchange coefficients and in data from the CsCl-extraction (Tab.2). Here K^+ shows a 2.8 times higher affinity than Na^+.

Magnesium is another element which might be affected by exchanger processes. It also shows an almost conservative concentration increase over time in the modeling and experimental data (Fig.5b & 6a). When presenting Mg^{2+} versus Cl^- (Fig.5d) measured data indicate a slight depletion compared to the conservative

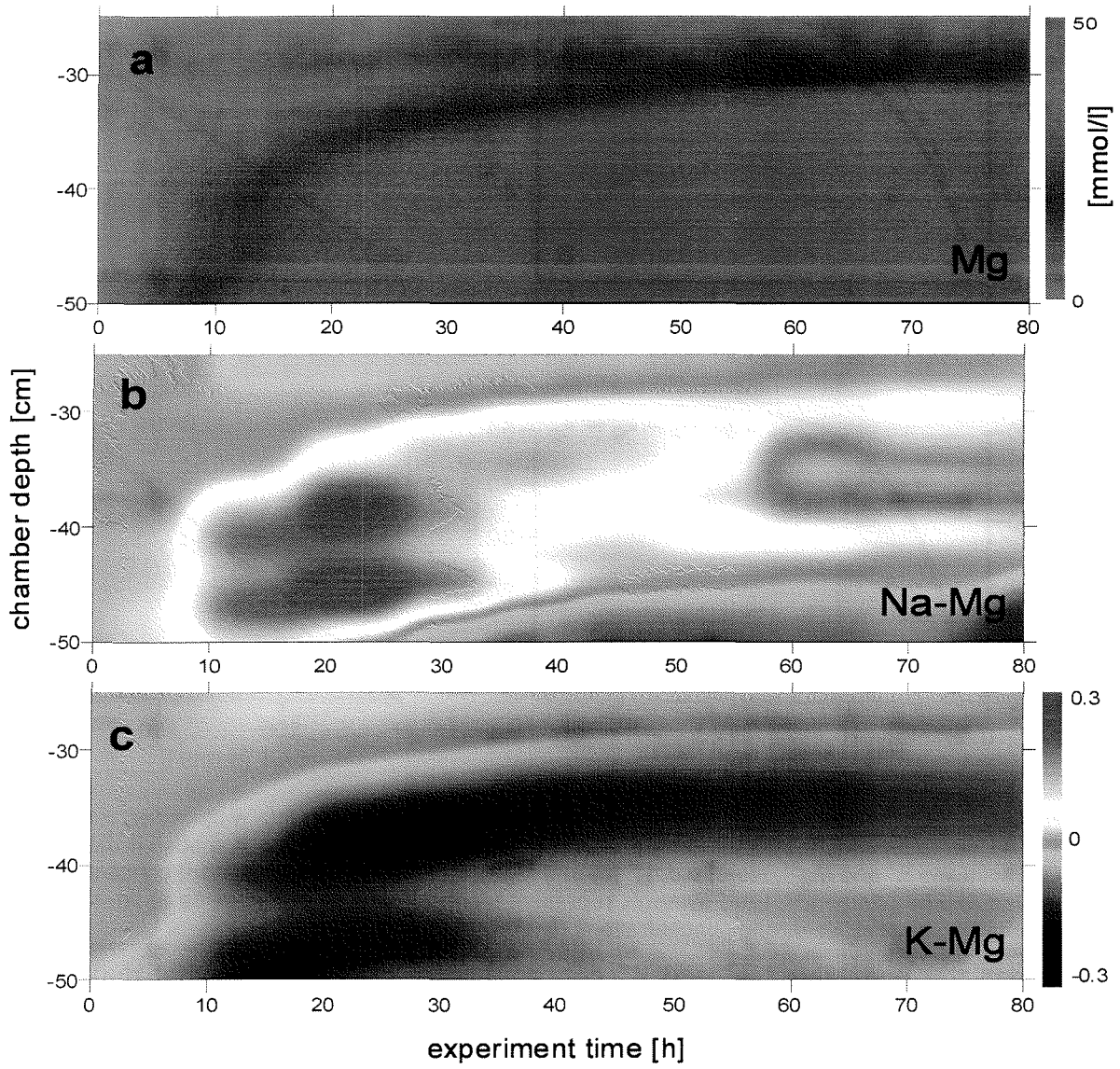

Figure 6a Change of Mg^{2+} concentration over time and depth ; **b,c:** Differences of normative concentrations between Na^{+}-Mg^{2+} and K^{+}-Mg^{2+}, displayer are their changes with depth and time of the experiment.

mixing ratio (line). To visualise this in the 2D diagram, the difference between the Na^{+} and Mg^{2+} concentrations is used (Fig.6b). The higher affinity of Mg^{2+} as well as its lower concentrations compared to Na^{+} result in observed stronger retention of Mg^{2+}. Comparing the Mg^{2+} and K^{+} concentrations similarly (Fig.6c), the rapid increase of the Mg^{2+} concentration apparently mask its higher affinity compared to K^{+} (Tab.2). However, a chemical process that is in contradiction to the selectivity coefficients may be possible. Hahn (1972) describes that two independent, but opposite processes may occur simultaneously during salinization, the release of

Mg^{2+} from exchanger sites and the uptake of Mg^{2+} with the formation of clay minerals. Furthermore, concentrations of K^+ from former column experiments showed an enhanced sorption compared to the prediction by the PHREEQC model (Panteleit et al., 2001a). A retardation of the K^+ breakthrough curve was also noticed by Beekmann and Appelo (1990). A possible mechanism for this might be the the incorporation of K^+ into newly formed clay minerals. Alternatively, a multi site exchanger can be considered, which has not been registered by the CsCl-extraction. But with respect to the good agreement of the modeled concentrations and the experimental data, the retention of K^+ generally could be caused by the concentration difference of K^+ and Mg^{2+}.

4. Conclusions and Outlook

Results from a 2D simulation of a salt water intrusion into an aquifer system show a linear increase of the total cation equivalent concentration, confirming the hypothesis that exchanger processes dominate during salt water intrusion. The concentration of Ca^{2+} shows a maximum due to its release from the exchanger sites, while the share of Ca^{2+} in the porewater decreased with increasing influence of the salt water. Whith salt water intrusion cations which are enriched in seawater (Na^+, K^+, Mg^{2+}) are adsorbed to exchanger sites. As a result the concentration of these species in the porewater becomes depleted. The intensity of the depletion of the different ions corresponds in general to the measured selectivity coefficients used as input parameters for one dimensional numeric modeling. Discrepancies between modeled and experimental data can be explained by inhomogeneities in the sediment packing of the flow chamber. The formation of clay minerals probably effects the concentration profiles of Mg^{2+} and K^+ due to enhanced adsorption of these species. This will be studied in a future experiment, during which a steady state with a stable position of the intrusion front will be developed. With stagnation of the salinization process exchanger reactions will become less important and the formerly masked effects from mineral formation and dissolution are expected to become more important for the porewater composition. These reactions will be effective until a complete equilibrium between the porewater and the solid phase establishes for the different areas of the fresh salt water transition zone.

References

Appelo C. A. J. and Greinaert W. (1991) Processes Accompanying the Intrusion of Salt Water. In *Hydrogeology of Salt Water Intrusion - A Selection of SWIM Papers* (ed. W. D. Breuck), pp. 291-303. Heise.

Appelo C. A. J. and Postma D. (1996) *Geochemistry, Groundwater and Pollution*. Balkema.

Appelo C. A. J. and Willemsen A. (1987) Geochemical Calculations and Observations on Salt Water Intrusions. 1. A Combined Geochemical/Mixing Cell Modell. *Journal of Hydrology* **94**, 313-330.

Appelo C. A. J., Willemsen A., Beekmann H. E., and Griffioen J. (1990) Geochemical Calculations and Observations on Salt Water Intrusions. 2. Validation of a Geochemical Model with Laboratory Experiments. *Journal of Hydrology* **120**, 225-250.

Beekmann H. E. and Appelo C. A. J. (1990) Ion chromatography of fresh- and salt-water displacement: Laboratory experiments and multicomponent transport modelling. *Journal of Contaminant Hydrology* **7**, 21-37.

Besenecker H., H. v. D. C., Hofmann W., Höhndorf A., Knabe W., and Kuster H. (1981) Horizontbeständige Schwermineralanreicherungen in pliozänen Sanden des niedersächsischen Küstenraumes. *Geologisches Jahrbuch* **D 49**, 23 S. 9 Abb. 9 Tab.

Binot F., Druivenga G., Eckard H., Fulda C., Große K., Grossmann E., Höltscher F., Kantor W., Kessels W., Neuß M., Panteleit B., Rifai H., Suckow A., and Wonik T. (2002) Forschungsbohrung Cuxhaven Lüdingworth 1 und 1A CAT-LUD 1 und CAT-LUD 1A - Ergebnisse, Vol. GGA-Report # 121 520. Leibnitz Institute for Applied Geosciences (GGA-Institut), Germany.

Brunauer S., Emmett P. H., and Teller E. (1938) Adsorption of gases in multimolecular layers. *Journal of Physical Chemistry* **60**, 309-319.

Cooper H. H. (1959) A hypothesis concerning the dynamic balance of fresh water and salt water in a coastal aquifer. *Journal of Geophysical Research* **64**(4), 461-467.

El-Baruni S. S. (1995) Deterioration of quality of groundwater from Suani wellfield, Tripoli, Libya. *Hydrogeological Journal* **3**(2), 58-64.

Elsner H. and Simon P. (1994) Midlum-Holssel Heavy Metal Deposit in Northwestern Germany. *Angewandte Geologie* **40**(1), 25-30.

Friedhoff T. (2001) Wasserhaushaltsuntersuchungen im tiedebeeinflussten Einzugsgebiet der Medem (Land Hadeln). Diplomarbeit, Hochschule Bremen.

Fulda C. (2002) Numerische Studie zur Salz-/Süßwasserverteilung im Rahmen der Cuxhavener Forschungsbohrung. *Mitteilungen der Deutschen Geophysikalischen Gesellschaft* **Sonderband II**, 10-26.

Gaines G. L. and Thomas H. C. (1953) Adsorption studies on clay minerals. II. A formulation of the thermodynamics of exchange and adsorption. *J. Chem. Phys.* **21**, 714-718.

Grasshoff K., Ehrhardt M., and Kremling K. (1999) Methods of Seawater Analysis, pp. 600. Wiley-VCH.

Hahn J. (1972) Diagenetisch bedingte Veränderungen im Chemismus intrudierter Meerwässer und ihre Beziehungen zum Chemismus von Tiefengrundwässern in Nordwestdeutschland. *Geologisches Jahrbuch*(90), S.245-264.

Hahn J. (1982) Grundwasserbeschaffenheit bei Aquiferen in Lockergesteinen in Nordostniedersachsen, Anthropogene Einflüsse auf die Grundwasserbeschaffenheit in Niedersachsen., pp. 145-159. Inst. Stadtbauwesen, Technische Universität Braunschweig.

Henry H. R. (1959) Salt Intrusion into Fresh-Water Aquifers. *Journal of Geophysical Research* **64**(11), 1911 -1919.

Kuster H. and Meyer K.-D. (1979) Glaziäre Rinnen im mittleren und nordöstlichen Niedersachsen. *Eiszeitalter u. Gegenw.* **29**, 135-156.

Martinez M. E. and Bocanegra E. M. (2002) Hydrochemistry and cation-exchange processes in the coastal aquifer of Mar Del Plata, Argentinia. *Hydrogeology Journal* **online**(s10040-002-0195-7).

Oude Essink G. H. P. (2001) Improving fresh groundwater supply-problems and solutions. *Ocean & Coastal Management* **44**(5-6), 429-449.

Panteleit B., Binot F., Kessels W., Schulz H. D., and Kantor W. (2001a) Geological and geochemical characteristics of a salinization-zone in a Coastal Aquifer. In *New Approaches Characterising Goundwater Flow*, Vol. 2 (ed. K.-P. Seiler and S. Wohnlich), pp. 1237-1241. A.A.Balkema.

Panteleit B., Kessels W., Kantor W., and Schulz H. D. (2001b) Geochemical characteristics of salinization-zones in the Coastal Aquifer Test Field (CAT-Field) in North Germany. *SWICA-M3 Saltwater Intrusion and Coastal Aquifers*.

Parkhurst D. L. and Appelo C. A. J. (1999) PHREEQC for Windows - A Hydrogeochemical Transport Model. U.S.G.S.

Reardon E. J., Dance J. T., and Lolcama J. L. (1983) Field Determination of Cation Exchange Properties for Calcareous Sand. *Ground Water* **21**(4), 421-428.

Reilly T. E. and Goodman A. S. (1985) Quantitative Analysis of Saltwater-Freshwater Relationships in Groundwater Systems - A Historical Perspective. *Journal of Hydrology* **80**, 125-160.

Siemon B., Sengpiel K.-P., Rehli H.-J., Röttger B., and Eberle D. (2001) Identification of Saltwater Intrusions in Coastal Aquifers Using the BGR Helicopter-borne Geophysical System. *SWICA-M³ 2001*.

Sposito G. (1989) *The Chemistry of Soils*. Oxford University Press.

Steinich B., Escolero O., and Martin L. E. (1998) Salt water intrusion and nitrate contamination in the valley of Hermosillo and El Sahaural coastal aquifers, Sonora, Mexico. *Hydrogeological Journal* **6**(4), 518-526.

Thorenz C., Kosakowski G., Kolditz O., and Berkowitz B. (in print) An Experimental and Numerical Investigation of Saltwater Movement in Coupled Saturated/Partially-Saturated Systems. *Water Ressources Research*.

Vandenbohede A. and Lebbe L. (2002) Numerical modelling and hydrochemical characterisation of a fresh-water lens in the Belgian coastal plain. *Hydrogeology Journal* **online**(DOI 10.1007/s10040-002-0209-5).

TEIL V Geochemical Processes in the Salt-Fresh Water Transition Zone – Comparing Results of a Sand Tank Experiment with Field Data from the Coastal Aquifer Test Field at the German North Sea Coast

Geochemical Processes in the Salt-Fresh Water Transition Zone – Comparing Results of a Sand Tank Experiment with Field Data from the Coastal Aquifer Test Field at the German North Sea Coast

B. Panteleit[1]; K. Hamer[1]; R. Kringel[2]; W. Kessels[2]; H.D. Schulz[1]

[1]University of Bremen, Dep. of Geosciences, PB 330440, 28334 Bremen, Germany
[2]Leibnitz Institute for Applied Geosciences, Stilleweg 2, 30655 Hannover, Germany

Abstract

Geochemical processes, occurring in a stable transition zone between salt and fresh water, were simulated in a 2D, multi layer flow chamber experiment. Mixing, calcite dissolution and oxidative degradation of organic matter were identified as the main controlling factors. The results of the chamber experiment were compared to field data and verified by thermodynamic modeling. Similarity in most ion distributions suggest the general applicability of the experimental method. Differences in the redox conditions between field and experiment were reflected by the oxidants involved in the mineralisation of organic carbon: while field data show evidence of sulfate reduction, the presence of oxygen in the laboratory experiment resulted in the reoxidation of sulfides.

1. Introduction

This study was conducted within an interdisciplinary project of the Leibnitz Institute of Applied Geosciences. The aim of the project is to develop a dynamic hydrogeochemical model of a Coastal Aquifer Test Field (CAT-Field, (Kessels et al., 2000), supported by geophysical measurements. The CAT-Field is located at the German North Sea coast between the Elbe and Weser river estuaries (Fig.1). The goal of this study was to characterise the geochemical processes in the salt-fresh water transition zone in the CAT-Field and to verify them by means of an 2D laboratory simulation experiment, which provides well defined boundary conditions and intense sampling possibilities.

The 2D flow chamber experiment represents a geological section inland from the coastline (Panteleit et al., 2002). The first phase of the experiment simulated exchanger reactions during the intrusion of salt water into a sand tank (Panteleit et al., 2003). After the intrusion of the salt water a stable position of the salt-fresh water interface established. Diffusion and dispersion processes expand the initially sharp

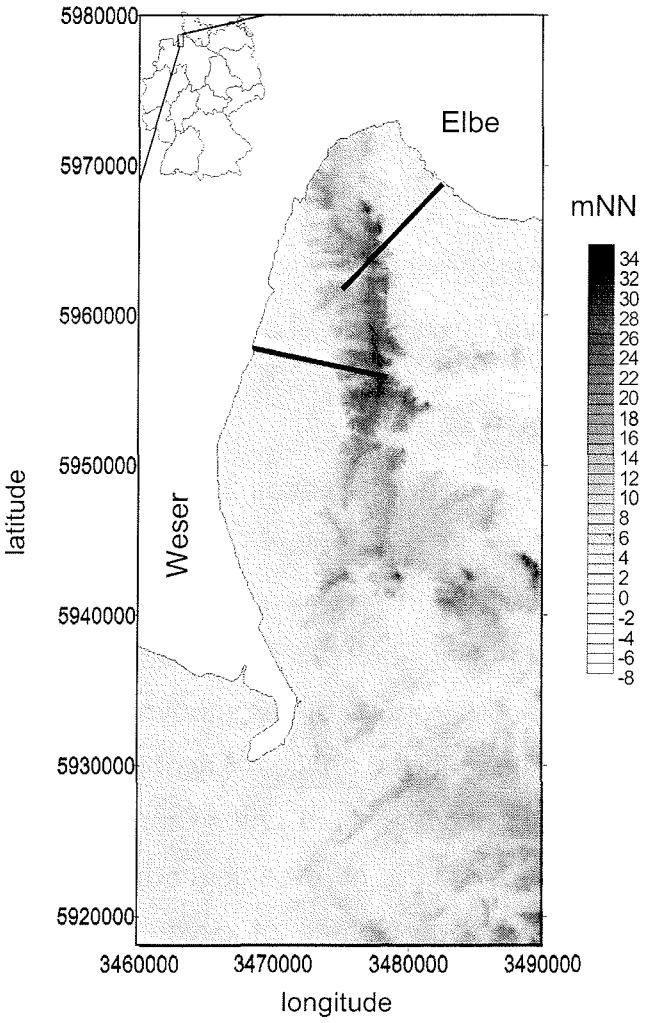

Figure 1: Position and topography (mNN) of the CAT-Field, bordered by the mouths of the rivers Elbe and Weser. The Geest ridge, acting as groundwater recharge area, is characterised by darker colours from north to south in the centre of the CAT-Field. Geological transects, to which the set-up of the chamber experiment refers, are indicated as lines. (source: DGM 50; LVM Niedersachsen, Fulda 2002)

interface into a zone of transition between the two end member water types. As shown from column experiments (Panteleit et al., 2001b), subsequent to hydrochemical disequilibrium slow geochemical processes occur in the transition zone. This paper compares field data collected in the area of investigation with results of the experimental simulation. Geochemical processes in both systems will be characterised, verified by thermodynamic modeling and discussed.

2. Method

2.1. Field methods

In several field campaigns during 2001 and 2002 hydrochemical field samples were collected from a network of 51 screened wells and 26 geological drills in the CAT-Field (part 1). Most wells are between 10 and 70 m in depth. Among them there are also four multi level well clusters and a fully screened research well with a depth of 120 m (Binot et al., 2002; Panteleit et al., subm.).

A vertical flow-through cell was employed to accommodate probes used for the simultaneous determination of pH, E_H, dissolved O_2, temperature and electric conductivity (EC) for all wells. The chamber was flooded from below using a diver pump (Grundfos MP1). Final measurements were recorded after equilibration of the measuring probes. Samples were passed through a 40 µm cellulose filter and either acidified (nitric acid), stored untreated, or immediately titrated for alkalinity (Cook and Miles, 1980).

For the analysis of porewater about 200 g field fresh sediments from cores, previously stored at 4° C, were centrifuged for 12 minutes at 2000 U/min to separate the porewater. E_H and pH of these porewater samples were measured potentiometricly. Due to the small sample volume alkalinity was determined by Gran titration (Grasshoff et al., 1999). The remaining sample volume was acidified with nitric acid for later cation analysis.

Cation analysis were performed by inductive coupled plasma atom emission spectroscopy (ICP-AES; Perkin Elmer, Optima 3000) for Na^+, Ca^{2+}, K^+, Mg^{2+}, Li^+, Sr^{2+}, Ba^{2+}, Mn^{2+} and Fe^{2+}. ICP-AES was also used to measure the elements Bor and Sulfur which are present in the anions BO^{3-} and SO_4^{2-}. Chloride was determined by high pressure liquid chromatography (HPLC; tsp P100 with a Kratos Spectroflow 773 absorbance spectrometer).

2.2. Laboratory simulation

For the laboratory scale simulation of the hydraulic and geochemical processes in the salt-fresh water transition zone a 2D sand tank experiment as shown in Figure 2 was designed. The sand tank itself consists of a sediment filled flow chamber of 1.90 m length, 0.50 m height, and 0.05 m width. The chamber was covered with a Plexiglas lid to minimise evaporation. To reproduce the geochemical environment encountered in the field, material from different layers of the aquifer was used to fill the flow chamber. These materials were collected from sediment cores during drilling in the investigation area (Binot et al., 2002; Panteleit et al., subm.). The chamber was filled in three layers using different sediment types to simulate the natural conditions (Fig.2). The uppermost layer (layer 1) with a thickness of 0.15 m consisted of eemian and holocene tidal flat and marsh sediments. These are characterised by a high content of calcite and organic compounds. The lithogene component consist of silt and clay with only very small amounts of fine sand. Accordingly the hydraulic

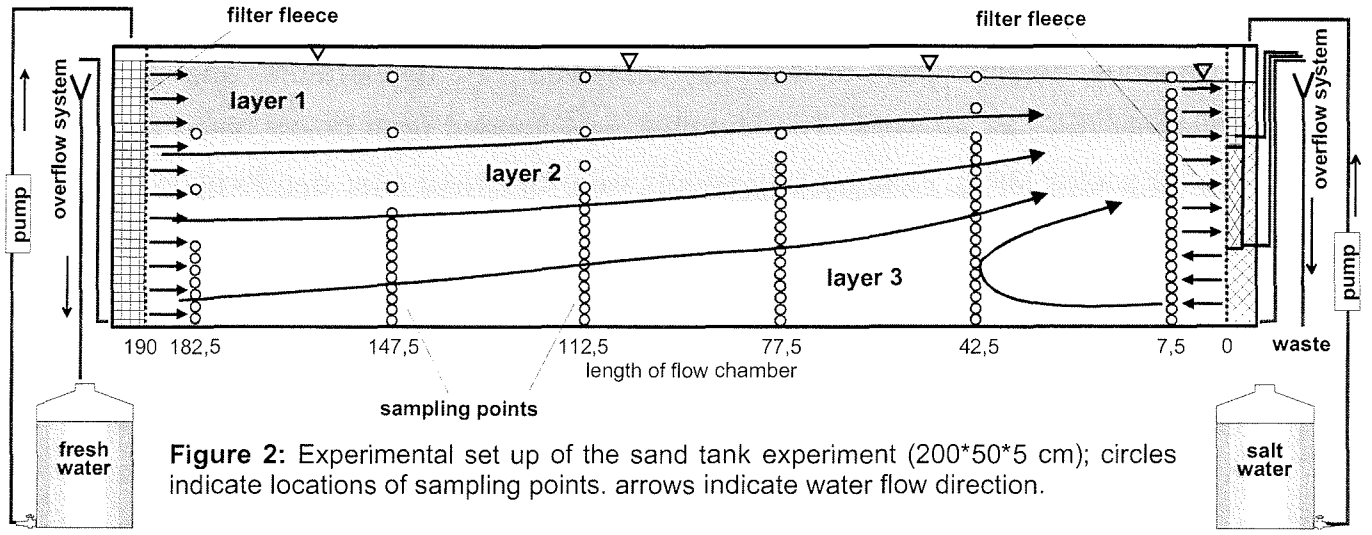

Figure 2: Experimental set up of the sand tank experiment (200*50*5 cm); circles indicate locations of sampling points. arrows indicate water flow direction.

	material	genesis	TIC g/kg	red S mmol/kg	LOI %	Kf m/s	nat. extension m below surface
Layer 1	silt & clay	tidal flat deposits	10	250	13.8	3.5*10-5	1-25
Layer 3	fine sand – fine gravel	glaciofluviatil	0,3	50	1.9	2.8*10-3	25- >90

Table 1: Hydrogeochemical characterisation of the aquifer layers used for the 2D flow chamber experiment (TIC = total inorganic carbon; red S = reduced sulfur compounds; LOI = loss on ignition)

conductivity (Kf-value), as estimated from sieve analysis according to Beyer (1964) is rather low (Tab.1). The deeper part of the chamber (layer 3) was filled to 0.25 m with glacifluviatile sands from the Drenthe stage. The texture of these sediments ranges from fine sand to fine gravel. Almost no or very low amounts of fine mineral textures, organic or carbonate fractions are present. The intermediate layer (layer 2) is a mixture of the material from layer 1 and 3. It has a thickness of 0.10 m.

Each side of the flow chamber is bordered by a water storage chamber (hatched in Fig.2). Two outflow chambers in the upper part of the salt water storage chamber avoid the intrusion of mixed water and ensure a constant salt concentration of the intrusion water. A filter fleece installed between the chambers prevented relocation of sediment while ensuring good hydraulic contact. To control the flow regime the water level in all four chambers can be adjusted separately through an overflow system. The inflow water on the fresh water side was artificially mixed and saturated with respect to calcite, simulating the groundwater composition from field samples as displayed in Table 3. Salt water was synthesised according to Grasshoff et al. (1999), diluted to the highest chloride concentration measured at the coastline of the CAT-Field, and also calcite saturated (Tab.5). The salt water was spiked with uranine

(disodiumfluoresceine) to allow a quick observation of the salt content of the porewater in the flow chamber.

An initial fresh water conditioning phase was followed by the salt water intrusion phase (part 4). A second conditioning phase lasted 9 weeks, during which a stable position of the transition zone between salt and fresh water established, while a constant hydraulic gradient of 3 mm/m was maintained in the chamber. The experimental design generates an overall discharge of about 90 ml/h for the three layers. At the end of the second conditioning phase porewater was sampled at 100 locations in the flow chamber. The sampling sites were arranged in 6 depth profiles, located at different intrusion lengths. Each depth profile had up to 25 sampling depths (Fig.2). At each point a soil moisture sampler was installed, that consisted of a porous polymer tube (diameter 2,5 mm) with a pore diameter of 1,1 µm. Polymer tubes penetrated the whole sediment and chamber width of 0.05 m, amounting to a relatively high sampling surface of almost 4 cm^2 per sampler. Thus the risk of disturbance of the hydraulic system and sealing of the sampling probes due to clogging was minimised. Samples were taken from top to bottom using a 10 ml syringe for each sampler. Water samples were treated as the extracted water from the sediment cores.

2.3. Thermodynamic modeling

Thermodynamic calculations were performed using the PHREEQC computer program (Parkhurst and Appelo, 1999). For a specification of equilibrium states between aqueous and solid phase, saturation indices (SI=log(ion activity in water sample/ion activity in equilibrium)) were determined for the analysed groundwater compositions. Analysed fresh water compositions were modified by stepwise implementation of the identified reactions (mixing, equilibration with the carbonate system, sulfate reduction and exchanger reactions).

3. Results

3.1. Field data

Typical concentrations for different ions analysed from the field samples are presented in Table 2 (detailed analysis data are given in the appendix).

species	pH	EH [mV]	Ca^{2+} [ppm]	Na^{+} [ppm]	Mg^{2+} [ppm]	K^{+} [ppm]	HCO_3^{-} [ppm]	SO_4^{2-} [ppm]	Cl^{-} [ppm]	log(pCO_2)
fresh water	7,1	90	17,0	15,0	41,0	11,8	575,0	134,0	45,0	-0,6
deep $NaHCO_3$ water	6,3	3,4	28,0	56,4	7,3	38,3	207,4	0	60,4	-2,3
shallow $NaHCO_3$ water	7,0	160	64,0	547,4	65,6	5,0	1318	28,8	461,5	-0,3
salt water	7,9	330	200,0	3301	396,1	133,0	237,9	864	6159	-1,3

Table 2: Typical concentration of major components for different water types as analysed from field samples

The distribution of cation and anion mixing ratios from field samples are shown in Figure 3 and Table 3. Data range from typical fresh water to seawater compositions. Major cations in fresh water are Ca^{2+} and Mg^{2+}, HCO_3^{-} is the major anion, while SO_4^{2-} and Cl^{-} are of minor importance. In a rough classification as indicated in Figure 3, the fresh waters are of the $CaHCO_3$ type. Water samples of typical seawater composition are of a NaCl type. The transition between these two water types is not linear but tends towards a $NaHCO_3$ type with Na^{+} and K^{+} contributing up to 81% of the total cation equivalent concentration ($TEC=\Sigma(n*X^{n+})$). HCO_3^{-} contributes 79% of the total anion equivalent concentration ($AEC=\Sigma(n*X^{n-})$), while almost no SO_4^{2-} was detected.

3.2. Laboratory experiment

Mixing ratios of water samples from the laboratory experiment are presented in relation to the field data (Fig.3). For a better comparison with field data extreme values are displayed in Table 3. Depending on the sampling location in the flow chamber, either Ca^{2+} or Na^{+} is the dominating cation, while Mg^{2+} reaches up to 22 % only. The anion triangle shows that SO_4^{2-} and Cl^{-} are the predominant species. HCO_3^{-} shares are in principle below 20% and negligible in samples with a high Cl^{-} content.

For the interpretation of the data and the identification of the major processes the spatial distribution of ion concentration (grey scale) and percentage (isolines) are essential. Figure 4a displays the joint distribution of Na^{+} and Cl^{-}. The salt water intrusion is indicated by a Cl^{-} concentration of more than 200 mmol/l. At the bottom of

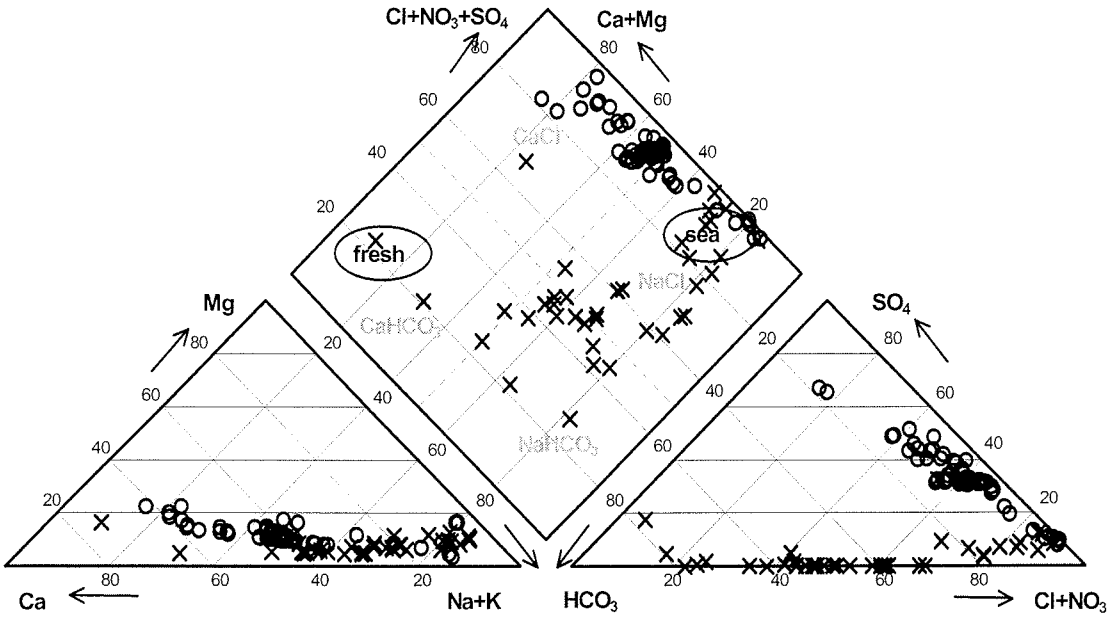

Figure 3: Piper plot of field samples (crosses) and experimental data (circles) from a flow chamber experiment. Typical compositions of sea- and fresh water and a rough classification of water types (dashed lines) are included into the middle diagram.

		Ca^{2+}	Mg^{2+}	$Na^{+} + K^{+}$	HCO_3^{-}	SO_4^{2-}	Cl^{-}
field	Min %	5	3	10	2	0	3
	Max %	76	18	83	78	19	84
Lab	Min %	3	3	17	0	8	17
	Max %	62	22	84	19	66	92

Table 3: Extreme values in the partitioning of ion composition from field and laboratory data.

the flow chamber the Cl^{-} intrusion reaches half of the flow chamber length. At the salt water inlet it reaches two third of the height. Na^{+} shows a similar distribution and so do the mixing ratios of both ions compared to the anion equivalent concentration and the cation equivalent concentration, respectively.

Ca^{2+} shows a more complex distribution (Fig.4b). High concentrations in both, the salt water dominated area and in the upper pleisto-holocene layers can be observed. In salt water affected pleisto-holocene layers Ca^{2+} concentrations reach up to a maximum of 45 mmol/l. Lowest concentrations were found in the galcigene sand under fresh water conditions. The observed distribution of the Ca^{2+} mixing ratio results mainly from changes in the Na^{+}/Ca^{2+} ratio. Since the Mg^{2+} content does not change significantly (Fig.3), thus the Ca^{2+} mixing ratio is equivalent to the inverse Na^{+} mixing ratio.

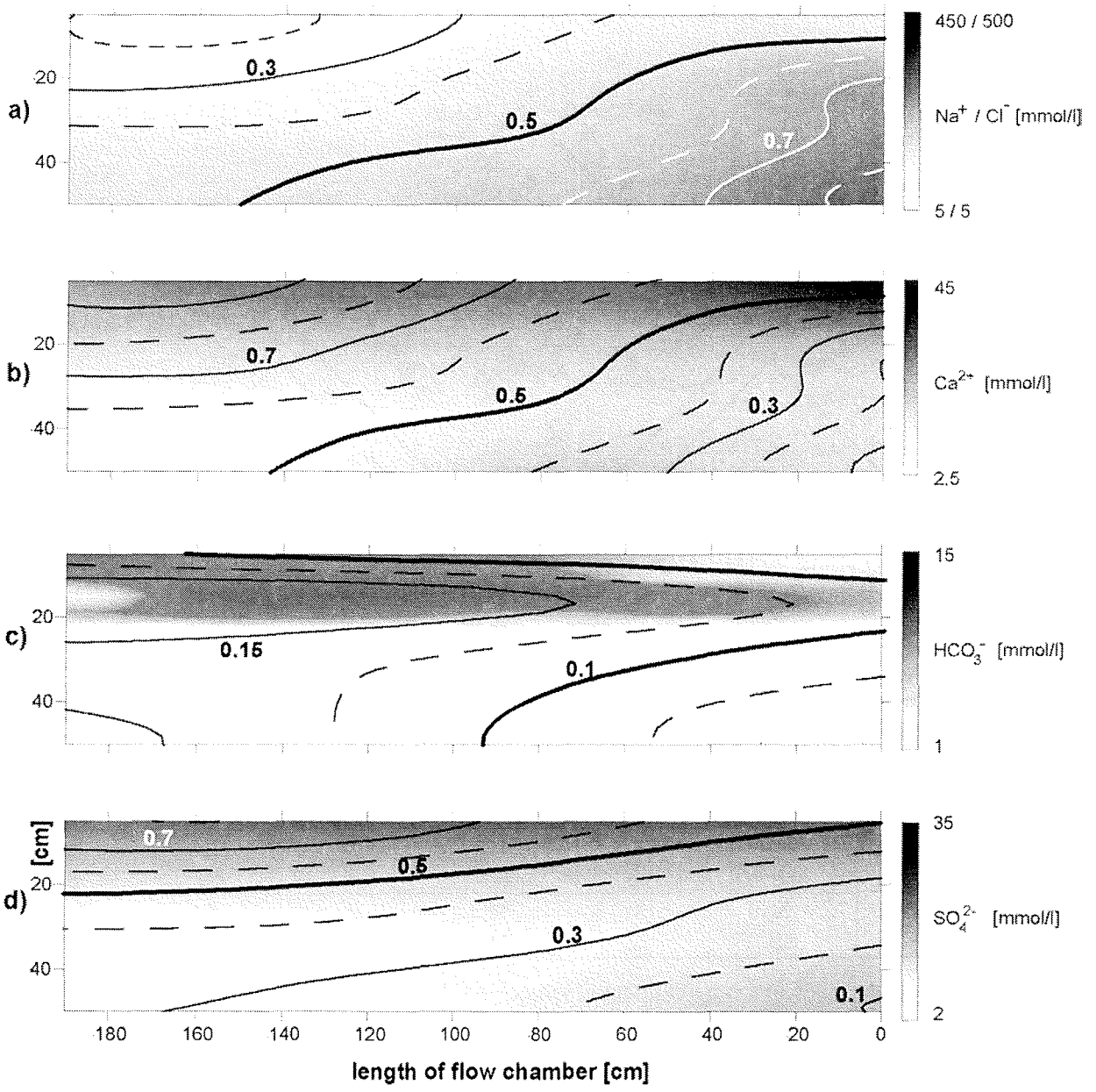

Figure 4: Spatial distribution of different ions in the flow chamber with the mixing zone in a steady state and at a stable position. Grey scale represents effective concentrations in mmol/l, lines indicate ion shares of the total cation and anion equivalent concentration, respectively.

The distribution of major anions is more complex than that of the cations. The distribution of HCO_3^- is displayed in Figure 4c. The concentration is highest (up to 15 mmol/l) in the upper layer of the pleisto-holocene sediments. In the transition layer measured HCO_3^- concentrations still reach 8 mmol/l, while in absence of the pleisto-holocene sediments a steep concentration decrease down to 1 mmol/l occurs. In the glacigene sands a slight HCO_3^- concentration increase towards the salt water dominated side is observed, though values do not rise above 2 mmol/l. The HCO_3^- /AEC ratio distribution delivers a different pattern. In the salt water dominated part

HCO_3^- has a low ratio of 0-5 %, while in the fresh water dominated part ratios up to 18 % are reached. In both regions the derived ratios are higher in the pleisto-holocene layer than in the layers containing glacigene sands.

The absolute concentration of SO_4^{2-} is highest (32.0 mmol/l) in the pleisto-holocene layers and decreases with depth (Fig.4d). In the deeper layers the SO_4^{2-} concentration correlates with the Cl^- concentration, resulting in higher values (26.4 mmol/l) in the salt water dominated side compared to the fresh water side (2.1 mmol/l). The SO_4^{2-}/AEC ratio is highest close to the surface at the fresh water side, and decreases with depth and towards the salt water side.

4. Discussion

4.1. Field Processes

The Piper plot in Figure 3 shows ion mixing ratios that are characteristic for fresh and seawater. Field samples from wells located inland match the typical ratios for fresh water, while samples from the coastal area resemble seawater. Considering a conservative mixing for the transition from seawater to fresh water, the data should plot on the conservative mixing line in between these two end member water types as indicated in Figure 5. Ion mixing ratios of field samples from the CAT-Field differ from this conservative mixing line towards higher Na^+ and HCO_3^- content (Fig.3) Typical groundwater samples from the CAT-Field (Tab.2) are indicated in Figure 5.

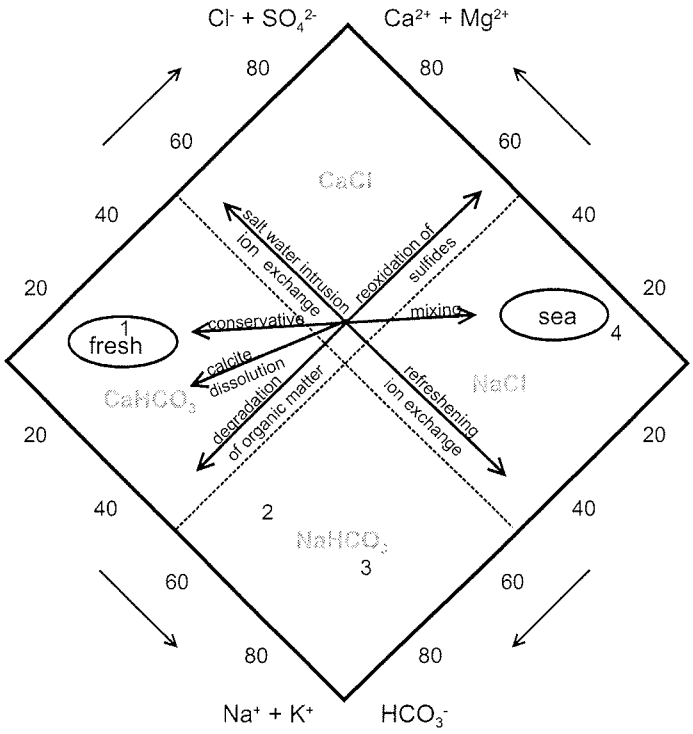

Figure 5: Piper plot showing typical compositions for fresh – and seawater and a rough classification of water types. Numbers indicate typical water samples from the CAT-Field (Tab.3). Arrows indicate reaction pathways as discussed in the text.

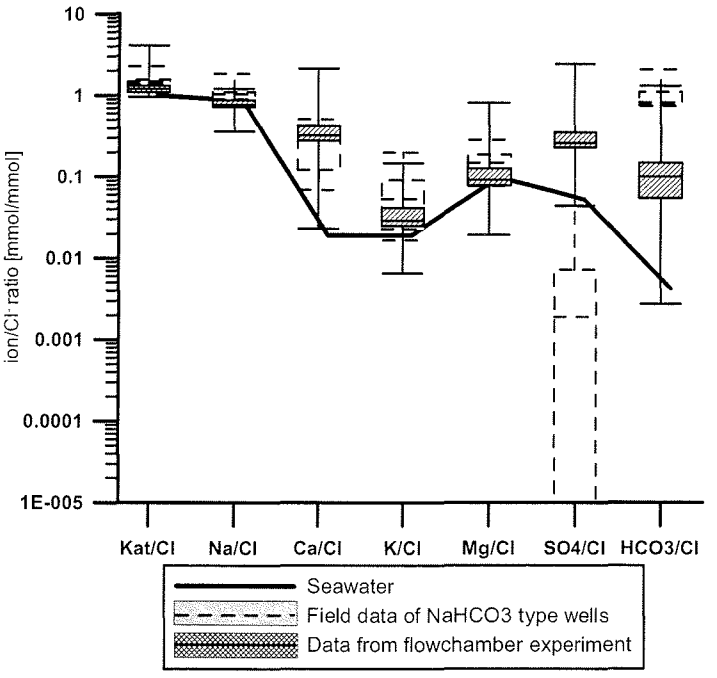

Figure 6: Ion/chloride ratios for different ions of the $NaHCO_3^-$ type field samples and samples from the flow chamber experiment compared to typical seawater ratios (line). Fat line in box indicates mean of samples, box edges are 1st and 3rd quartiles, bars are minimum and maximum values. Ratios above the seawater value indicate an ion releasing process (as for Ca^{2+}; HCO_3^- and experimental SO_4^{2-}), ratios below the seawater value a consuming process (SO_4^{2-} field data)

Sample 2 originates from the glacigene layers in a depth of 17.5 m, while sample 3 was collected in the holocene layers (4.5 m depth). Chemical processes that are alterating the hydrochemistry of the water result from conservative mixing, calcite dissolution, sulfate reduction and exchanger reactions. These different processes are calculated using PHREEQC (Parkhurst and Appelo, 1999), their effects will be discussed separately in the following.

4.1.1. Mixing

The effect of mixing on the hydrochemistry can be derived from the measured Cl^- concentration, since Cl^- is supposed to behave conservative. This is done in a first step of the thermodynamical calculations. The Cl^- concentration of fresh groundwater was adapted to that of the selected samples (2 and 3 in Fig.5) by adding salt water with a factor of 0.067 and 0.0023, respectively.

4.1.2. Calcite dissolution

The dissolution of calcite is a process which is often found to alterate the chemical composition of groundwater in coastal aquifers (Custodio and Bruggeman, 1987). Sediment cores from the CAT-Field show varying calcite content, but calcite is present in all layers down to 60 m. Shelfs of conches can be found in the quaternary layers of marine origin (tidal flat sediments), while glacigene sediments contain disperse calcite (Binot et al., 2002). The increased Ca^{2+}/Cl^- ratio compared to the seawater value of 0.019 (Fig.6) clearly indicates a Ca^{2+} releasing process. The

dissolution of calcite would increase the concentration of dissolved carbon species as well as the Ca^{2+} concentration (equation 1).

$$CaCO_3 + H_2O \rightarrow Ca^{2+} + HCO_3^{2-} + OH^- \quad (1)$$

This process affects the concentration of both, cations and anions. Accordingly, this reaction moves the sample projection in the Piper diamond more or less to the left (Fig.5). Thus the tendency of the samples towards a $NaHCO_3$ type can not be explained by the calcite dissolution alone.

One driving force for the dissolution of calcite is the ionic strength effect. According the Debye-Hückel theory (Atkins 1990) the activity coefficient depends non linearly on the ionic strength. Therefore a mixture of two water types, both initially equilibrated with respect to calcite, may be undersaturated after mixing. Another driving process is the reaction with carbonic acid (H_2CO_3). Water, equilibrated with respect to calcite under the atmospheric CO_2 pressure ($10^{-3.5}$ atm), enters the aquifer. There it is exposed to a higher CO_2 partial pressure in the soil air, which results from respiration of organic matter. According to the new equilibrium conditions additional protons may associate with the carbonate-ion that is released from calcite to form bicarbonate (Appelo and Postma, 1996), leading to the overall reaction

$$CaCO_3 + CH_2O + O_2 \rightarrow Ca^{2+} + 2HCO_3^- \quad (2).$$

Sanford and Konikow (1989) calculated the expected calcite dissolution or precipitation rate for different CO_2 pressures, temperatures and fresh - seawater mixing ratios. Their thermodynamic calculations showed that calcite dissolution is most significant in mixtures containing less than 50% seawater. Supersaturation results for solutions with a composition closer to seawater. But even from supersaturated solutions with a saturation index of up to 0.3, the precipitation of calcite might be inhibited by the presence of magnesium, organic acids or phosphate. The later two affect precipitation even at concentrations below 1 µmol/l (Berner, 1975; Berner et al., 1978; Reddy, 1977; Tomson, 1983; Walter and Hanor, 1979). However, for typical samples from the CAT-Field (Tab.4) a calcite dissolution is clearly indicated by the negative saturation indices that are resulting from thermodynamic calculations (Tab.4).

The effect of calcite dissolution upon the mixtures of fresh and salt water was calculated in a second step (Tab.4, column 3). Each sample was assumed to be in

	fresh water (1)	calculated stepwise reaction				sampled water	salt water (4)
species		step 1: mixing of fresh and salt water	step 2: equilibration with calcite and pCO_2	step 3: oxidation of C_{org} by SO_4^{2-} reduction	step 4: exchanger equilibration	$NaHCO_3$ water (4.5 m depth) (3)	
pH	7.1	7.1	6.24	6.25	6.25	7	7.9
EH [mV]	90	860	915	-150	-150	160	330
Ca^{2+} [ppm]	177.0	178.4	401.6	322.3	352.2	64.0	200
Na^{+} [ppm]	15.0	232.8	232.8	232.8	219.5	547.4	3301
Mg^{2+} [ppm]	41.0	63.7	63.7	63.7	72.3	65.6	396.1
K^{+} [ppm]	11.8	19.5	19.5	19.5	19.0	5.0	133
HCO_3^{-} [ppm]	575.0	529.5	1167	1204	1203	1318	237.9
SO_4^{2-} [ppm]	134.0	180.5	180.5	**28.8**	**28.8**	28.8	864
Cl^{-} [ppm]	45.0	**434.2**	**434.2**	**434.2**	**434.2**	461.5	6159
$log(pCO_2)$	-0.6	-1.46	**-0.3**	**-0.3**	**-0.3**	-0.3	-1.3
SI calcite	-0.56	0.22	**0**	**0**	**0**	-0.69	-1.04
SI gypsum	-1.34					-2.41	-1.00
SI dolomite	-1.64					-1.24	-1.63
SI pyrite		-247.22	-245	12.85	12.85		
mixing ratio		0.067				0.067	
species	fresh water (1)	step 1: mixing of fresh and salt water	step 2: equilibration with calcite and pCO_2	step 3: oxidation of C_{org} by SO_4^{2-} reduction	step 4: exchanger equilibration	$NaHCO_3$ water (17.5 m depth) (2)	salt water (4)
pH	7.1	7.1	7.6	7.63	7.63	6.3	7.9
EH [mV]	90	860	830	-250	-250	3.4	330
Ca^{2+} [ppm]	177.0	176.9	66.4	43.2	75.8	28	200
Na^{+} [ppm]	15.0	23.0	23.0	23.0	21.4	56.4	3301
Mg^{2+} [ppm]	41.0	41.8	41.8	41.8	23.4	7.3	396.1
K^{+} [ppm]	11.8	12.1	12.1	12.1	10.9	38.3	133
HCO_3^{-} [ppm]	575.0	551.7	227.7	265.0	265.4	207.4	237.9
SO_4^{2-} [ppm]	134.0	135.7	135.7	**1.0**	**1.0**	0	864
Cl^{-} [ppm]	45.0	**59.3**	**59.3**	**59.3**	**59.3**	60.4	6159
$log(pCO_2)$	-0.6	-1.46	**-2.3**	**-2.3**	**-2.3**	-2.3	-1.3
SI calcite	-0.56	0.3	**0**	**0**	**0**	-0.38	-1.04
SI gypsum	-1.34					-5.98	-1.00
SI dolomite	-1.64					-1.25	-1.63
SI pyrite		-246.5	-248	12.6	12.06		
mixing ratio		0.0023				0.0023	

Table 4: Concentrations of typical water samples from the CAT-Field are shaded grey, numbers in brackets refer to the position of the sample projection in Fig.4. Concentrations derived from thermodynamic calculations using PHREEQC (Parkhurst and Appelo, 1999) are presented for several calculation steps. Bold printed parameters were fitted to match field concentrations.

equilibrium with the calcite present in the sediment, and the local CO_2 pressure as measured at the well location. In case of sample (3), which originates from the organic rich holocene layer, calculations suggest calcite dissolution as a result of the high CO_2 partial pressure of $10^{-0.3}$ atm. For the sandy glacigene layer (sample 2), the low CO_2 partial pressure of $10^{-2.3}$ atm results in a calculated calcite precipitation, since the mixed solution was slightly supersaturated with respect to calcite (SI = 0.3).

But with respect to the discussed inhibition of calcite precipitation and the Ca^{2+}/Cl^- ratio in the field samples, precipitation of calcite in the CAT-Field aquifer seems to be unlikely. However, for model calculations the calcite precipitation is the most important process with respect to the concentrations of Ca^{2+} and HCO_3^-, approaching the concentrations of the corresponding sample.

4.1.3. Sulfate reduction

Besides calcite dissolution, the mineralisation of organic carbon (simplified as CH_2O) is another source for HCO_3^- in the pore water of sediments. The organic matter in the system investigated here is mainly present in the Pleisto - Holocene layers (Tab.1). The mineralisation product CO_2 dissolves in water and converts to carbonic acid according to the present equilibrium conditions. For the oxidation of organic matter an oxidant is required. In the very upper layer this will be oxygen from the atmosphere or dissolved in the pore water:

$$CH_2O + O_2 \rightarrow CO_2 + H_2O \rightarrow H^+ + HCO_3^- \quad (3)$$

Fine sediments in the upper layer hamper the deep penetration of atmospheric gases. The upconing of groundwater was already expected for the marsh areas (Fulda, 2002). This is supported by the field data (Tab.4), as no fresh, oxidising groundwater is recharged in the CAT-Field. The suboxic conditions are reflected in the low E_H values and high iron concentrations of the samples that are taken in a depth of 4.5 m. After all oxygen has been consumed by aerobic respiration, anaerobic micro organisms as e.g. a bacteria of the genus Desulfovibrio may gain energy from dissimilatory sulfate reduction (Jørgensen, 1982; Kasten and Jørgensen, 2000). The products of sulfate reduction are a broad range of reduced sulfur species, which may be precipitated in a number of metastable metal sulfide minerals, and finally transformed and immobilised to pyrite (Morse et al., 1987). Equation 4 summarises the system of sulfate reduction reactions:

$$2CH_2O + SO_4^{2-} \rightarrow 2CO_2 + 2H_2O + S^{2-} \rightarrow H_2S + 2HCO_3^- \quad (4)$$

The oxidation of organic carbon through sulfate reduction or oxidative respiration affect the anion mixing ratios in the Piper plot only. With respect to the Piper diamond of Figure 3 these reactions would result in a shift of the sample projection parallel to the cation axis (Fig.5). Source of SO_4^{2-} is seawater, where concentrations are generally two orders of magnitude higher than in fresh water (Bowen, 1979). SO_4^{2-} is delivered from sea salt, entrained in the air from the nearby North Sea surface and

precipitated onto the uppermost layer in the CAT-Field, or added to deeper layers of the aquifer by seawater intrusion. Accordingly, samples with a high Cl^- content, which represent samples close to the shoreline, have the highest SO_4^{2-} concentrations. The SO_4^{2-}/Cl^- ratio of $NaHCO_3$ type field samples (Fig.6) lie well below the typical value for seawater of 0.05, indicating that the decreasing SO_4^{2-} content is not due to conservative mixing only.

Decreasing SO_4^{2-} concentrations are typical for regions with seawater intrusion (Magaritz and Luzier, 1985; Mercado, 1985; Nadler et al., 1980). Since the decrease can not be explained by conservative mixing only, it suggests reduction processes as a sulfate sink. The cited authors assign the decrease of sulphate to degradation of organic matter through sulphate reducing bacteria. In contrast, Gomis-Yagües et al. (2000) discuss gypsum precipitation and dissolution as factor resulting in the decrease of SO_4^{2-} concentration during seawater intrusion. They admit that usually the activities that are reported for SO_4^{2-} and Ca^{2+} from groundwater samples taken in seawater intrusion studies do not reach the solubility product for gypsum. Thus the gypsum precipitation can only occur if additional Ca^{2+} will be available through ion exchange reactions. In the CAT-Field the Ca^{2+}/Cl^- ratio increased (Fig.6), however thermodynamic calculations suggest that gypsum precipitation is not possible, because the saturation indices are negative for all field samples (Tab.4). This confirms the former conclusion mentioned before that an active intrusion of salt water can be excluded for the CAT-Field. Consequently, no excessive release of Ca^{2+} from exchanger sites occurs. On the other hand, in the CAT-Field conditions appear to be favourable for microbiological sulfate reduction:

In the pleisto-holocene layers a high amount of organic matter is present (Tab.1). According to equation 4, 0.6 mmol/l CH_2O (which equals to 7.2 mg/l DOC) are necessary to balance the observed sulfate concentration decrease, which averages 0.3 mmol/l SO_4^{2-}. Since samples show a DOC content of 5 - 50 mg/l sufficient reactive organic matter seems to be available to facilitate the SO_4^{2-} reduction process.

According to the energy budget, sulfate reduction only takes place if no other oxidants that would deliver more energy are present (Froelich et al., 1979). The E_H values of <180 mV (Tab.3) in the samples indicate that the lack of suitable oxidants

in pore water of the Pleisto - Holocene layers in the CAT-Field support SO_4^{2-} reduction.

The produced H_2S should be able to form iron sulfide minerals, consequently excess Fe^{2+} should be available and the iron sulfides detectable. Own data (Tab.1) as well as investigations from Dellwig et al. (2001) proofed the presence of pyrite and reduced sulfur in sediment cores from the region. Measured iron concentration in the groundwater suggest the supply of Fe^{2+} through the fresh water flow. The notwithstanding low pyrite content can be explained by reoxidation processes (Lowson, 1982; Schulz et al., 1994), resulting in a more complicated model than the straight Froelich scheme (Froelich et al., 1979). According to Giblin and Howarth (1984) an oxidative dissolution of iron sulfides in coastal regions could be induced by salt water flushing and plant activity. In any case, the characteristic foul smell was noticed easily during the drilling works, giving a qualitative detection of the presence of H_2S.

Data of stable isotope ratio would deliver a definite proof for the SO_4^{2-} reduction pathway, since during microbiological SO_4^{2-} reduction ^{32}S is preferentially consumed rather than the heavier ^{34}S (Robertson et al., 1989). Using stable isotopes (Dellwig et al. (1999; 2001) documented the microbiological reduction of SO_4^{2-} in a number of sediment cores that were collected in a region a few kilometres west of the CAT-Field. Furthermore, they determined seawater as the main source for SO_4^{2-}.

Another option to identify driving processes could be the utilisation of radio tracer methods as described by Jørgensen (2000). Neither stable isotopes nor radio tracers were applied in this project. The measured sediment characteristics and the observed sulfate depletion suggest the mineralisation of organic carbon by dissimilatory sulfate reduction. As discussed, a series of published studies in the region support the conclusion that the sulfate depletion is a consequence of the sulfate reduction by organic matter decomposing micro organisms. As HCO_3^- is a product of this reaction the water type will be shifted towards a HCO_3^- type by the increased HCO_3^- content as documented in Figure 3.

The degradation of organic matter was implemented in the thermodynamic calculations through reduction the SO_4^{2-} concentration down to that of the corresponding sample (sampled water in column 7, Tab.4). The concentrations of HCO_3^- and S^{2-} were raised according to equation 4. Reflecting the observations in the

CAT-Field, the E_H decreased in this calculation step and the solution becomes supersaturated with respect to metal sulfides (e.g. pyrite in Tab.4). Additionally the increase of HCO_3^- resulted in a precipitation of calcite, which is reflected in the decrease of the Ca^{2+} concentration.

4.1.4 Exchanger reactions

Cations, adsorbed reversibly to negative charged surfaces, are exchanged with each other due to equilibrium disturbance after the cation mixing ratios in the aqueous phase changed, e.g. through seawater intrusion (Appelo and Greinaert, 1991; Beekmann and Appelo, 1990; Panteleit et al., 2003). The rather weakly bound ions are exchanged almost immediately, thus a new equilibrium is reached rapidly. Therefore, if exchanger reactions are identified in field measurements in coastal areas, it is generally considered an indication for a recent movement of the salt - fresh water interface. Examples for an active salinisation or refreshening of coastal aquifers that are showing patterns of exchanger reactions were found all over the world (e.g. Kim et al., 2003; Martinez and Bocanegra, 2002; Vandenbohede and Lebbe, 2002).

An increasing Na^+ content of the pore water samples as observed in the CAT-Field would be the result of the exchange of adsorbed Na^+ through Ca^{2+}:

$$2NaX + Ca^{2+} \leftrightarrow CaX_2 + 2Na^+ \qquad K = \frac{[Na^+]^2[CaX_2]}{[NaX]^2[Ca^{2+}]} \qquad (5),$$

whith X representing the negative charged exchanger site on the surface of the aquifer material. Since this exchanger reaction affects the cation ratio in the water only, it would result in a shift of the sample projection in the Piper diamond parallel to the anion axis towards the lower right (Fig.5). The deviation from the conservative mixing line as observed in the field samples would occur during a refreshening of the aquifer. In this case Ca^{2+} rich water displaces a water body with a higher Na^+ ratio of the cations and the subsequent exchange reaction responds according to the law of mass action.

Figure 6 displays the ratios of different ions to Cl^- as measured in groundwater samples from the CAT-Field in comparison to typical seawater ratios. Assuming the increased Na^+ ratio of the cations would result from ion exchange of adsorbed Na^+ by Ca^{2+} during refreshening, then this must be reflected in higher Na^+/Cl^- ratios as well as in a lower Ca^{2+}/Cl^- ratio. However, figure 6 shows that the Na^+/Cl^- ratio matches

the seawater value of 0.98 and the Ca^{2+}/Cl^- ratio is even higher than the seawater value. Consequently, in the subsoil of the investigation area, the ion exchange reaction did not cause the observed deviation from the conservative mixing between sea- and fresh water.

Even if the position of the transition zone is stable, the processes discussed before alterate the composition of the porewater. Consequently, exchanger processes resulting from these alterations were included as a final step in the thermodynamic calculations. For the calculations the exchanger characteristics derived from samples used in the column experiments (Panteleit et al., 2001a) were employed. The results of the thermodynamic calculation step showed only slight changes in the cation concentrations. The still remaining differences with respect to pH and the cation concentrations can be related to the fact that the material for the column experiment does not originate from the location of the studied water samples, while the complex exchanger characteristics vary significantly, due to natural heterogeneity.

4.2. Laboratory simulation

For a better understanding of the processes occurring in the transition zone between salt and fresh water the described chamber experiment was designed and performed. In this chapter the presented experimental data will be compared to field data. This comparison will be done separately for cations and anions, respectively.

Since the salt water has a much higher ion content than the fresh water, the Na^+ concentration and content (Fig.4a) of individual samples reflects the distribution of seawater in the flow chamber. Sediments are free of easily soluble sodium, therefore seawater is the only source of Na^+. The only possible sink for Na^+ its adsorption to exchanger sites, which in turn will cause a release of weakly bound Ca^{2+}. However, these rapid exchange processes occur only during the movement of the salt water front. Consequently, they were completed during the first phase of the flow chamber experiment (Panteleit et al., 2003).

More complex is the concentration pattern of Ca^{2+} (Fig.4b). Clearly two sources can be distinguished. Due to the higher ion content of the seawater the Ca^{2+} concentrations are highest in the salt water dominated part of the chamber. Rising concentrations in the upper layer, which is containing pleisto-holocene material, identify the silty and clayey material as another source for Ca^{2+}. This experimental

result corresponds to the observations from the CAT-Field, where ion strength effects next to enhanced CO_2 pressure from the degradation of organic matter were identified as major factors controlling the calcite dissolution.

The spatial distribution of the Ca^{2+}/TEC ratio does not reflect the calcite dissolution and is conditioned by the high Na^+ content of the seawater. High shares of Ca^{2+} were found in the fresh water filled areas, with decreasing Ca^{2+} mixing ratios in areas where salt water turns towards the Na^+ type water. This result is found in both, field and laboratory data as reflected in the corresponding allocation of data points in the cation triangle of Figure 3.

Due to the conservative behaviour of Cl^- both, the Cl^- concentration and mixing ratio distribution depend directly on the amount of salt water in the pore water. Cl^- and Na+ distributions (Fig.4a) correlate well with seawater, showing a constant Na^+/Cl^- ratio of 0.98 (Fig.6).

While processes concerning the chloride and the cation distribution were simulated well through the flow chamber experiment, the measured anion distributions differ significantly between field and laboratory data. These deviations can be explained by different constrains inherent to the laboratory experiment:

The HCO_3^- concentration is highest in layer 1 and shows a steep decrease between layer 2 and 3. Layer 1 and 2 contain organic substances in the Pleisto - Holocene material, while layer 3 consists of glacigene sands that are almost free of organic matter. Microbiological degradation of organic matter produces CO_2, which dissolves to carbonic acid in the pore water which then partly dissociates according to equation 3. Salt water is a second, though less important, source for HCO_3^-, causing the slightly higher concentrations in the salt water dominated part of layer 3. Due to the high ion content in the salt water the effective HCO_3^- concentrations are slightly higher than in the fresh water.

The HCO_3^-/AEC ratios are lowest in the salt water dominated part of the chamber and increase towards the fresh water area in the flow chamber. Highest ratios are found in the pleisto-holocene layers. Field and laboratory observations coincide. However, in the flow experiment high SO_4^{2-} concentrations result in maximum HCO_3^- ratios to the anion equivalen concentration that stays well below those of the field samples (Tab.2, Fig.4d).

Sulfate correlates negatively with Cl^-. Mixing ratios of SO_4^{2-} are lowest in the salt water, while fresh water has generally higher mixing ratios. The flow chamber experiment shows a steep gradient of SO_4^{2-} with depth. Compared to field data the fresh water in the chamber holds a very high content of SO_4^{2-} (Tab.2). Clearly two different sources for SO_4^{2-} can be distinguished. The first source is the salt water, intruding into the flow chamber system. The second source are the pleisto-holocene deposits, with high SO_4^{2-} concentrations measured in layers 1 and 2. This observation is in contradiction to the very low SO_4^{2-} concentrations measured in the holocene layers of the CAT-Field. The pleisto–holocene sediments hold reduced sulfur species as metal sulfide minerals. During the chamber experiment these reduced species get in contact with oxidising waters and atmospheric oxygen and reoxidise to SO_4^{2-} (equation 6):

$$S^{2-} + 2O_2 \rightarrow SO_4^{2-} \qquad (6).$$

This oxygen consuming process may cause the smaller enrichment of HCO_3^- in the laboratory experiment compared to field conditions, as reflected in the lower HCO_3^-/Cl^- ratio in Figure 6. The observed high SO_4^{2-} concentrations in the upper two layers of the chamber experiment also result in a higher SO_4^{2-}/Cl^- ratio compared to seawater. In contrast the SO_4^{2-}/Cl^- ratio from field samples are well below the seawater value due to sulfate reduction (Fig.6).

As for the field samples, thermodynamic calculations were performed for three flow chamber samples, each representing one sediment layer (Tab.5). The processes included in the calculations are those discussed above. Thus, the first to steps (mixing and equilibration with calcite and the CO_2 pressure) are identical with the field sample calculation. In the third step, SO_4^{2-} is added from sulfide oxidation until the calculation data reach the measured SO_4^{2-} concentration. Finally the exchanger sites are equilibrated with the new solution composition. In this step, the calculated cation concentrations approach the measured ones, however the exchange capacity seems to be underestimated.

	fresh water	calculated stepwise reaction				sampled water	salt water
species		step 1: mixing of fresh and salt water	step 2: equilibration with calcite and pCO_2	step 3: oxidation of sulfides	step 4: exchanger equilibration	shallow flow chamber water	
pH	7		5.8	5.7	5.7	7.4	7.8
EH [mV]	200		790	985	985	-40	100
Ca^{2+} [ppm]	117.6		7720	1792	1720	984	478.5
Na^{+} [ppm]	123.7		124.0	124.0	134.3	174.4	9997
Mg^{2+} [ppm]	17.1		17.1	17.1315	55.2	102.1	1121
K^{+} [ppm]	12.1		12.1	12.1	15.2	26.2	357
HCO_3^{-} [ppm]	102.1		1952	1647	1647	752.6	160
SO_4^{2-} [ppm]	197.1		196.8	**2880**	**2880**	2852	2636
Cl^{-} [ppm]	255.0		255.6	255.6	255.6	275.04	17850
SI calcite	-0.61		**0**	**0**	**0**		
log(pCO_2)	-2.21		**0.37**	**0.37**	**0.37**	0.37	
mixing ratio						0.001	
species	fresh water	step 1: mixing of fresh and salt water	step 2: equilibration with calcite and pCO_2	step 3: oxidation of sulfides	step 4: exchanger equilibration	Intermediate flow chamber water	salt water
pH	7	7	6.9	6.9	6.9	7.1	
EH [mV]	200	750	755	885	885	0	100
Ca^{2+} [ppm]	117.6	138.8	248.0	452.0	480.0	446.1	478.5
Na^{+} [ppm]	123.7	701.5	701.5	701.5	670.2	580.2	9997
Mg^{2+} [ppm]	17.1	81.6	81.6	81.6	67.3	64.2	1121
K^{+} [ppm]	12.1	14.9	14.9	14.9	16.0	35.7	357
HCO_3^{-} [ppm]	102.1	101.3	416.6	455.7	455.7	125.3	160
SO_4^{2-} [ppm]	197.1	339.8	339.8	**793.0**	**793.0**	820.2	2636
Cl^{-} [ppm]	255.0	**1285.1**	**1285.1**	**1285.1**	**1285.1**	1233.2	17850
SI calcite	-0.61	-0.77	**0**	**0**	**0**		
Log(pCO_2)	-2.21	-2.13	**-1.44**	**-1.44**	**-1.44**	-1.44	
mixing ratio		0.06				0.06	
species	fresh water	step 1: mixing of fresh and salt water	step 2: equilibration with calcite and pCO_2	step 3: oxidation of sulfides	Step 4: exchanger equilibration	Deep flow chamber water	salt water
pH	7	7.1	6.8	6.7	6.7	6.8	
EH [mV]	200	710	-80	910	910	200	
Ca^{2+} [ppm]	117.6	224.8	399.2	516.0	648.0	1039	478.5
Na^{+} [ppm]	123.7	3036	3036	3036	2967	2328	9997
Mg^{2+} [ppm]	17.1	342.6	342.6	342.6	342.6	279.7	1121
K^{+} [ppm]	12.1	26.6	26.6	26.6	27.4	61.2	357
HCO_3^{-} [ppm]	102.1	108.0	432.4	388.6	388.6	122.9	160
SO_4^{2-} [ppm]	197.1	624	918.7	**1248**	**1248**	1376	2636
Cl^{-} [ppm]	255.0	**5467**	**5467**	**5467**	**5467**	5242	17850
SI calcite	-0.61	-0.64	**0**	**0**	**0**		
log(pCO_2)	-2.21	-2.23	**-1.17**	**-1.17**	**-1.17**	-1.17	
mixing ratio		0.4				0.4	

Table 5: concentrations of input water and analysed pore water from the flow chamber experiment are shaded in grey. Concentrations of the thermodynamic calculation using PHREEQC (Parkhurst and Appelo, 1999) are presented for different calculation steps. Bold printed parameters were fitted to simulate processes.

5. Conclusions

Processes that occur during salt water intrusion into a fresh water aquifer can be simulated well through the presented flow chamber experiment. Cation distribution correlate well between experimental and field data. Given a stable position of the transition zone between salt and fresh water the cation distribution is controlled by mixing, redox processes and the dissolution of calcite. The calcite dissolution is a result of two processes, first the changing ion strength in the mixing zone of two water types, which were previously in equilibrium with the mineral phase, second the enhanced CO_2 concentration of porewater due to the degradation of organic matter contained in the sediments.

Different redox conditions between field and flow chamber experiment, affect the anion distribution. In the open chamber experiment redox sensitive sediments were exposed to oxygen, while being under reduced conditions in the field. A closed chamber system could have maintained reducing conditions, simulating field conditions to a certain degree after removing sediments from in situ and packing the chamber.

In both systems, field and flow chamber, the degradation of organic material is a driving process controlling the anion distribution and causing elevated HCO_3^- concentrations. Organic material is present in high concentrations in the upper pleisto-holocene layer, while it is absent or not easy degradable in the deeper, glacigene sediments. In the CAT-Field oxygen for the reduction of the organic carbon is only available in the uppermost layer. This is due to the low gas permeability of coherent sediments as well as to the present groundwater flow regime. In the deeper part of the pleisto-holocene layer sulfate is reduced and fixed in the sediment as sulfide. SO_4^{2-} probably is replenished by seawater intrusion in deeper layers and by seaspray in the surface layer. In the flow chamber experiment the sulfides are reoxidised in the presence of oxygen, resulting in high sulfate concentrations in the sediment layers containing pleisto -holocene material.

Acknowledgements

Antje Weitz is thanked for discussion, debates and helpful reviews which improved the paper and ideas. Thank you to Toni Wienrich, Yvonne Habenicht , Jens Berger and Markus Helms for their aid in constructing, sampling and analysing the flow chamber.

References

Appelo C. A. J. and Greinaert W. (1991) Processes Accompanying the Intrusion of Salt Water. In *Hydrogeology of Salt Water Intrusion - A Selection of SWIM Papers* (ed. W. D. Breuck), pp. 291-303. Heise.

Appelo C. A. J. and Postma D. (1996) *Geochemistry, Groundwater and Pollution*. Balkema.

Atkins P. (1990) *Pysikalische Chemie*. VCH.

Beekmann H. E. and Appelo C. A. J. (1990) Ion chromatography of fresh- and salt-water displacement: Laboratory experiments and multicomponent transport modelling. *Journal of Contaminant Hydrology* **7**, 21-37.

Berner R. A. (1975) The role of magnesium in the crystal growth of calcite and aragonite from sea water. *Geochimica Cosmochimica Acta* **39**(4), 489-504.

Berner R. A., Westrich J. T., Graber R., Smith J., and Martens C. S. (1978) Inhibition of aragonite precipitation from supersaturated seawater: a laboratory and field study. *American Journal of Science* **278**, 816-837.

Beyer W. (1964) Zur Bestimmung der Wasserdurchlässigkeit von Kiesen und Sanden aus der Kornverteilung. In *Wasserwirtschaft - Wassertechnik*, pp. 165-169.

Binot F., Druivenga G., Eckard H., Fulda C., Große K., Grossmann E., Höltscher F., Kantor W., Kessels W., Neuß M., Panteleit B., Rifai H., Suckow A., and Wonik T. (2002) Forschungsbohrung Cuxhaven Lüdingworth 1 und 1A CAT-LUD 1 und CAT-LUD 1A - Ergebnisse, Vol. GGA-Report # 121 520. Leibnitz Institute for Applied Geosciences (GGA-Institut), Germany.

Bowen H. J. M. (1979) *Environmental Chemistry of the Elements*. Academic Press.

Cook J. M. and Miles D. L. (1980) *Methods for the chemical analysis of groundwater*. Institute of Geological Sciences, Hydrogeology Unit.

Custodio E. and Bruggeman G. A. (1987) *Groundwater Problems in Coastal Areas*. UNESCO.

Dellwig O., Watermann F., Brumsack H.-J., and Gerdes G. (1999) High-resolution Reconstruction of a Holocene Coastal Sequence (NW Germany) Using Inorganic Geochemical Data and Diatom Inventories. *Estuarine, Coastal and Shelf Science* **48**, 617-633.

Dellwig O., Watermann F., Brumsack H.-J., Gerdes G., and Krumbein W. E. (2001) Sulphur and iron geochemistry of Holocene coastal peats (NW Germany): a tool for palaeoenvironmental reconstruction. *Palaeogeography, Palaeoclimatology, Palaeoecology* **167**, 359-379.

Froelich P. N., Klinkhammer G. P., Bender M. L., Luedtke M. L., Heath G. R., Cullen D., Dauphin P., Hammond D., Hartmann B., and Maynard V. (1979) Early oxidation of organic matter in pelagic sediments of the eastern equatorial Atlantic: suboxic diagenesis. *Geochimica Cosmochimica Acta* **43**, 1075-1090.

Fulda C. (2002) Numerische Studie zur Salz-/Süßwasserverteilung im Rahmen der Cuxhavener Forschungsbohrung. *Mitteilungen der Deutschen Geophysikalischen Gesellschaft* **Sonderband II**, 10-26.

Giblin A. E. and Howarth R. W. (1984) Porewater evidence for a dynamic sedimentary iron cycle in salt marshes. *Limnol. Oceanogr.* **29**(6), 47-63.

Gomis-Yagües V., Boluda-Botella N., and Ruiz-Beviá F. (2000) Gypsum Precipitation/Dissolution as an Explanation of the Decrease of Sulphate Concentration during Seawater Intrusion. *J. Hydr.* **228**, 48-55.

Grasshoff K., Ehrhardt M., and Kremling K. (1999) Methods of Seawater Analysis, pp. 600. Wiley-VCH.

Jørgensen B. B. (1982) Ecology of the bacteria of the sulphur cycle with special reference to anoxic-oxic interface environments. *Phil. Trans. R. Soc. Lond.* **B 298**, 543-561.

Jørgensen B. B. (2000) Bacteria and Marine Biogeochemistry. In *Marine Geochemistry* (ed. H. D. Schulz and M. Zabel), pp. 173-208. Springer-Verlag.

Kasten S. and Jørgensen B. B. (2000) Sulfate reduction in Marine Sediments. In *Marine Geochemistry* (ed. H. D. Schulz and M. Zabel), pp. 263-282. Springer-Verlag.

Kessels W., Dörhöfer G., Fritz J., and Fulda C. (2000) Das Forschungsprojekt "Bremerhaven-Cuxhavener Rinne" zur Beurteilung von Grundwasservorkommen in Rinnensystemen. *Arbeitshefte Wasser* **2000**(1), 189-203.

Kim Y., Lee K.-S., Koh D.-C., Lee D.-H., Lee S.-G., Park W.-B., Koh G.-W., and Woo M.-C. (2003) Hydrogeochemical and isotopic evidence of groundwater salinization in a coastal aquifer: a case study in Jeju volcanic island, Korea. *Journal of Hydrology* **270**, 282-294.

Lowson R. T. (1982) Aqueous oxidation of pyrite by molecular oxygen. *Chem. Rev.;* **82**, 461-497.

Magaritz M. and Luzier J. E. (1985) Water-Rock Interactions and Seawater-Freshwater Mixing Effects in the coastal dunes aquifer, Coos Bay, Oregon. *Geochimica Cosmochimica Acta* **49**, 2515-2525.

Martinez M. E. and Bocanegra E. M. (2002) Hydrochemistry and cation-exchange processes in the coastal aquifer of Mar Del Plata, Argentinia. *Hydrogeology Journal* **online**(s10040-002-0195-7).

Mercado A. (1985) The Use of Hydrogeochemical Patterns in Carbonate Sand and Sandstone Aquifers to Identify Intrusion and Flushing of Saline Water. *Ground Water* **23**(5), 635-645.

Morse J. W., Millero F. J., Cornwell J. C., and Rickard D. (1987) The Chemistry of the Hydrogen Sulfide and Iron Sulfide Systems in Natural Waters. *Earth-Science Reviews* **24**, 1-42.

Nadler A., Magaritz M., and Mazor E. (1980) Chemical reactions of seawater with rocks and freshwater: experimental and field observation on brackish waters in Israel. *Geochimica Cosmochimica Acta* **44**, 879-886.

Panteleit B., Binot F., and Kessels W. (subm.) Mud Tracer Test During Soft Rock Drilling. *Water Resouces Research*.

Panteleit B., Binot F., Kessels W., Schulz H. D., and Kantor W. (2001a) Geological and geochemical characteristics of a salinization-zone in a Coastal Aquifer. In *New Approaches Characterising Goundwater Flow*, Vol. 2 (ed. K.-P. Seiler and S. Wohnlich), pp. 1237-1241. A.A.Balkema.

Panteleit B., Kessels W., Kantor W., and Schulz H. D. (2001b) Geochemical characteristics of salinization-zones in the Coastal Aquifer Test Field (CAT-Field) in North Germany. *SWICA-M3 Saltwater Intrusion and Coastal Aquifers*.

Panteleit B., Kessels W., and Schulz H. D. (2003) Geochemical processes in the salt-freshwater transition zone - exchanger reactions in a 2D-sand-tank experiment. In *Geochemical Processes in soil and groundwater -measurement - modeling - upscaling* (ed. A. Hadeler and H. D. Schulz), pp. 596-610. Wiley VCH.

Panteleit B., Schulz H. D., and Kessels W. (2002) Geochemical processes in the salt-freshwater transition zone - preliminary results of a sand tank experiment. *Proceedings 17th Salt Water Intrusion Meeting, Delft 6-10 May 2002*, 29-38.

Parkhurst D. L. and Appelo C. A. J. (1999) PHREEQC for Windows - A Hydrogeochemical Transport Model. U.S.G.S.

Reddy M. M. (1977) Crystallisation of calcium carbonate in the presence of trace concentrations of phosphorous containing anions. *Journal of Crystal Growth* **41**, 287-295.

Robertson W. D., Cherry J. A., and Schiff S. L. (1989) Atmospheric sulfur deposition 1950-1985 inferred from sulfate in groundwater. *Water Resources Research* **25**, 1111-1123.

Sanford W. E. and Konikow L. F. (1989) Simulation of Calcite Dissolution and Porosity Changes in Saltwater Mixing Zones in Coastal Aquifers. *Water Resouces Research* **25**(4), 655-667.

Schulz H. D., Dahmke A., Schinzel U., Wallmann K., and Zabel M. (1994) Early diagenetic processes, fluxes, and reaction rates in sediments of the South Atlantic. *Geochimica Cosmochimica Acta* **59**(9), 2041-2060.

Tomson M. B. (1983) Effect of precipitation inhibitors on calcium carbonate scale formation. *Journal of Crystal Growth* **62**, 106-112.

Vandenbohede A. and Lebbe L. (2002) Numerical modelling and hydrochemical characterisation of a fresh-water lens in the Belgian coastal plain. *Hydrogeology Journal* **online**(DOI 10.1007/s10040-002-0209-5).

Walter L. M. and Hanor J. S. (1979) Effect of orthophosphate on the dissolution kinetics of biogenic magnesian calcites. *Geochimica Cosmochimica Acta* **43**, 1377-1385.

Anhang

A – Lokation der Probenahmestellen für das Grundwasser

B – Analysenwerte des Grundwassers

C – Analysenwerte der Säulenversuche

D – Analysenwerte des Porenwassers aus dem Beckenversuch während der Intrusion von Salzwasser

E – PHREEQC - Eingabefile für die Berechnung der Austauscherprozesse in Becken- und Säulenversuch

F – Analysenwerte des Porenwassers aus dem Beckenversuch aus der Endbeprobung

G – PHREEQC - Eingabefile für die Berechnung der Geochemischen Prozesse im CAT-Field

Bohrungskürzel	Rechtswert	Hochwert	NN-Höhe OK-Gelände	Entteufe unt. Gel.	Filterstrecke unter Gelände	
					OK Filter	UK Filter
			m	m	m	m
CAT_ALM105F	3483350.00	5967130.00	1.50	32.50	? 20	? 30
CAT_ALM176F	3484160.00	5966885.00	1.50	43.10	? 33	?41
CAT_BOY02	3485095.00	5962610.00	1.00	27.00	26.00	27.00
CAT_BOY03	3484730.00	5961832.00	1.00	19.00	18.00	19.00
CAT_DBE01	3485148.00	5967244.00	1.00	27.00	0.00	6.50
CAT_DOS 03	3482233.12	5962580.68	0.50	53.03	51.03	52.03
CAT_DOS 04	3482231.34	5962581.40	0.50	26.45	23.45	25.45
CAT_DOS 05	3482229.55	5962582.30	0.50	7.18	5.18	6.18
CAT_DOS07	3482625.49	5963466.09	1.00	25.00	ca. 22	ca. 24
CAT_GER 01	3482945.34	5964337.38	0.97	10.50	9.50	10.50
CAT_GER 02	3482942.04	5964339.00	0.96	24.35	23.35	24.35
CAT_GER 03	3482945.86	5964338.95	1.02	32.00	31.00	32.00
CAT_GER 04	3482942.60	5964340.30	0.98	42.50	41.50	42.50
CAT_GER 05	3482944.00	5964339.00	1.00	51.00	50.00	51.00
CAT_HAD 02	3482961.00	5966217.00	0.75	33.00	31.00	33.00
CAT_LAF 01	3483635.68	5964059.63	1.25	7.00	6.00	7.00
CAT_LAF 02	3483634.86	5964059.79	1.26	14.00	13.00	14.00
CAT_LAF 03	3483633.83	5964060.59	1.17	24.00	23.00	24.00
CAT_LAF 04	3483632.97	5964060.71	1.19	34.00	33.00	34.00
CAT_LAF 05	3483632.00	5964061.00	1.16	44.00	43.00	44.00
CAT_LUD 49F	3482782.00	5963750.00	1.09	63.40	54.80	62.80
CAT_LUD01	3482733.10	5963647.60	1.00	120.00	8.00	117.00
CAT_LUD01A	3482732.12	5963645.50	1.00	120.00	13.00	118.90
CAT_LUD01B	3482727.93	5963643.59	1.00	6.50	5.50	6.50
CAT_NIE 01	3483679.00	5965810.00	0.04	29.00	19.00	29.00
CAT_OFA01	3484085.00	5966585.00	2.00	49.00	46.00	47.00
CAT_OFA02	3484085.00	5966583.00	2.00	12.80	10.30	11.30
CAT_OFA03	3484085.00	5966581.00	2.00	8.00	5.30	6.30
CAT_OFA04	3484085.00	5966579.00	2.00	28.00	24.80	25.80
CAT_PIE 03	3482128.00	5964269.00	1.50	32.40	29.40	31.40
CAT_SCH 01	3483574.00	5965747.00	1.36	26.00	22.00	26.00
CAT_SET 01A	3481963.95	5964767.72	0.87	12.20	11.20	12.20
CAT_SET 01B	3481962.45	5964767.05	0.88	10.86	8.86	9.86
CAT_SET 02	3481966.87	5964766.22	0.89	22.30	21.30	22.30
CAT_SET 03	3481963.00	5964765.75	0.76	33.80	32.80	33.80
CAT_SET 04	3481965.65	5964763.80	0.79	37.60	36.60	37.60
CAT_SET 05	3481965.00	5964766.00	0.85	44.10	43.10	44.10
CAT_SRD01	3483416.00	5967177.00	1.50	19.00	18.00	19.00
CAT_WEF02	3481909.00	5962978.00	1.00	19.00	18.00	19.00
CAT_WOB01	3473885.00	5968125.00	19.00	18.25	16.25	17.25
MA 18	3480025.00	5963200.00	1.00	21.00	14.50	19.50
MA 19	3480020.00	5963200.00	1.00	6.50	3.00	6.00
UE 103 (2218HY20)	3482450.00	5962140.00	1.00	232.00	51.00	53.00
UE 111 (2118HY163)	3481750.00	5963460.00	1.00	387.00	187.00	189.00
UE 91 (2118HY161)	3479620.00	5964980.00	1.00	323.00	37 und 172	39 und 174

Fundort	Tiefe	pH	EC	K	Na	Cl	Mg	Ca	SO4	HCO3	Fe(II)	Mn	Br	Li	O2	EH
	m		µS/cm	mg/l	mg/l	mg/l	mg/l	mg/l	mg/l	mg/l	mg/l	mg/l	mg/l	mg/l	mg/l	mV H2
CAT_LAF 01	7	7,1	1150	11,23	13,66	44	38,28	175	134	575	2,595	1,248	0,08	0,03		
CAT_LAF 02	14	7,5	848	16,56	107,7	155	18,89	19,76	2,3	217	0,0309	0,1339	0,03	0,012		
CAT_LAF 03	24	7,5	797	3,708	87,9	152	8,33	53	0,2	193	0,2803	0,3605	0,33	0,017		
CAT_LAF 04	34	7,7	1220	4,929	152,1	290	11,06	64,1	0	178	0,0414	0,185	0,52	0,025		
CAT_LAF 05	44	7,5	4700	22,14	637	1390	62,8	197,1	116	162	0,203	0,712	0,25	0,074		
CAT_GER 01	10,5	7,8	748	2,644	73,7	140,12	6,99	56,6	0,5	183	0,0554	0,4546	0,25	0,01	0,3	80
CAT_GER 02	24,35	7,7	816	2,607	83,4	161	7,6	60	0	180	0,0638	0,4027	0,01	0,01	0,6	90
CAT_GER 03	32	7,8	1200	4,065	147,8	281,6	10,7	63,9	0,11	181	0,0434	0,2689	0,7	0,018	0	70
CAT_GER 04	42,5	7,6	5620	18,99	793	1694,8	72,3	243,1	181,04	164	0,1111	0,4847	4,39	0,07	0,1	80
CAT_GER 05	65	7,4	8460	46,4	1104	2722	187,4	310,5	185,74	190	0,1088	0,88	5,37	0,124	0,1	90
CAT_SET 01A	12,2	7,3	16500	108,3	3013	5029,1	381,4	170,6	0	2240	0,3911	1,347	3,78	0,113	0,1	100
CAT_SET 02	22,3	7,5	1150	5,76	145	248,21	10,87	62,1	0	229	0,0932	0,608	0,58	0,01	0,1	80
CAT_SET 03	33,8	7,7	791	3,335	80,6	151,6	8,89	54,7	0	179	0,0579	0,2514	0,13	0,01	0,2	90
CAT_SET 04	37,6	7,7	890	3,362	93,5	182,44	9,84	60,3	0	188	0,0523	0,2167	0,33	0,012	0,1	90
CAT_SET 05	62	7,8	2220	12,41	306,2	596,01	26,32	81,2	53,61	153	0,115	0,2023	0,43	0,031	0,2	60
UE90F		8,1	232	1,209	9,2	15,43	2,563	33,94	6,68	104	0,157	0,1061	0	0,006	0,1	40
UE90T		8,3	256	0,988	12,21	15,5	2,044	38,59	8,64	118	0,1001	0,0414	0	0,021	0,1	30
UE 91 (2118HY161) F	38	7	192	1,118	9,31	16,14	1,601	21,49	4,47	78,1	6,87	0,1432	0,05	0,009	0,2	150
UE 91 (2118HY161) T	173	7,6	15200	12,51	2300	4816,6	250	614	705,77	159	4,501	0,387	11,6	0,375	0,2	70
UE 103 (2218HY20)	52	7,5	1760	13,61	229,3	380,73	25,75	88,4	0	363	5,09	0,531	0,77	0,026	0,2	80
UE84F		6,5	386	1,464	22,21	58,83	5,47	39,35	27,48	34,9	0,0066	0	0,08	0	4,7	440
UE84T		6,5	200	1,081	13,53	27,3	2,997	17,42	16,47	29,9	0,2781	0,0051	0,04	0,004	3,7	340
UE111	188	7,3	3200	9,12	260,8	443,55	27,55	85,1	0,77	419	2,218	0,567	1,5	0,03	0,5	150
MA9/1		7	5250	135,5	387	643,97	70,1	264,1	267,03	1980	15,56	1,174	1	0,016	6	100
MA9/2		6,8	1610	22,05	116,9	144,1	25,54	132,7	80,4	590	3,546	2,62	0,5	0	0,5	170
MA9/3		6,6	662	2,102	26,94	48,26	15,41	79,6	48,41	171	0,0107	0,0362	0,2	0	3,8	310
MA9/4		6,6	717	1,563	40,57	52,97	11,63	78	60,41	175	0,0056	0,0295	0,3	0	0,4	280
MA9/5		7,4	271	0,923	11,61	27,06	2,477	36,18	26,03	77,5	0,604	0,1106	0,08	0,006	0,2	170
CAT_SCH 01	24	8	3660	47,7	534	915	84,2	74,3	44	510	0,0135	0,4147	0,38	0,043	0,1	0

Fundort	Tiefe	pH	EC	K	Na	Cl	Mg	Ca	SO4	HCO3	Fe(II)	Mn	Br	Li	O2	EH
	m		µS/cm	mg/l	mg/l	mg/l	mg/l	mg/l	mg/l	mg/l	mg/l	mg/l	mg/l	mg/l	mg/l	mV H2
CAT_LUD 49F	58,8	7,2	4460	12,16	645	1210	60,1	161,4	28,9	423	3,869	0,826	0,59	0,054	0	80
CAT_PIE 03	30,4	8	779	2,324	72,1	127	7,95	70,2	0,5	238	0,0831	0,738	0,42	0,017	0	130
CAT_HAD 01		8,1	875	4,433	106,7	175	8,3	47,27	0	189	0,522	0,2506	0,52	0,013	0,1	50
CAT_HAD 02	32	7,8	3350	15,91	441,8	928	45,37	146	46,2	209	0,4814	0,556	2,6	0,03	0,2	120
CAT_OST 58F		7,5	3840	30,52	591	932	74	80,2	0,2	652	1,797	0,686	2,9	0,029	0	80
CAT_TWI 01F		7,2	2500	98,5	274,3	451	40,49	100,8	52,8	608	0,2931	0,539	0,84	0,033	0,1	80
CAT_MUH 01F		7,3	4450	43,59	717	1100	74,4	69,3	0,2	697	2,531	0,802	3,4	0,03	0,1	10
CAT_HEE 17F		7,5	13310	85,7	2158	4090	272	256	366	656	0,574	0,956	11	0,086	0,1	0
CAT_NIE 01	24	7,6	7640	48,54	1216	2220	118	154,9	98,3	500	0,592	0,559	6,2	0,054	0,1	0
UE 93-II		7,6	204	1,533	12,07	17,4	3,286	24,25	8,1	85,8	1,733	0,0875	0,03	0,004	0	50
UE 93-III		7,1	33300	29,3	6320	11800	413	796	450	92	0,728	1,122	18	0,607	0	230
UE 93-I		8,3	293	1,105	13,9	19,4	3,396	42,82	39,7	93,9	0	0	0,06	0	8,8	430
UE 94 I		6,4	165	1,333	10,79	17,8	2,671	15,64	15	30,2	0	0	0,05	0	8,9	460
UE 94 II		6,1	129	1,124	13,14	16,5	1,277	9,22	7,3	34	0,3154	0,0691	0	0,004	0,1	310
MA 18	17	6,3	538	5	55	58,9	6,77	27,5	0	207	9,25	0,603	0,31	0,005	0,5	200
MA 19	4,5	7	2930	38,3	547	460	66,4	63,2	32,1	1317			2,2		3,6	160
Dicke Berta		7,9	19800	133	3440	6160	397	199	867	238	0,091	0,303	20	0,065	11,1	330
CAT_DBE01	3,25	7,3	11100	125	1754	2773	140	287	386	945	0,131	1,18	11,7	0,13	1,8	360
Dicke Berta		8,1	17000	117	2859	5340	346	176	740	147	0,027	0,009	16,8	0,059	6,5	330
CAT_DOS 05	5,68	7,3	7710	63,5	1236	1534	208	119	62,8	1990	0,17	0,52	5,87	0,068	2,5	110
CAT_DOS 03	51,53	7,6	1280	6,8	115	264	20	90,3	0,4	220	0,641	0,372	0,88	0,026	0,1	90
CAT_DOS 04	24,45	7,6	701	3,5	71,6	109	5,71	51,7	0	201	1,42	0,415	0,36	0,014	0,1	90
CAT_WEF01		7,7	577	2,6	57,6	98,1	5,9	44	0	159	0,129	0,467	0,33	0,014	6,9	210
CAT-LUD 01 (54m)	53	8,5	870	3,2	96,1	163	7,08	49,8	0,6	180	0,028	0,16	0,52	0,023		270
CAT-LUD 01 (87m)	87	8,1	18400	73,9	2591	6340	340	950	605	136	14,6	2,99	21	0,27	0	0
CAT_BOY03	18,5	6,6	709	6,9	62,7	91,2	17,6	51,8	1,77	283	2,66	0,43	0,36	0,014		
MA9/4		6,7	514	1,4	20,5	45,7	9,32	62,7	81,6	79,6	0,007	0,032	0,15	0	1,3	340
MA9/5		7,4	262	0,9	11,8	25,8	2,28	34,4	24,8	73,2	0,677	0,117	0,09	0,007	0	150
UE84T		6,3	227	1,1	14,9	28,7	3,58	20,1	29,5	31,6	0,259	0,009	0,1	0,004	2,7	330

Fundort	Tiefe	pH	EC	K	Na	Cl	Mg	Ca	SO4	HCO3	Fe(II)	Mn	Br	Li	O2	EH
	m		µS/cm	mg/l	mg/l	mg/l	mg/l	mg/l	mg/l	mg/l	mg/l	mg/l	mg/l	mg/l	mg/l	mV H2
UE84F		6,4	387	1,4	22	52,4	5,21	37,9	25,6	31,5	0	0,002	0,07	0	7,6	360
UE90F		8	231	1,2	9,2	15,1	2,59	34,1	7,15	105	0,131	0,111	0,03	0,006	0,1	50
UE90T		8,2	256	0,9	11,9	15	1,98	37,2	8,85	120	0,093	0,048	0,03	0,021	0	40
MA9/2		6,8	1022	12,5	59	74,4	19,4	94,5	66,5	309	3,87	1,7	0,35	0	0,7	180
MA9/1		7,1	4410	109	296	433	53,4	273	435	1560	20,1	1,18	0,83	0,012	2,5	60
MA9/3		6,6	567	1,8	22,8	46,9	11,9	63,1	47	88,1	0,016	0,018	0,18	0	2,8	390
CAT_SET 01B	9,36	7,5	17600	113	3361	5240	456	188	0	2470	0,111	0,334	19	0,1	0	120
1/98T		7,8	368	1,1	16,6	25,2	3,8	53,2	55,9	121	0,025	0,029	0,17	0	0	130
1/98F		5,4	193	5,8	10,2	20,4	5,72	10,5	28,69	2	0	0,019	0,1	0	10,3	480
UE94/I		6,2	162	1,3	9,6	17,8	2,69	15,6	16,8	31	0,012	0,003	0,1	0	9,1	380
UE94/II		6,1	129	1,1	12,6	16,7	1,24	9,87	9,58	32,2	0,245	0,028	0,04	0	0,1	280
UE93/I		8,1	290	1	10,4	17,5	3,13	43,1	41,3	90,6	0,009	0,002	0,06	0	9	370
UE93/II		7,3	204	1,3	10,4	16,7	2,97	24,4	9,49	78,7	2	0,092	0,04	0	0	70
UE93/III		7,1	33400	31,4	6540	12300	431	837	523	93	0,813	1,11	23,9	0,564	0	150
CAT_ALM105F	25	7,1	4690							740,21182						106
CAT_ALM176F	35,5	7,2	10700							949,98182						19
CAT_SRD01	17	7	1302							524,94838						228
CAT_OFA01	48,2	7	18810							1150,0008					0,35	141
CAT_OFA02	8,8	7,5	4620							651,14967					0,1	187
CAT_OFA03	3,8	7,2	887							793,26323						86
CAT_OFA04	23,3	7,2	10720							745,65357						117
Analysen aus	Kernzentrifugater															
CAT-OFA 1V	3	7,8	854,48107	9,9505146	84,469042		21,764403	139,42957	163,76926	291,77511						
CAT-OFA 1V	6	7,8	355,7568	17,483415	12,291504		19,462447	147,4861	147,59982	267,62007						
CAT-OFA 1V	9	7,9	1067,522	46,081222	115,17743		32,836708	47,68108	96,232508	388,99983						
CAT-OFA 1V	10	8	2178,3155	49,317663	274,52098		34,250521	44,110044	130,99024	367,34922						
CAT-OFA 1V	27,5	8	449,83752	11,055856	25,942413		30,676808	83,779191	180,91227	301,83946						
CAT-OFA 1V	48,1	8	20532,834	186,04512	4094,1387		449,05216	317,73054	993,3033	354,53367						
CAT-OFA 1V	49	7,8	5246,4028	50,018814	715,83333		68,138212	65,430666	192,4469	253,82257						

Fundort	Tiefe	pH	EC	K	Na	Cl	Mg	Ca	SO4	HCO3	Fe(II)	Mn	Br	Li	O2	EH
	m		µS/cm	mg/l	mg/l	mg/l	mg/l	mg/l	mg/l	mg/l	mg/l	mg/l	mg/l	mg/l	mg/l	mV H2
CAT-OFA 1V	51	7,8	20540,154	181,6032	4096,8609		458,8312	325,72745	985,59976	454,71117						
CAT-LUD 1	34,52		902,72881	8,9994291	91,429381		5,791055	55,976817	74,100786							
CAT-LUD 1	35,68		4526,1206	13,061251	611,30099		13,191739	64,674043	51,484412							
CAT-LUD 1	42,83		1703,517	11,162423	206,52992		11,151104	67,91617	131,47917							
CAT-LUD 1	43,5		3065,6861	9,9943784	401,46193		7,2389585	40,344368	95,885704							
CAT-LUD 1	45,5		1123,7604	14,330741	123,27339		5,9327726	62,514335	57,021297							
CAT-LUD 1	47,1		9611,2986	19,319638	1383,7456		19,021835	18,916132	552,0307							
CAT-LUD 1	47,5		2051,3624	5,7564018	256,35233		4,5567969	41,38335	31,093655							
CAT-LUD 1	48,17		7896,2428	14,876873	1111,9758		11,16694	10,18668	287,21347							
CAT-LUD 1	48,53		6284,7772	19,681047	868,49503		31,480749	134,30616	154,74866							
CAT-LUD 1	50,13		8512,597	14,880127	1207,8848		13,880366	7,2519355	235,15765							
CAT-LUD 1	50,83		6744,9839	15,53095	937,10128		10,924463	20,515733	202,29594							
CAT-LUD 1	50,5		6176,3521	15,052026	852,42384		14,29185	68,401015	131,62997							
CAT-LUD 1	57,59		5842,5253	14,858445	803,14575		10,402524	19,787972	214,85264							
CAT-LUD 1	58,38		3498,0646	20,4928	463,39185		24,437637	152,06497	168,71407							
CAT-LUD 1	58,5		4191,7919	23,041493	563,06497		32,870107	247,14837	267,1843							
CAT-LUD 1	59,18		5578,2844	15,212941	764,3418		13,856375	70,788569	80,332748							
CAT-LUD 1	59,79		5179,3382	23,501915	706,05962		39,298941	272,72567	322,1219							
CAT-LUD 1	60,15		5707,9647	20,556903	783,3642		34,982895	215,31259	139,37085							
CAT-LUD 1	60,49		5330,0866	28,248097	728,04213		45,895838	350,37312	318,53723							
CAT-LUD 1	60,85		5384,0204	18,435473	735,91851		23,971375	127,7885	112,26076							
CAT-LUD 1	61,55								0							
CAT-LUD 1	62,48		7374,6148	21,625786	1032,1124		33,401518	173,80227	191,344							
CAT-LUD 1	63,13		6271,6543	25,243586	866,54812		58,917043	363,40111	206,14199							
CAT-LUD 1	64,14		6087,2187	15,659184	839,23696		11,378024	39,022727	77,574691							
CAT-LUD 1	65,52		8749,5838	47,196002	1245,2542		106,08404	593,66757	383,02175							
CAT-LUD 1	66,13		8468,707	51,004867	1200,9953		130,45179	472,50457	382,04351							
CAT-LUD 1	66,85		8941,6495	66,922906	1275,7567		191,08499	586,71083	496,40877							
CAT-LUD 1	67,52		8869,3149	81,135952	1264,2457		210,23483	493,64477	449,16531							

Säule / Versuch	Poren-	Na	K	Ca	Mg	Sr	Fe	Mn	Li	Cl	SO4	HCO3
	volumen	mg/l	mg/l	mg/l	mg/l	mg/l	µg/l	mg/l	µg/l	mg/l	mg/l	mg/l
künstl. Grundwasser		804,7	27,0	293,0	79,8	4,4	8,0		0,0	1759,8	257,1	21,6
künstl. Salzwasser		2136,8	31,7	135,9	558,9	1,5	8,0		0,0	4759,6	553,8	53,1
Säule A SV1	0,0	870,7	27,8	299,3	38,8	4,3	< 0,01	0,6	7,7	1321,2	299,3	88,0
Säule A SV1	0,5	866,6	27,5	304,6	39,9	4,4	278,2	0,7	10,6	1387,8	301,3	104,3
Säule A SV1	1,5	2113,7	58,3	315,4	175,4	4,7	597,0	1,2	14,7	3538,9	605,7	130,7
Säule A SV1	3,6	2248,9	84,8	149,8	259,2	1,8	231,8	0,8	8,3	3603,3	630,1	117,3
Säule A SV1	6,0	2259,2	86,7	136,8	265,2	1,6	153,5	0,5	6,6	3777,3	631,1	114,7
Säule A SV1	7,8	2263,0	87,2	135,0	265,2	1,6	147,7	0,4	6,7	3617,6	632,8	109,0
Säule A SV2	0,0	2541,2	95,2	149,1	309,3	1,9	137,3	0,2	8,0		709,9	
Säule A SV2	0,1	2301,8	86,7	133,2	281,3	1,7	135,9	0,2	4,5		644,1	
Säule A SV2	0,3	2303,0	86,2	132,6	280,5	1,7	74,5	0,2	5,0		643,6	
Säule A SV2	0,4	2327,9	87,8	135,1	285,5	1,7	76,1	0,2	6,4		654,5	
Säule A SV2	0,5	2269,5	85,3	131,6	277,5	1,7	66,2	0,1	6,2	4187,6	637,5	33,5
Säule A SV2	0,7	2224,8	84,9	124,7	262,9	1,6	48,0	0,1	5,0		622,7	
Säule A SV2	0,8	1886,9	74,2	98,6	207,2	1,2	34,5	0,1	9,9		525,2	
Säule A SV2	1,0	1530,9	65,7	80,8	169,7	1,0	0,0	0,1	9,8		435,8	
Säule A SV2	1,1	1297,3	61,1	75,3	156,7	0,9	0,0	0,1	6,4		382,2	
Säule A SV2	1,3	1131,1	57,1	78,2	149,4	0,9	0,0	0,1	5,6	2016,4	346,4	30,1
Säule A SV2	1,4	1024,6	53,5	89,6	143,7	1,0	0,0	0,1	8,5		325,2	
Säule A SV2	1,6	964,7	50,2	108,7	134,0	1,3	0,0	0,1	0,0		313,3	
Säule A SV2	1,7	923,5	46,8	131,3	122,6	1,6	0,0	0,1	0,0		306,1	
Säule A SV2	1,9	903,6	43,7	153,9	111,1	2,0	0,0	0,1	0,0		301,5	
Säule A SV2	2,0	883,0	40,4	174,7	99,5	2,4	0,0	0,1	0,0	1708,7	298,8	25,0
Säule A SV2	2,2	872,6	38,0	192,3	90,1	2,7	0,0	0,1	0,0		298,0	
Säule A SV2	2,3	863,6	36,4	206,9	81,5	3,0	0,0	0,1	0,0		295,7	
Säule A SV2	2,5	857,4	34,6	221,2	74,1	3,4	60,8	0,1	0,0		294,1	
Säule A SV2	2,7	847,9	33,2	229,9	68,0	3,5	36,5	0,1	0,0		292,3	27,4
Säule A SV2	2,8	844,6	32,1	237,1	62,9	3,7	36,8	0,1	0,0	1721,1	292,1	
Säule A SV2	3,0	843,7	31,3	243,9	60,0	3,9	51,8	0,1	0,0		294,7	
Säule A SV2	3,1	840,4	30,7	249,2	56,3	4,0	50,1	0,1	0,0		292,8	
Säule A SV2	3,3	835,0	29,8	252,8	53,5	4,1	51,3	0,1	0,0		292,2	
Säule A SV2	3,5	833,8	28,7	261,6	48,6	4,3	0,0	0,0	0,0		290,9	26,1
Säule A SV2	3,6	849,2	28,9	268,7	48,2	4,5	0,0	0,0	0,0	1672,2	296,3	
Säule A SV2	3,8	849,6	28,7	270,8	47,0	4,5	0,0	0,0	5,1		296,3	
Säule A SV2	4,0	858,3	29,2	269,8	48,9	4,4	62,9	0,1	5,5		297,9	
Säule A SV2	4,1	851,8	28,7	269,4	47,9	4,5	66,0	0,1	0,0		295,8	
Säule A SV2	4,3	849,2	28,7	271,1	46,7	4,5	77,3	0,1	0,0		295,6	28,1
Säule A SV2	4,5	847,2	28,5	272,0	45,6	4,6	69,1	0,1	0,0	2016,4	296,0	
Säule A SV2	5,0	840,3	27,6	272,8	43,7	4,6	74,8	0,1	3,8		292,5	
Säule A SV2	5,9	837,5	26,7	275,5	42,2	4,7	61,0	0,1	11,6		293,4	
Säule A SV2	6,8	837,4	26,9	276,3	41,6	4,7	65,7	0,1	0,0		293,1	
Säule A SV2	17,2	849,5	28,2	288,0	40,6	3,4	94,3	0,2	0,0		302,7	28,4
Säule A SV3	0,1	850,0	30,1	296,0	42,0	2,9	75,6	0,3	4,3		709,9	
Säule A SV3	0,2	852,9	29,8	297,0	42,4	3,0	65,3	0,3	4,3		644,1	
Säule A SV3	0,4	887,7	31,1	308,7	44,2	3,1	48,7	0,3	6,1		643,6	
Säule A SV3	0,5	843,2	29,5	297,1	42,1	3,0	49,3	0,3	1,8		654,5	
Säule A SV3	0,6	875,0	30,3	319,9	45,5	3,2	57,0	0,4	8,1	1808,2	637,5	33,5
Säule A SV3	0,7	1026,5	33,0	388,1	55,6	3,9	62,3	0,4	4,4		622,7	
Säule A SV3	0,8	1302,9	36,9	457,7	68,6	4,7	72,7	0,5	4,7		525,2	
Säule A SV3	0,9	1584,0	40,9	489,9	83,6	5,1	78,7	0,5	7,2		435,8	
Säule A SV3	1,0	1801,1	44,1	478,0	100,2	5,0	76,8	0,6	2,5		382,2	
Säule A SV3	1,1	1996,7	49,2	432,9	129,2	4,6	73,3	0,6	1,6	3831,4	346,4	30,1
Säule A SV3	1,3	2119,2	56,0	377,4	158,9	3,9	67,8	0,6	8,0		325,2	
Säule A SV3	1,4	2174,7	60,9	339,9	179,8	3,5	66,3	0,5	2,7		313,3	
Säule A SV3	1,5	2204,4	65,4	307,2	194,4	3,1	55,6	0,5	7,9		306,1	
Säule A SV3	1,6	2219,2	68,8	280,6	208,6	2,8	50,2	0,5	4,9		301,5	
Säule A SV3	1,7	2220,8	71,1	258,1	218,8	2,5	43,3	0,5	4,0	4065,9	298,8	25,0
Säule A SV3	1,7	2302,4	75,3	247,2	234,3	2,3	40,6	0,5	2,8		298,0	
Säule A SV3	1,8	2207,4	74,6	224,3	234,2	2,0	27,7	0,5	13,2		295,7	
Säule A SV3	1,9	2314,4	78,7	219,2	250,1	1,9	31,3	0,5	16,4		294,1	
Säule A SV3	2,0	2327,8	79,8	207,6	253,3	1,8	29,7	0,5	12,1		292,3	27,4
Säule A SV3	2,1	2301,0	80,6	198,4	257,5	1,6	26,6	0,4	11,9	4303,5	292,1	
Säule A SV3	2,2	2296,8	80,4	191,0	261,1	1,5	19,5	0,4	16,4		294,7	
Säule A SV3	2,3	2289,4	80,6	183,5	261,9	1,4	19,1	0,4	10,2		292,8	
Säule A SV3	2,4	2304,2	81,5	179,5	264,8	1,4	23,0	0,4	17,3		292,2	
Säule A SV3	2,5	2278,2	80,7	173,3	264,6	1,3	23,6	0,4	10,2		290,9	26,1

Säule / Versuch	Poren-	Na	K	Ca	Mg	Sr	Fe	Mn	Li	Cl	SO4	HCO3
	volumen	mg/l	mg/l	mg/l	mg/l	mg/l	µg/l	mg/l	µg/l	mg/l	mg/l	mg/l
Säule A SV3	2,6	2305,0	81,5	170,7	268,5	1,2	23,2	0,4	15,0	4180,7	296,3	
Säule A SV3	2,7	2284,9	81,5	166,4	268,9	1,2	19,7	0,4	7,8		296,3	
Säule A SV3	2,8	2301,0	81,8	164,2	271,7	1,1	19,9	0,4	10,9		297,9	
Säule A SV3	2,9	2278,7	82,1	161,4	272,7	1,1	18,5	0,4	12,7		295,8	
Säule A SV3	3,0	2286,5	81,5	158,3	271,7	1,0	20,4	0,4	13,7		295,6	28,1
Säule A SV3	3,1	2281,6	81,9	156,5	272,4	1,0	13,9	0,3	16,6	4210,0	296,0	
Säule A SV3	3,2	2264,8	80,9	154,0	270,8	1,0	20,2	0,3	19,2		292,5	
Säule A SV3	3,3	2269,8	81,4	153,8	274,2	0,9	8,0	0,3	8,1		293,4	
Säule A SV3	3,4	2337,6	84,4	157,4	283,6	0,9	10,0	0,3	12,3		293,1	
Säule A SV3	3,5	2328,1	83,3	155,4	281,6	0,9	17,7	0,3	14,3		302,7	28,4
Säule A SV3	3,6	2321,9	83,6	154,5	281,5	0,9	11,9	0,3	15,6	4331,2		
Säule A SV3	3,7	2325,9	83,6	153,7	281,7	0,9	8,8	0,3	9,6			
Säule A SV3	3,8	2321,4	83,5	152,4	282,4	0,9	21,9	0,3	11,2			
Säule A SV3	3,9	2314,0	83,2	151,8	282,1	0,9	7,4	0,3	9,8			
Säule A SV3	4,0	2324,1	83,4	151,3	282,5	0,8	17,2	0,3	14,1			
Säule A SV3	4,1	2321,3	83,1	150,3	282,1	0,8	15,0	0,3	16,6	4277,8		
Säule A SV3	4,2	2298,0	82,3	149,1	279,4	0,8	12,4	0,3	4,0			
Säule A SV3	4,3	2302,0	82,2	148,5	279,3	0,8	10,5	0,3	6,4			
Säule A SV3	4,4	2293,7	82,0	148,5	278,3	0,8	8,1	0,3	0,2			
Säule A SV3	4,5	2297,3	82,0	148,1	280,5	0,8	11,5	0,3	3,7			
Säule A SV3	4,6	2287,3	81,8	147,1	278,9	0,8	10,5	0,3	5,9	4218,2		
Säule A SV3	4,7	2283,9	81,9	146,8	279,9	0,8	9,5	0,3	9,4			
Säule A SV3	4,8	2278,3	81,4	146,4	278,7	0,8	11,5	0,3	1,8			
Säule A SV3	4,9	2295,3	81,4	146,3	279,5	0,8	11,3	0,3	6,6			
Säule A SV3	5,0	2284,9	81,7	146,0	279,6	0,8	15,9	0,2	2,3			
Säule A SV3	5,1	2281,4	81,3	144,8	276,9	0,8	18,3	0,2	8,6	4295,0		
Säule A SV3	5,1	2283,4	80,9	145,7	276,3	0,8	7,6	0,2	8,9			
Säule A SV3	5,2	2273,6	81,1	144,9	277,7	0,7	6,5	0,2	3,3			
Säule A SV3	5,3	2305,7	82,2	146,4	281,7	0,7	16,4	0,2	2,6			
Säule A SV3	5,8	2248,1	80,3	142,6	275,5	0,7	7,6	0,2	2,4			
Säule A SV3	6,3	2364,3	85,2	151,4	289,8	0,8	14,1	0,2	6,8			
Säule B SV1	0,0	815,8	26,1	283,2	36,9	4,3	< 0,01	0,5	7,8	1499,4	283,3	88,0
Säule B SV1	0,7	813,4	25,9	286,8	37,7	4,3	508,5	0,6	10,3	1477,9	283,2	112,2
Säule B SV1	1,9	2183,4	60,5	280,5	194,3	4,2	832,9	1,0	13,4	3777,1	625,2	139,0
Säule B SV1	4,6	2248,2	85,8	144,0	259,7	1,7	329,5	0,6	7,1	3891,9	629,9	115,6
Säule B SV1	7,4	2234,8	86,7	136,4	264,3	1,6	251,1	0,4	6,9	4019,1	629,0	116,6
Säule B SV1	9,5	2234,0	87,2	134,4	265,7	1,5	290,4	0,3	6,4	4080,2	629,5	114,2
Säule B SV2	0,0	2379,8	89,0	148,7	291,8	1,8	107,3	0,2	6,7		667,5	
Säule B SV2	0,1	2290,6	85,4	142,1	279,9	1,7	224,7	0,1	7,9		630,5	
Säule B SV2	0,3	2280,9	85,0	140,9	280,0	1,7	92,1	0,1	7,4		641,0	
Säule B SV2	0,5	2284,2	85,0	141,0	280,1	1,7	72,6	0,1	0,0		637,5	
Säule B SV2	0,7	2026,7	75,2	124,9	248,3	1,5	69,4	0,1	4,8	4098,8	563,8	34,9
Säule B SV2	0,9	2298,4	85,5	140,2	278,1	1,7	65,8	0,1	6,5		644,5	
Säule B SV2	1,0	1913,6	72,1	102,6	203,5	1,2	47,3	0,1	0,0		532,0	
Säule B SV2	1,2	1440,8	59,3	70,9	140,5	0,8	52,9	0,1	6,3		399,3	
Säule B SV2	1,4	1142,4	56,4	66,5	132,7	0,7	0,0	0,0	0,0		336,7	
Säule B SV2	1,6	990,2	55,9	71,7	142,9	0,8	0,0	0,0	0,0	1734,4	308,0	26,1
Säule B SV2	1,8	910,8	54,1	80,0	149,4	0,9	0,0	0,1	6,9		298,1	
Säule B SV2	2,0	881,8	51,8	96,7	146,1	1,0	0,0	0,1	4,7		294,2	
Säule B SV2	2,2	872,9	48,2	124,4	134,3	1,3	0,0	0,1	0,0		293,6	
Säule B SV2	2,3	865,9	44,2	157,2	117,7	1,8	0,0	0,1	0,0		294,0	
Säule B SV2	2,5	857,2	40,4	186,0	101,9	2,3	0,0	0,1	6,0	1685,9	293,6	25,6
Säule B SV2	2,7	852,3	37,3	209,7	88,8	2,7	0,0	0,1	0,0		293,3	
Säule B SV2	2,9	844,6	34,7	226,9	78,1	3,1	0,0	0,0	0,0		291,4	
Säule B SV2	3,1	843,3	32,8	241,5	70,3	3,4	0,0	0,0	4,3		292,0	
Säule B SV2	3,3	841,4	31,3	251,6	63,5	3,7	0,0	0,0	0,0		291,7	
Säule B SV2	3,5	839,6	30,1	260,1	58,9	3,8	0,0	0,0	6,4	1685,3	289,7	26,5
Säule B SV2	3,7	842,4	29,4	268,2	55,5	4,0	0,0	0,0	0,0		293,3	
Säule B SV2	3,9	845,0	29,0	274,0	52,6	4,2	0,0	0,0	4,0		292,5	
Säule B SV2	4,1	836,4	28,2	275,8	50,3	4,3	0,0	0,0	0,0		291,8	
Säule B SV2	4,3	838,8	29,1	273,5	51,6	4,2	57,0	0,0	4,2		291,6	
Säule B SV2	4,6	852,5	29,3	281,1	50,4	4,4	77,4	0,1	4,6	1681,5	297,6	26,1
Säule B SV2	4,8	825,1	28,1	273,9	47,6	4,3	61,3	0,0	0,0		287,3	
Säule B SV2	5,0	849,7	28,1	288,9	46,0	4,6	0,0	0,0	7,5		296,1	
Säule B SV2	5,2	846,7	27,9	289,6	45,3	4,6	0,0	0,0	0,0		295,6	
Säule B SV2	5,4	840,0	27,5	288,5	44,4	4,6	0,0	0,0	0,0		294,0	

Säule / Versuch	Poren-	Na	K	Ca	Mg	Sr	Fe	Mn	Li	Cl	SO4	HCO3
	volumen	mg/l	mg/l	mg/l	mg/l	mg/l	µg/l	mg/l	µg/l	mg/l	mg/l	mg/l
Säule B SV2	5,6	846,5	27,3	290,5	43,9	4,7	33,5	0,1	0,0	1657,8	294,3	27,8
Säule B SV2	6,3	821,7	26,3	285,9	42,0	4,6	0,0	0,0	0,0		286,8	
Säule B SV2	7,4	824,3	26,2	288,5	41,2	4,7	0,0	0,0	0,0		287,0	
Säule B SV2	8,5	824,3	26,3	289,6	40,6	4,7	0,0	0,0	0,0		287,2	
Säule B SV2	21,4	860,5	28,0	303,9	43,0	3,4	148,0	0,2	8,6		305,1	28,1
Säule B SV3	0,1	723,3	22,9	256,2	36,1	2,6	47,0	0,4	0,0			
Säule B SV3	0,3	851,2	27,1	300,7	42,3	3,0	50,2	0,4	0,2			
Säule B SV3	0,6	903,8	29,0	320,5	44,9	3,2	53,0	0,4	3,2			
Säule B SV3	0,7	856,8	27,4	308,0	43,1	3,1	42,9	0,3	0,0			
Säule B SV3	0,9	928,7	28,8	349,1	48,9	3,5	36,4	0,4	8,4	1957,6	274,9	34,9
Säule B SV3	1,0	1162,3	32,6	435,5	61,7	4,4	41,1	0,5	11,1			
Säule B SV3	1,1	1486,0	37,2	509,2	76,9	5,1	45,4	0,6	7,2			
Säule B SV3	1,3	1776,2	40,2	521,3	92,4	5,3	45,4	0,6	4,6			
Säule B SV3	1,4	1976,3	43,5	491,3	111,6	5,1	39,6	0,6	14,0			
Säule B SV3	1,7	2135,2	49,1	420,2	143,3	4,4	38,7	0,6	4,9	4108,6	457,9	26,1
Säule B SV3	1,9	2217,4	56,1	351,3	173,8	3,7	31,4	0,6	8,4			
Säule B SV3	2,0	2222,1	61,1	309,2	193,5	3,1	31,6	0,6	9,0			
Säule B SV3	2,1	2238,8	65,3	275,3	208,2	2,7	26,0	0,6	4,5			
Säule B SV3	2,3	2240,8	68,2	248,1	219,9	2,4	23,3	0,5	5,2			
Säule B SV3	2,4	2221,4	70,7	227,5	230,5	2,1	27,2	0,5	12,8	4166,5	473,5	25,6
Säule B SV3	2,6	2339,4	76,5	220,8	248,6	1,9	29,3	0,5	16,4			
Säule B SV3	2,7	2328,5	77,7	205,9	252,5	1,8	18,5	0,5	13,1			
Säule B SV3	2,9	2302,2	78,6	194,2	256,9	1,6	14,2	0,5	18,7			
Säule B SV3	3,0	2317,7	79,9	187,1	262,3	1,5	10,4	0,5	13,6			
Säule B SV3	3,1	2302,8	80,4	179,6	263,7	1,4	10,3	0,5	14,7	4340,5	472,9	26,5
Säule B SV3	3,3	2293,5	80,3	173,7	266,1	1,3	7,0	0,4	14,7			
Säule B SV3	3,4	2304,5	81,3	169,6	268,3	1,2	15,8	0,4	12,0			
Säule B SV3	3,6	2300,1	81,8	166,4	271,0	1,2	13,6	0,4	10,4			
Säule B SV3	3,7	2302,8	82,0	164,0	272,7	1,1	14,5	0,4	11,1			
Säule B SV3	3,9	2286,6	81,6	160,2	271,8	1,0	10,0	0,4	10,5	4222,7	480,7	26,1
Säule B SV3	4,0	2292,1	81,7	158,7	274,8	1,0	8,4	0,4	11,4			
Säule B SV3	4,1	2282,1	81,8	157,3	275,8	1,0	11,8	0,4	10,5			
Säule B SV3	4,3	2284,1	81,6	155,8	275,8	0,9	7,9	0,4	12,1			
Säule B SV3	4,4	2282,6	81,8	154,3	276,0	0,9	33,2	0,4	14,0			
Säule B SV3	4,6	2282,5	82,2	154,3	278,1	0,9	13,8	0,4	13,7	4119,1	464,5	27,8
Säule B SV3	4,7	2290,1	82,3	152,4	276,5	0,9	11,3	0,3	13,8			
Säule B SV3	4,9	2281,1	82,0	151,4	277,4	0,9	6,8	0,3	5,6			
Säule B SV3	5,0	2357,4	85,4	156,2	286,6	0,9	9,2	0,3	13,6			
Säule B SV3	5,1	2358,3	85,5	155,2	286,6	0,9	20,5	0,3	15,2			28,1
Säule B SV3	5,3	2336,5	84,4	153,8	285,0	0,9	15,6	0,3	4,3	4300,2	480,6	
Säule B SV3	5,4	2384,0	86,0	155,2	288,4	0,8	14,2	0,3	6,3			
Säule B SV3	5,6	2336,1	84,7	152,3	284,0	0,8	19,8	0,3	4,1			
Säule B SV3	5,7	2320,1	84,9	151,8	283,5	0,8	7,1	0,3	4,2			
Säule B SV3	5,9	2310,8	84,3	150,2	281,8	0,8	13,7	0,3	7,6			
Säule B SV3	6,0	2299,9	84,1	148,8	279,8	0,8	10,4	0,3	6,1	4310,5	522,3	
Säule B SV3	6,1	2296,0	83,7	148,7	280,8	0,8	13,7	0,3	5,7			
Säule B SV3	6,3	2300,8	83,2	147,7	279,6	0,8	13,3	0,3	6,4			
Säule B SV3	6,4	2302,4	83,6	148,1	281,5	0,8	22,2	0,3	5,4			
Säule B SV3	6,6	2372,1	87,2	153,3	291,8	0,8	13,8	0,3	8,1			
Säule B SV3	6,7	2284,8	83,1	146,4	279,7	0,8	18,5	0,3	1,3	4204,8	510,1	
Säule B SV3	6,9	2273,2	82,9	145,9	278,0	0,8	13,7	0,3	6,9			
Säule B SV3	7,0	2274,8	83,0	145,7	278,3	0,8	13,0	0,3	4,4			
Säule B SV3	7,1	2267,6	82,4	145,1	277,2	0,8	10,9	0,3	5,2			
Säule B SV3	7,3	2264,1	82,8	145,4	278,6	0,8	5,8	0,3	8,5			
Säule B SV3	7,4	2261,1	82,2	144,7	277,5	0,7	12,9	0,3	7,8	4281,3	527,5	
Säule B SV3	7,6	2255,3	82,2	144,4	277,6	0,7	12,2	0,3	8,1			
Säule B SV3	7,7	2255,4	82,1	144,6	278,1	0,7	8,5	0,2	5,8			
Säule B SV3	7,9	2271,5	83,3	146,3	281,7	0,7	17,3	0,3	5,4			
Säule B SV3	8,6	2156,7	77,4	136,8	265,1	0,7	16,5	0,2	7,7			
Säule B SV3	9,3	2162,9	78,9	139,2	265,0	0,7	13,9	0,2	6,1			

Proben lokation	Laufzeit	SO4	Na	Ca	K	Mg	Proben lokation	Laufzeit	SO4	Na	Ca	K	Mg
Spalte-Zeile	h	mg/l	mg/l	mg/l	mg/l	mg/l	Spalte-Zeile	h	mg/l	mg/l	mg/l	mg/l	mg/l
FW Zufluß	0,0	639,8	471,1	368,1	30,1	41,8	1-4	37,7	2617,8	10907,6	406,9	394,7	1209,7
SW Zufluß	0,0	2547,2	10397,8	399,5	358,1	1159,1	1-5	37,7	2602,5	10787,2	413,4	391,9	1190,6
1-10	4,8	746,8	542,3	413,3	35,8	51,1	1-6	37,7	2561,1	10798,8	447,3	346,8	1178,6
1-12	4,8	690,0	510,0	394,1	31,3	45,2	1-7	37,7	2600,0	10767,5	438,2	343,8	1192,4
3-4	4,8	703,8	516,4	396,9	31,5	47,7	1-8	37,7	2297,6	9147,0	662,1	267,5	966,3
1-2	4,9	725,0	652,7	478,9	33,5	56,7	2-1	37,7	678,4	509,9	398,0	30,1	44,0
1-1	4,9	1125,5	2543,3	608,5	74,8	268,9	2-2	37,7	665,4	503,9	392,0	31,0	44,9
1-3	4,9	650,4	492,7	387,3	31,4	42,6	1-9	45,1	2096,8	7628,1	695,2	209,5	814,0
1-4	4,9	700,9	545,6	415,0	34,7	48,4	1-10	45,1	968,5	2045,4	665,8	62,6	191,9
1-5	4,9	745,2	699,3	461,1	37,4	63,4	1-11	45,1	697,5	577,2	421,4	36,2	51,9
1-6	4,9	699,1	533,2	405,7	32,4	50,5	1-12	45,1	971,2	622,3	463,8	43,0	66,7
1-7	4,9	697,6	512,7	405,6	31,6	49,1	1-1	45,1	2604,8	10779,7	404,9	385,2	1228,6
1-8	4,9	695,8	509,9	405,2	31,9	48,8	1-2	45,1	2593,4	10755,0	424,0	383,5	1211,7
2-1	4,9	684,4	521,3	411,3	30,1	44,3	1-3	45,1	2579,7	10651,0	474,7	367,9	1172,8
2-2	4,9	672,8	508,8	395,9	30,4	44,1	1-4	45,1	2613,4	10859,5	401,3	391,1	1203,6
1-9	14,1	677,2	515,3	405,8	32,9	49,0	1-5	45,1	2592,6	10761,0	404,8	391,1	1190,4
1-10	14,1	683,2	490,1	389,2	32,8	47,2	1-6	45,1	2570,8	10802,9	416,8	353,1	1184,4
1-11	14,1	763,8	530,5	402,1	36,7	52,2	1-7	45,1	2620,5	10896,9	411,6	356,2	1205,5
1-12	14,1	1372,6	664,7	488,3	46,0	72,8	1-8	45,1	2479,5	10087,5	549,1	316,6	1096,4
1-1	14,1	2589,7	10621,7	576,1	332,6	1165,3	2-1	45,1	674,6	509,4	399,6	30,1	44,0
1-2	14,1	2027,8	7290,8	1111,2	172,7	724,8	2-2	45,1	667,1	502,5	392,6	30,8	45,0
1-3	14,1	873,2	1506,6	744,8	51,7	133,1	1-1	53,3	2608,8	10783,8	404,1	385,8	1228,2
1-4	14,1	1463,2	4914,6	645,7	155,5	509,0	1-2	53,3	2608,9	10699,0	412,8	386,1	1206,5
1-5	14,1	2126,9	7737,4	879,7	204,1	793,8	1-3	53,3	2573,6	10720,1	443,9	378,4	1184,4
1-6	14,1	1147,7	2691,6	971,0	63,5	252,0	1-4	53,3	2613,9	10833,1	400,8	393,5	1203,1
1-7	14,1	792,9	1028,4	674,2	40,5	96,9	1-5	53,3	2587,9	10852,6	400,9	392,5	1188,0
1-8	14,1	705,7	648,4	458,4	34,6	64,2	1-6	53,3	2564,6	10779,7	407,2	356,2	1187,4
2-1	14,1	677,5	509,2	399,4	30,3	43,6	1-7	53,3	2588,9	10890,5	404,3	359,1	1206,4
1-9	22,5	760,8	990,1	549,8	40,9	88,1	1-8	53,3	2548,3	10496,7	475,3	339,2	1152,6
1-10	22,5	679,7	508,6	402,8	33,4	48,5	2-1	53,3	719,2	641,7	459,8	32,6	55,6
1-11	22,5	722,2	514,3	396,4	36,0	50,2	2-2	53,3	668,9	508,1	396,8	31,3	45,2
1-12	22,5	1186,0	636,1	470,0	44,3	69,2	1-9	53,2	2295,9	8757,9	576,5	265,4	962,2
1-1	22,4	2602,2	10838,5	430,9	378,1	1215,2	1-10	53,2	1146,6	2974,8	677,6	91,0	306,6
1-2	22,4	2537,5	10258,5	775,5	293,9	1079,6	1-11	53,2	696,8	626,9	428,1	37,1	54,0
1-3	22,4	1985,3	7429,8	1359,8	170,7	677,4	1-12	53,2	1062,8	628,5	465,1	42,6	66,5
1-4	22,4	2528,3	10391,8	484,0	352,3	1135,5	1-9	61,8	2450,6	9771,3	508,5	307,9	1084,2
1-5	22,4	2560,2	10563,1	538,3	345,2	1123,4	1-10	61,8	1402,8	4145,3	703,5	127,7	447,2
1-6	22,4	2262,1	8695,3	1055,0	195,9	869,3	1-11	61,8	703,0	757,1	457,8	40,6	63,3
1-7	22,4	1958,9	6850,4	1078,9	147,1	684,8	1-12	61,8	1058,1	644,4	469,5	42,9	66,4
1-8	22,4	1308,2	3570,6	758,6	91,0	377,5	1-1	61,9	2596,9	10777,9	411,2	381,9	1222,1
2-1	22,4	674,8	504,5	395,7	29,9	43,7	1-2	61,9	2565,6	10729,9	397,0	387,6	1204,0
2-2	22,4	665,4	503,7	389,8	30,9	44,2	1-3	61,9	2605,8	10803,0	397,2	389,2	1203,2
1-9	29,7	1100,4	2535,9	782,6	66,4	235,3	1-4	61,9	2568,5	10772,2	431,9	386,2	1194,3
1-10	29,7	685,5	605,4	430,8	35,0	52,9	1-5	61,9	2583,2	10816,2	409,3	390,7	1183,5
1-11	29,7	713,1	513,5	400,3	35,4	50,1	1-6	61,9	2564,4	10785,9	393,0	359,0	1195,9
1-12	29,7	1220,0	627,8	465,3	43,9	67,5	1-7	61,9	2572,0	10686,7	440,0	352,0	1186,4
1-2	29,7	2597,4	10629,2	530,8	344,9	1182,0	1-8	61,9	2596,7	10743,3	398,8	360,3	1204,2
1-1	29,7	2604,4	10884,9	416,0	384,5	1224,6	2-1	61,9	675,7	515,7	399,8	31,3	45,6
1-4	29,7	2593,4	10844,7	409,6	383,7	1186,7	2-2	61,9	911,7	1392,1	631,7	41,7	132,4
1-3	29,7	2495,1	10033,6	829,5	286,5	1039,3	1-9	71,3	2490,6	9992,1	476,6	322,9	1100,1
1-6	29,7	2534,6	10489,6	590,4	303,9	1117,8	1-10	71,3	1544,1	4910,2	722,6	153,2	535,0
1-5	29,7	2572,1	10745,6	439,1	380,5	1174,6	1-11	71,3	717,2	893,4	485,6	45,4	74,6
1-8	29,7	1856,3	6585,6	768,2	179,5	699,8	1-12	71,3	998,5	652,8	469,5	42,8	66,8
1-7	29,7	2484,0	10008,6	604,3	287,0	1081,8	1-1	71,3	2610,7	10783,1	403,5	389,2	1232,4
2-2	29,7	664,6	506,5	392,3	31,3	44,7	1-2	71,3	2606,8	10787,1	408,4	392,3	1217,5
2-1	29,7	676,0	509,1	398,7	30,6	43,8	1-3	71,3	2594,8	10809,3	400,6	393,8	1195,1
1-9	37,6	1696,3	5317,4	836,6	136,0	557,8	1-4	71,3	2600,6	10814,8	423,3	388,8	1205,9
1-10	37,6	786,3	1135,0	568,7	42,9	93,5	1-5	71,3	2576,2	10804,3	406,4	392,6	1185,5
1-11	37,6	704,3	533,5	409,3	35,3	50,7	1-6	71,3	2569,7	10845,7	393,3	360,1	1197,2
1-12	37,6	1205,2	619,7	460,6	43,4	66,6	1-7	71,3	2580,1	10749,9	420,8	358,8	1197,9
1-1	37,7	2607,4	10831,7	407,6	384,4	1224,4	1-8	71,3	2613,5	10835,9	400,9	363,4	1212,3
1-2	37,7	2595,1	10809,5	443,3	374,6	1207,2	2-1	71,3	673,1	549,4	414,3	32,1	47,6
1-3	37,7	2578,5	10591,2	549,9	348,1	1152,7	2-2	71,3	1271,0	2940,9	761,3	66,3	306,4

```
TITLE Säulenversuch 1--Transport and ion exchange.
PRINT
        -reset            false
        -user_graph true
SOLUTION 0  Input water Simulated SW 20% (Analysenwerte)
         units   ppm
         pH      7.38
         pe      7.32
         temp    22.0
         Ca                125.153
         Mg                262.8
         Na                2221.8
         K                 88.00
         Fe                0.008
         Mn                0.005
         Sr                1.5
         Zn                0.001
         Si                8.91
         Cl                3916.1
         Alkalinity        96.3 as HCO3
         S                 624.5 as SO4
         Li                0.006
         B                 3.3     as BO3
         F                 0.15
         O(0)              1.0      O2(g)    -0.7
           P                         0.44    as PO4
           Br                        13.3
SOLUTION 1-50  Output nach Konditionierung mit künstl. GW
         units   ppm
         pH      7.61
         pe      6.2
         temp    22.0
         Ca                290.0
         Mg                38.0
         Na                840.00
         K                 26.8
         Fe                0.008
         Mn                0.55
         Sr                4.3
         Zn                0.0004
         Si                9.47
         Cl                1445.0
         Alkalinity        88.0 as HCO3
         S                 291.5 as SO4
         Li                0.008
         B                 0.391     as BO3
         O(0)              1.0      O2(g)    -0.7
         Br                         3.8

EXCHANGE_MASTER_SPECIES
         X       X-
         Xa      Xa-
EXCHANGE_SPECIES # erster Austauscher ' nach Gaines & Thomas' ####
         X- = X-
         log_k             0.0

         Na+ + X- = NaX
         log_k    0.0
         -gamma   4.0      0.075

         K+ + X- = KX
         log_k    0.4728
         -gamma   3.5      0.015
         delta_h  -4.3    # Jardine & Sparks, 1984

         Li+ + X- = LiX
         log_k    1.6226
         -gamma   6.0      0.0
         delta_h  1.4     # Merriam & Thomas, 1956

         NH4+ + X- = NH4X
         log_k    0.6
         -gamma   2.5      0.0
         delta_h  -2.4    # Laudelout et al., 1968

         Ca+2 + 2X- = CaX2
         log_k    1.3473
         -gamma   5.0      0.165
```

```
        delta_h  7.2     # Van Bladel & Gheyl, 1980

        Mg+2 + 2X- = MgX2
        log_k   1.1632
        -gamma  5.5      0.2
        delta_h  7.4     # Laudelout et al., 1968

        Sr+2 + 2X- = SrX2
        log_k   1.2879
        -gamma  5.26     0.121
        delta_h  5.5     # Laudelout et al., 1968

        Ba+2 + 2X- = BaX2
        log_k   0.91
        -gamma  5.0      0.0
        delta_h  4.5     # Laudelout et al., 1968

        Mn+2 + 2X- = MnX2
        log_k   1.3341
        -gamma  6.0      0.0

        Fe+2 + 2X- = FeX2
        log_k   0.44
        -gamma  6.0      0.0

        Cu+2 + 2X- = CuX2
        log_k   0.6
        -gamma  6.0      0.0

        Zn+2 + 2X- = ZnX2
        log_k   0.8
        -gamma  5.0      0.0

        Cd+2 + 2X- = CdX2
        log_k   0.8

        Pb+2 + 2X- = PbX2
        log_k   1.05

        Al+3 + 3X- = AlX3
        log_k   0.41
        -gamma  9.0      0.0

        AlOH+2 + 2X- = AlOHX2
        log_k   0.89
        -gamma  0.0      0.0
######## zweiter Austauscher  'nach Gapon'#############
        Xa- = Xa-
        log_k            0.0

        Na+ + Xa- = NaXa
        log_k   0.0
        -gamma  4.0      0.075

        K+ + Xa- = KXa
        log_k   0.4728
        -gamma  3.5      0.015
        delta_h  -4.3    # Jardine & Sparks, 1984

        Li+ + Xa- = LiXa
        log_k   1.6226
        -gamma  6.0      0.0
        delta_h  1.4     # Merriam & Thomas, 1956

        NH4+ + Xa- = NH4Xa
        log_k   0.6
        -gamma  2.5      0.0
        delta_h  -2.4    # Laudelout et al., 1968

        0.5Ca+2 + Xa- = Ca0.5Xa
        log_k   1.2059
        -gamma  5.0      0.165
        delta_h  7.2     # Van Bladel & Gheyl, 1980

        0.5Mg+2 + Xa- = Mg0.5Xa
        log_k   0.683
        -gamma  5.5      0.2
        delta_h  7.4     # Laudelout et al., 1968
```

```
        0.5Sr+2 + Xa- = Sr0.5Xa
        log_k   -0.0299
        -gamma  5.26    0.121
        delta_h  5.5    # Laudelout et al., 1968

        0.5Ba+2 + Xa- = Ba0.5Xa
        log_k   0.91
        -gamma  5.0     0.0
        delta_h  4.5    # Laudelout et al., 1968

        0.5Mn+2 + Xa- = Mn0.5Xa
        log_k   -0.239
        -gamma  6.0     0.0

#        0.5Fe+2 + Xa- = Fe0.5Xa
#        log_k   0.44
#        -gamma  6.0     0.0

        0.5Cu+2 + Xa- = Cu0.5Xa
        log_k   0.6
        -gamma  6.0     0.0

        0.5Zn+2 + Xa- = Zn0.5Xa
        log_k   0.8
        -gamma  5.0     0.0

        0.5Cd+2 + Xa- = Cd0.5Xa
        log_k   0.8

        0.5Pb+2 + Xa- = Pb0.5Xa
        log_k   1.05

#        0.333Al+3 + Xa- = Al0.333Xa
#        log_k   0.41
#        -gamma  9.0     0.0

        0.5AlOH+2 + Xa- = (AlOH)0.5Xa
        log_k   0.89
        -gamma  0.0     0.0

EXCHANGE 1-50
        equilibrate 1
        X               0.03134# Austauscher nach Gaines & Thomas
        Xa              0.0# Austauscher nach Gapon
SELECTED_OUTPUT
        -file           Säule1trn.sel
        -totals         Na Cl K Ca Li Fe Mn Sr Mg
USER_GRAPH
       -headings PV Na Cl K Ca Li Mn Fe Sr Mg
       -chart_title "Säulenversuch 1, Säule A"
       -axis_titles "PORE VOLUME" "MILLIMOLES PER KILOGRAM WATER"
       -axis_scale x_axis 0 auto 1 0.1
       -axis_scale y_axis 0 auto 0.25 0.05
       -axis_scale secondary_y_axis 0 auto 0.25 0.05
       -initial_solutions false
       -plot_concentration_vs time
       -start
       10 GRAPH_X (STEP_NO + 0.5) / 50
       20 GRAPH_Y TOT("Na")*1000, TOT("Cl")*1000, TOT("K")*1000, TOT("Ca")*1000
       30 GRAPH_SY TOT("Li")*1000, TOT("Mn")*1000, TOT("Fe")*1000, TOT("Sr")*1000, TOT
("Mg")*1000
       -end
TRANSPORT
        -cells          50
        -length         0.01
        -shifts         300
        -time_step      900.0
        -flow_direction  forward
        -boundary_cond   flux    flux
        -diffc          5.0e-11
        -dispersivity    0.017
        -correct_disp    true
        -punch          50
        -punch_frequency 1
        -print          50
        -print_frequency 25
END
```

Becken-	Becken-	Eh	pH	Ca	K	Mg	Na	SO4	HCO3	Mn	Sr	Li	Cl
länge [cm]	tiefe [cm]			[mg/l]	[mg/l]	[mg/l]	[mg/l]	[mg/l]	[mg/l]	[mg/l]	[mg/l]	[mg/l]	[mg/l]
-7,5	-7,0	-58,3	7,2	1641,2	111,0	424,0	731,1	2927,8	304,0	69,5	9,9	275,6	3127,9
-7,5	-9,0			1396,0	113,7	406,3	1112,7	2562,2		67,7	8,0	229,7	3669,0
-7,5	-11,0	-78,3	7,2	1347,4	113,9	391,6	1855,8	2544,5	393,0	64,8	7,4	209,7	4468,3
-7,5	-13,0	-71,3	7,2	1175,3	108,6	346,7	1864,8	2293,5	459,8	58,0	6,6	188,7	4171,9
-7,5	-15,0	-85,4	7,3	881,0	95,1	248,2	2464,9	1874,7	479,8	42,0	4,9	159,0	4552,9
-7,5	-17,0	-10,6	7,4	645,4	78,6	169,3	2647,2	1540,9	480,3	29,5	3,7	132,6	4399,9
-7,5	-19,0	-50,5	7,1	643,9	77,4	177,9	3703,7	1339,4	444,6	29,9	3,9	117,9	6227,5
-7,5	-21,0	-42,0	7,0	493,7	60,2	122,9	4205,6	1081,7	357,0	20,4	3,1	93,7	6793,8
-7,5	-23,0	-21,5	7,0	493,7	50,5	92,9	4292,1	832,5	206,5	17,0	3,4	80,8	7100,9
-7,5	-25,0	-28,5	6,9	480,2	75,7	259,2	4313,2	1203,3	141,4	26,8	8,8	77,8	7402,1
-7,5	-27,0		7,0	466,6	321,7	1052,9	9492,5	2434,5	211,9	3,3	1,2	23,1	16933,4
-7,5	-29,0			450,7	351,8	1104,4	9778,4	2520,9		2,0	0,8	21,9	17581,2
-7,5	-33,0		7,7	441,4	343,5	1075,4	9621,0	2471,3	154,2	2,0	0,8	21,2	17176,7
-7,5	-35,0	146,8	7,9	437,7			9535,8		159,2	1,9	0,7	22,5	15411,9
-7,5	-37,0		7,8	433,9	341,0	1066,6	9450,7	2458,3	79,0	2,0	0,8	22,8	16926,1
-7,5	-39,0	119,8	7,8	449,4	348,7	1101,6	9825,7	2515,0	158,5	2,1	0,8	24,0	17554,0
-7,5	-41,0	98,2	7,5	432,5	336,1	1056,8	9513,6	2418,6	168,7	2,3	0,8	20,2	16965,3
-7,5	-43,0		7,6	478,5	357,0	1120,6	9996,9	2635,6	158,7	2,9	1,0	26,6	17844,2
-7,5	-45,0		7,3	463,0	342,4	1077,8	9629,2	2534,1	141,3	2,8	0,9	23,2	17196,2
-7,5	-47,0		7,8	461,1	341,8	1074,1	9596,3	2520,6	161,1	2,7	0,9	24,0	17129,0
-7,5	-49,0		7,7	465,9	347,7	1086,3	9723,4	2536,4	141,4	2,9	0,9	24,4	17374,4
-7,5	-7,0			957,2	60,5	205,8	1146,4	3024,2		41,4	5,2	227,0	1934,1
-42,5	-11,0	-63,9	7,3	882,6	54,6	195,5	1049,5	2546,1	326,2	50,1	4,7	200,7	1777,6
-42,5	-15,0	-71,9	7,5	788,5	52,2	167,5	929,5	2128,1	600,7	40,3	4,4	166,8	1480,3
-42,5	-17,0	-38,0	7,3	701,5	48,9	136,8	817,7	1757,8	641,8	32,0	3,9	141,7	1301,7
-42,5	-19,0	-32,5	7,2	590,3	46,5	116,6	739,1	1419,8	548,5	27,0	3,5	127,3	1222,3
-42,5	-21,0	-41,1	7,0	499,7	41,4	96,2	672,1	1116,9	217,6	20,8	3,1	101,9	1309,6
-42,5	-25,0	-42,3	7,2	426,6	36,5	74,4	596,9	868,3	215,5	13,3	3,0	71,7	1174,7
-42,5	-27,0	5,7	7,3	417,6	34,4	66,4	570,5	799,5	159,9	9,2	3,3	61,7	1172,7
-42,5	-29,0		7,1	431,5	34,6	68,2	581,1	829,3	137,8	8,7	3,5	63,3	1210,3
-42,5	-31,0		7,2	415,9	33,3	62,4	568,6	763,2	142,4	6,4	3,5	54,1	1189,5
-42,5	-33,0		7,1	422,6	33,6	61,9	562,8	776,6	142,4	5,6	3,6	56,9	1180,5
-42,5	-35,0	-77,5	7,0	437,0	34,6	64,6	579,7	812,6	139,1	5,8	3,5	52,4	1216,5
-42,5	-37,0		7,9	420,6	33,2	61,2	554,3	773,8	100,0	4,5	3,7	50,7	1187,0
-42,5	-41,0			406,7	32,9	64,9	543,5	750,3				0,0	1223,2
-42,5	-43,0		7,1	447,3	333,9	1080,7	9639,3	2505,8	141,1	2,4	0,9	29,3	17205,8
-77,5	-7,0			1024,7	56,5	195,3	1024,1	3076,1		39,2	5,0	206,2	1792,3
-77,5	-15,0	-42,3	7,4	823,0	51,2	171,2	871,3	2248,0	766,2	43,1	4,5	171,9	1279,6
-77,5	-19,0	84,9	8,0	582,6	44,7	109,6	703,8	1377,3	444,4	23,3	3,5	109,8	1228,6
-77,5	-21,0	-27,2	7,4	517,5	39,5	94,6	644,5	1147,1	358,5	19,7	3,4	96,1	1186,2
-77,5	-23,0	-23,9	7,3	473,0	38,2	84,5	619,9	1010,4	281,4	16,3	3,2	84,1	1181,2
-77,5	-25,0	164,9	7,1	461,1	37,4	80,7	605,1	972,6	216,6	15,1	3,2	77,3	1193,8
-77,5	-27,0	-10,1	7,1	430,8	35,4	68,9	575,5	849,4	188,8	9,4	3,4	64,3	1157,5
-77,5	-29,0	-20,7	7,1	425,5	34,0	65,0	555,8	809,7	186,6	6,9	3,5	58,6	1134,1
-77,5	-31,0		7,0	420,7	33,5	62,0	554,1	780,9	143,3	5,2	3,7	50,6	1159,1
-77,5	-33,0		7,2	419,5	33,9	61,3	550,2	774,7	140,3	4,2	3,7	51,3	1155,1
-77,5	-35,0	-73,7	7,0	446,1	35,7	64,2	580,2	820,2	125,3	3,6	3,7	54,0	1233,2
-77,5	-37,0	-28,5	7,5	421,6	35,0	60,6	549,6	772,5	109,2	3,1	3,8	52,3	1175,3
-77,5	-39,0	-48,6	7,3	407,1	33,6	58,5	541,7	752,2	104,5	2,9	3,7	50,5	1147,3
-77,5	-41,0	-7,2	7,1	423,2	34,6	60,6	557,5	776,6	112,3	3,0	3,8	48,6	1185,3
-77,5	-43,0		7,4	448,3	34,7	64,9	576,9	775,2	102,8	4,1	4,2	55,1	1281,0
-77,5	-47,0		6,8	1038,7	61,2	279,7	2328,1	1376,3	122,9	11,5	9,3	75,6	5241,9
-77,5	-49,0		6,8	1071,9	81,8	581,2	4576,6	1983,1	125,1	13,2	8,8	70,5	9224,0
-112,5	-7,0			983,6	60,2	205,7	340,5	3065,8		45,0	5,3	235,8	705,5
-112,5	-15,0	126,6	7,7	858,3	55,0	186,6	340,5	2396,2	803,8	45,1	4,9	185,8	440,4
-112,5	-25,0	-45,9	7,2	461,7	37,9	82,0	340,5	980,1	289,5	15,3	3,3	81,0	740,0
-112,5	-27,0	-30,0	7,0	432,9	36,1	67,9	340,5	843,6	201,3	8,6	3,5	65,0	793,0
-112,5	-29,0		7,2	464,9	38,0	71,1	340,5	879,6	208,8	7,2	3,6	60,1	829,4
-112,5	-31,0		7,3	427,4	34,5	62,7	340,5	789,8	143,0	4,9	3,7	53,9	838,1
-112,5	-33,0		7,2	430,2	35,6	63,7	340,5	806,3	147,1	5,6	3,6	57,0	832,8

Becken-	Becken-	Eh	pH	Ca	K	Mg	Na	SO4	HCO3	Mn	Sr	Li	Cl
länge [cm]	tiefe [cm]			[mg/l]	[mg/l]	[mg/l]	[mg/l]	[mg/l]	[mg/l]	[mg/l]	[mg/l]	[mg/l]	[mg/l]
-112,5	-35,0	126,0	7,6	181,8	23,7	26,3	340,5	402,8	134,9	1,6	1,5	27,7	571,5
-112,5	-37,0	183,8	7,7	149,8	21,3	21,9	293,3	346,9	113,7	1,4	1,3	27,0	479,7
-112,5	-39,0	177,8	7,2	155,5	21,4	22,9	268,0	329,4	107,3	1,4	1,3	27,7	471,1
-112,5	-41,0	207,8	7,6	170,5	22,5	25,2	290,5	353,3	106,3	1,6	1,5	30,2	523,1
-112,5	-43,0		6,9	341,1	30,7	50,0	486,5	660,1	120,4	3,0	3,0	38,9	976,5
-112,5	-45,0		7,0	361,6	31,3	54,9	511,0	688,0	142,5	3,5	3,5	47,4	1033,1
-112,5	-47,0		6,8	399,8	32,5	59,3	545,0	743,8	139,7	3,4	3,4	42,0	1126,3
-112,5	-49,0		7,1	390,4	32,0	57,3	533,4	728,8	117,1	3,4	3,3	45,0	1110,0
-147,5	-7,0			1019,1	66,1	229,8	226,5	3064,4		44,2	5,4	241,9	673,2
-147,5	-15,0	17,5	7,5	848,9	57,3	194,4	226,5	2298,2	784,5	43,9	5,0	180,3	353,8
-147,5	-25,0	-48,3	7,0	481,4	39,6	90,7	226,5	1016,3	325,6	17,5	3,3	83,3	579,2
-147,5	-29,0		7,4	447,4	36,4	69,7	226,5	817,7	198,8	6,7	3,6	58,3	668,3
-147,5	-31,0		7,2	387,8	33,2	57,8	226,5	705,8	136,4	4,3	3,4	49,5	641,3
-147,5	-33,0		7,7	194,0	24,7	29,1	226,5	370,0	130,3	1,7	1,6	29,0	453,6
-147,5	-35,0	164,5	7,3	194,1	23,2	29,0	226,5	333,8	100,0	1,6	1,6	21,0	496,8
-147,5	-37,0	191,6	8,0	184,6	22,9	27,7	214,5	320,1	103,1	1,6	1,6	19,8	466,2
-147,5	-39,0	179,3	6,9	188,5	23,0	28,2	218,8	326,4	102,4	1,6	1,6	20,2	477,0
-147,5	-41,0		7,4	181,7	22,7	27,5	214,5	318,0	113,7	1,6	1,6	22,2	455,2
-147,5	-43,0		6,9	187,7	22,8	28,2	242,9	345,4	108,6	1,7	1,6	26,5	494,3
-147,5	-45,0		7,0	180,0	22,3	27,1	249,6	347,3	110,3	1,6	1,6	28,7	485,1
-147,5	-47,0		7,1	179,0	22,3	26,9	255,4	348,6	110,5	1,5	1,6	26,6	490,2
-147,5	-49,0		7,0	177,4	22,5	27,0	257,4	349,1	159,7	1,4	1,6	25,0	461,8
-182,5	-15,0	48,4	6,7	533,7	38,8	105,2	214,9	1153,3	235,0	24,7	3,1	101,9	646,1
-182,5	-25,0		6,9	417,0	33,0	69,2	214,9	781,2	170,2	10,9	3,3	56,2	636,0
-182,5	-35,0	189,8	7,4	186,9	16,0	26,9	214,9	317,9	99,0	1,4	1,4	15,7	465,6
-182,5	-37,0	179,4	7,7	183,5	15,9	26,4	209,5	311,6	97,6	1,3	1,5	18,1	455,3
-182,5	-39,0	175,8	7,0	192,9	16,5	27,9	221,1	336,0	97,1	1,5	1,5	17,9	477,1
-182,5	-41,0	256,3	7,3	190,2	16,4	27,6	217,4	325,0	110,3	1,4	1,5	17,6	466,2
-182,5	-43,0		7,3	157,8	14,7	22,7	182,8	283,4	112,1	1,3	1,2	16,1	368,6
-182,5	-45,0		7,2	125,7	12,7	18,4	148,9	222,9	98,6	1,0	1,0	12,6	297,3
-182,5	-47,0		6,8	117,6	12,1	17,1	123,7	197,1	104,3	0,8	0,8	14,0	255,0
-182,5	-49,0		7,3	118,6	12,2	17,6	133,7	210,8	101,9	1,0	0,9	11,3	265,5
.	.												

```
TITLE SIMULATION OF FIELDPROCESSES
        units   ppm
        pH      7.1
        pe      0.481
        density 1.000
        temp    10.0
        redox   O(0)/O(-2)
        Ca              177
        Mg              41
        Na              15   charge
        K               11.8
        Fe              2.2
        Mn              1.3
        Sr                      0.93
        Ba              0.015
        Si              74   as SiO2
        Cl              45
        Alkalinity      575  as HCO3
        S(6)            134 as SO4
        Li              0.03
        N(-3)           0.09    as NH4
        B               0.55    as BO2
        F               0.25
        O(0)            0.9  #   O2(g)   -0.7
          P                     0.3    as PO4
SAVE Solution 1
END
EXCHANGE_MASTER_SPECIES
        X       X-
        Xa      Xa-
EXCHANGE_SPECIES # erster Austauscher ' nach Gaines & Thomas' ####
        X- = X-
        log_k           0.0

        Na+ + X- = NaX
        log_k   0.0
        -gamma  4.0     0.075

        K+ + X- = KX
        log_k   0.4728
        -gamma  3.5     0.015
        delta_h  -4.3   # Jardine & Sparks, 1984

        Ca+2 + 2X- = CaX2
        log_k   1.3473
        -gamma  5.0     0.165
        delta_h  7.2    # Van Bladel & Gheyl, 1980

        Mg+2 + 2X- = MgX2
        log_k   1.1632
        -gamma  5.5     0.2
        delta_h  7.4    # Laudelout et al., 1968

######## zweiter Austauscher  'nach Gapon'#############
        Xa- = Xa-
        log_k           0.0

        Na+ + Xa- = NaXa
        log_k   0.0
        -gamma  4.0     0.075

        K+ + Xa- = KXa
        log_k   0.4728
        -gamma  3.5     0.015
        delta_h  -4.3   # Jardine & Sparks, 1984

        0.5Ca+2 + Xa- = Ca0.5Xa
        log_k   1.2059
        -gamma  5.0     0.165
        delta_h  7.2    # Van Bladel & Gheyl, 1980

        0.5Mg+2 + Xa- = Mg0.5Xa
        log_k   0.683
        -gamma  5.5     0.2
        delta_h  7.4    # Laudelout et al., 1968

EXCHANGE
        equilibrate with solution 1
```

```
        X               0.03134# Austauscher nach Gaines & Thomas
        Xa              0.0# Austauscher nach Gapon
SAVE exchange 1
END
SOLUTION 2  CAT-DB
        units   ppm
        pH      7.9
        pe      0.481
        density 1.000
        temp    10.0
        Ca              199
        Mg              397
        Na              3440   charge
        K               133
        Fe              0.091
        Mn              0.303
        Sr                      2.42
        Ba              0.02
        Si              9.5   as SiO2
        Cl              6160
        Alkalinity      238  as HCO3
        S               867 as SO4
        Li              0.065
        N(-3)           0.09    as NH4
        B               5.46    as BO2
        F               0.561
        O(0)            11.1  #   O2(g)   -0.7
          P                     0.44    as PO4
SAVE Solution 2
END
MIX 1
     1     1
     2     0.067
SAVE Solution 3
END
EQUILIBRIUM_PHASES 1
        CO2(g)          -0.3
        Calcite
REACTION 1 Abbau Corg durch Sulfatreduktion
        SO4             -1
        H2S             +1
        HCO3            +2
        0.001745 moles in 1 steps
USE Solution 3
SAVE Solution 4
END
EQUILIBRIUM_PHASES
USE Solution 4
EXCHANGE
        equilibrate with solution 1
        X               0.03134# Austauscher nach Gaines & Thomas
        Xa              0.0# Austauscher nach Gapon
SAVE Solution 5
END
```